5-2024

Controlled Delivery of Peptide and Gasotransmitter for Promoting Vascular Endothelialization

Shirin Changizi
Florida Institute of Technology, schangizi2019@fit.edu

Controlled Delivery of Peptide and Gasotransmitter for Promoting Vascular Endothelialization

by

Shirin Changizi

A dissertation submitted to the Department of Biomedical Engineering and Science

of

Florida Institute of Technology

in partial fulfillment of the requirements

for the degree of

Doctor of Philosophy

in

Biomedical Engineering

Melbourne, Florida

May 2024

We the undersigned committee hereby approve the attached dissertation, "Controlled Delivery of Peptide and Gasotransmitter for Promoting Vascular Endothelialization"

By

Shirin Changizi

Christopher A. Bashur, Ph.D.
Associate Professor
Chemistry and Chemical Engineering
Major Advisor

Vipuil Kishore, Ph.D.
Associate Professor
Chemistry and Chemical Engineering

Yi Liao, Ph.D.
Professor
Chemistry and Chemical Engineering

Venkat Keshav Chivukula, Ph.D.
Assistant Professor
Biomedical Engineering and Science

Linxia Gu, Ph.D.
Professor and Department Head
Biomedical Engineering and Science

Abstract

Title: Controlled Delivery of Peptide and Gasotransmitter for Promoting Vascular Endothelialization

Author: Shirin Changizi

Advisor: Christopher A. Bashur, Ph.D.

Endothelial cells (ECs) are vital for maintaining proper vascular function and regulating processes such as hemostasis and inflammation. Disruption of endothelial cells integrity can lead to several pathological conditions, including coronary artery disease, vascular cognitive impairment, and dementia (VCID). Alterations in ECs distribution may lead to compromised blood-brain barrier (BBB) function, facilitating the passage of blood components and contributing to conditions such as Alzheimer's disease. Additionally, disruptions in ECs function can lead to early-stage thrombosis and intimal hyperplasia, resulting in graft failure in small-diameter (<6mm) tissue-engineered vascular grafts (TEVGs). Current strategies to enhance endothelialization at the BBB and TEVGs encounter several challenges. Therefore, restoring EC function at the targeted site is crucial for preventing disease progression and ensuring the success of vascular grafts.

This study aimed to develop innovative approaches for drug delivery to the BBB and TEVGs to improve endothelialization and mitigate associated risks. To this end, microbubbles (MBs) and electrospun-based constructs were employed to deliver

active compounds. MBs were engineered using perfluorocarbon (PFC) to transport carbon monoxide and restore endothelial cells at the BBB *in vitro*. Furthermore, fibrin-coated polycaprolactone (PCL) constructs were utilized to deliver the UPI peptide and enhance endothelialization in proposed TEVGs, both *in vitro* and *in vivo*. Additional modifications were implemented to optimize the release profile of the UPI peptide and evaluate its specificity for endothelialization. The findings of this study suggest that these novel techniques hold promise for improving endothelialization at targeted sites.

Table of Contents

List of figures

Attribution

Chris A. Bashur – Ph.D., serves as the advisor and committee chair in the department of BCES at the Florida Institute of Technology and has been instrumental in guiding the research process.

Yi Liao – Ph.D., affiliated with the Department of BCES at the Florida Institute of Technology, played a crucial role in providing valuable expertise in chemistry, including synthesis techniques for my carbon monoxide delivery study.

Hong Chen – Ph.D., affiliated with Harward Medical School, synthesized the novel UPI peptide, and provided us with this peptide for research.

Gabrielle Bazemore – was a master's student who performed animal surgeries for the peptide project.

Jennifer VanSant – was a master's student who first developed the high boiling point microbubbles and taught me how to fabricate the microbubbles.

Osamah Alghazwat, Ph.D., helped me install carbon monoxide to load my samples.

Mahyar Sameti – Ph.D., guided me at the beginning of my PhD by teaching me different techniques. He also initially started the peptide project (chapter 2).

Isabelle Marquette - an undergraduate student who helped analyze the stability of PFC-based microbubbles.

Adnan Elgattar – Ph.D., helped me with synthesizing a sensor for measuring the carbon monoxide contents within the microbubbles.

Acknowledgement

I want to thank my supervisor for his guidance. He has helped to learn critical thinking and research skills.

I would love to thank Dr. Keshav who has been great at advising me in different aspects of my life. He is a role model who showed me that I can be a researcher and be a daughter, a partner, and a friend.

I would like to thank my family, my mom, my sister, and brother that have been supporting me through all my wishes. Even though I am far away, they always showed me how it feels to have a great family who supports you through every step of your life.

I want to thank Leo, my husband who made me feel at home and helped me through these years. There were days that I wanted to give up and he pushed me for the better.

I also want to appreciate my friends who made it easier to leave away from all the loved ones. Soroush, Beste, Nithya, Mariam, Ruthie, Arnold, and Ana, thanks for putting up with me. All of you has helped me in a time of my journey.

Lastly, I would like to thank my lab mates, specifically Zack and Rubens for making the lab a better place to work.

Dedicated to my loving family.

Especially my mom

Chapter 1: Introduction

1.1 Introduction

Endothelial cells (ECs) play several critical roles in controlling vascular function. Their function is necessary to control homeostasis, thrombosis, inflammation, vascular wall remodeling, and other physiological and pathological processes [1]. ECs form a layer in the blood vessels, which provides a selective barrier for transporting molecules between tissue and blood. Any disturbance of these cells causes coagulation, inflammation, and vasoconstriction.

ECs dysfunction and its roles in various diseases such as coronary artery disease, peripheral artery disease, and vascular cognitive impairment have raised the interest in developing drug delivery methods to improve their function. Research groups have investigated the delivery of therapeutic molecules to ECs to improve their function and response. Further research has shown that delivering vascular endothelial growth factor (VEGF) via scaffolds enhances endothelialization, cell infiltration, and graft remodeling [2].

For this purpose, the primary goal of this research is to improve endothelization at small diameters < 4mm tissue engineering vascular grafts (TEVGs) and at the blood-brain barrier (BBB). Several drug delivery techniques have been employed to deliver therapeutic compounds to the targeted regions to achieve this. The strategies adopted include the delivery of carbon monoxide (CO) to the BBB using perfluorocarbon (PFC)-based microbubbles (MBs), as well as the implantation of an

acellular graft designed for the targeted delivery of a specific peptide to facilitate endothelization in small-diameter vascular grafts. Moreover, in this study, we performed survival surgery on rodents for one week, which allowed us to assess the rapid endothelization of grafts after delivery of our specific peptide.

This section addresses critical clinical needs and highlights fabrication challenges in developing effective drug delivery systems for enhancing endothelization in small-diameter vascular grafts and at the BBB. Various methodologies and approaches are discussed to provide insights into advancing vascular tissue engineering.

1.2 Endothelial cells

ECs have a cobblestone shape, cover the luminal surfaces of blood vessels in the human body, and are in contact with the blood circulation system. ECs are one of the main parts of the vascular system [3]. These cells prevent intimal hyperplasia and thrombosis [4]. ECs have organ-adaptation properties, and their shape and function can be adjusted for different organs [5]. ECs, for instance, form the BBB in the nervous system, and ECs in the endocardium adapt to the constant heartbeat [6].

ECs are also very adaptive to different blood flow of the vessels. Further, ECs can regulate flow-mediated dilation and low-flow vasoconstriction, and loss of these functions increases the risk of different diseases [3], [4]. A monolayer of ECs is present in the anatomical structure of veins, capillaries, and arteries [7].

1.3 Artery anatomical structure

Coronary arteries have three main layers: the inner layer or tunica intimal, media, and adventitia. The inner layer is in direct contact with blood and comprises the endothelium, basement membrane, and elastic lamina. The endothelium consists of a single layer of ECs that play a crucial role in preserving vascular permeability, homeostasis, blood flow regulation, and the secretion of numerous molecules integral to metabolic and immunologic functions [8]. The basement membrane, which provides structural support for the ECs layer is comprised of collagen type I and III, fibronectin, and large molecules such as GAGs. The elastic lamina provides flexibility for this structure [9], [10]. The second or tunica media layer is mainly formed from smooth muscle cells, elastic fibers, and collagen [10]. The smooth muscle cell layers are bound to the elastic lamina, separating these layers from the other layers [11]. Smooth muscle cells actively help the artery's contraction to control the blood flow, partially facilitated by signaling pathways from ECs and provide mechanical stability for the vessel [10]. The outermost layer, the tunica adventitia is comprised of connective tissue such as collagen, fibroblasts, and mast cells. Most parasympathetic and sympatric nerves are in this layer [11]. A deep comprehension of arterial anatomy holds significance for advancements in tissue engineering and regenerative medicine. Transitioning from the structural complexities of arterial layers allows the development of biological substitutes and therapeutic interventions for developing TEVGs.

1.4 Tissue engineering and regenerative medicine

Regenerative medicine combines research, clinical approaches, and technologies, including tissue engineering, gene therapy, and cell therapy. Regenerative medicine aims to stimulate the body to generate new cells for organ generation without embedding or recruiting any cells via scaffolds [12], [13]. Tissue engineering is part of regenerative medicine. However, tissue engineering depends on scaffolds as a fundamental component. Biodegradable or bioresorbable scaffolds can allow the biomaterial to be substituted by cells and promote functional tissue generation [14]. Scaffold degradation and resorption rate are essential for tissue replacement.

The tissue engineering terminology was created almost 30 years ago and is an interdisciplinary field composed of different sciences, including biomaterials, cell biology, mechanical engineering, and biotechnology [13]. Tissue engineering can help to develop biological substitutes to restore, maintain, or improve the organ's functions [12]. Tissue engineering strategies are comprised of four main components: 1. Cells 2. Growth factors 3. Scaffold, and 4. Bioreactors. These components can be designed to mimic biological organs/tissues close to humans' structure and function [13], and are important for both tissue engineering and regenerative medicine.

1.4.1 Cells

Different cell types can be used for regeneration, such as multipotent stem cells, autologous cells, allogenic cells, and iPSC [13]. According to the biological and

structural requirements of the application, the cell sources can be different. There are two main approaches to harvesting cells for tissue engineering and regenerative medicine: biopsy and stem cell technique. The organ biopsy technique can be applied to most organs, including the kidney and liver. For instance, smooth muscle cells and urothelial cells can be isolated from bladder biopsy. However, the nervous system cannot go under any biopsy. Harvesting stem cells is an alternative method of overcoming this obstacle [13].

Numerous strategies have been used to enhance the endothelialization of TEVGs. These include pre-seeding techniques to establish a complete endothelium layer before implantation and using acellular grafts to recruit cells post-grafting. In pre-seeding techniques of TEVGs, ECs are used to establish a cellular layer to prevent intimal hyperplasia and early-stage thrombosis after implantation *in situ*. Moreover, in acellular grafts, ECs may migrate to the mid grafts from the anastomosis site or through pores in the graft via ingrowth of capillaries [15]. Further, circulating endothelial progenitor cells (EPCs) can adhere, proliferate, and differentiate to ECs and improve endothelization [16].

1.4.2 Growth factors

Cell proliferation, migration, differentiation, and cell-matrix interaction can be improved by releasing desired signaling molecules, such as growth factors, from carriers [17]. These signaling molecules can be embedded into the scaffold and delivered to the targeted tissue. Carriers are needed to increase the efficacy and release of these molecules [18]. The controlled release of these molecules can affect

cell propagation, vascularization, and tissue generation. Growth factors can act on different cell types with the same or different effects and influence the secretion of other growth factors [18]. Different growth factors have been used for tissue-engineered vascular grafts. For example, VEGF has been used to improve endothelization in multilayer electrospun polycaprolactone (PCL) constructs *in vitro* [19]. In this study, VEGF and heparin were incorporated into the PCL constructs, resulting in the early release of VEGF and endothelization of the hydrophobic constructs, followed by sustained release of heparin for long-term antithrombogenicity [19].

1.4.3 Scaffold

The scaffold or artificial extracellular matrix (ECM) for tissue engineering provides structural integrity and supports cells to proliferate, migrate, and differentiate. These scaffolds must meet requirements to enhance organ/tissue generation and cellular activity [12]. These properties include biocompatibility, biodegradability, proper mechanical strength, and porosity. Biocompatibility is essential in understanding the host's immune response to foreign body material [20]. The durability and success of implants and drug carriers depend on their interaction with the immune response. Toxicity, implant size, and implant bioreaction with surrounding tissue can induce foreign body reactions [20]. The scaffold provides the structure and mechanical strength of the tissue, such as rigidity, viscoelasticity, and elasticity. Appropriate mechanical properties are crucial for cell attachment and proliferation [14]. A low Young's modulus, for example, can reduce cell attachment

and proliferation, while a high modulus can induce stress shielding. Moreover, pore size is also an essential part of the scaffold as it allows transfer of oxygen and nutrition and diffuses growth factors [21]. Porous scaffolds also provide a high surface-to-volume ratio, which can increase cell attachment and proliferation [21].

1.4.4 Bioreactors

Bioreactors are devices that provide biological and biochemical processes under controlled conditions. Bioreactors are used in diverse areas, such as wastewater treatment, fermentation, food processing, and recombinant protein processes [22]. Bioreactors have also been used for over 30 years to produce vaccines and other pharmaceutical components. In tissue engineering, bioreactors mimic the mechanical, biochemical, and biological cues of the native body in monitored conditions, including pH, temperature, oxygen, and pressure *in vitro* [23]. Moreover, bioreactors provide accurate information about the living tissue's responses to mechanical and biochemical stimulations in the system. To mature an engineered tissue *in vitro* before implantation, researchers attempt to enhance cellular growth by incorporating growth factors and bioreactors [24].

1.5 Biomaterial choice

Biomaterials used in the TEVGs have two general categories based on their origin: 1. Natural and 2. Synthetic [25].

1.5.1 Natural biomaterials

Natural materials, including chitosan, collagen, elastin, and hyaluronan, are often in the tissue engineering interest as they can have proper biocompatibility and availability [25]. These materials often mimic the ECM components that induce cell attachment, proliferation, migration, nutrition, and oxygen exchange with other tissues [26]. For example, collagen is the primary protein in the human body, a vital element of the ECM. It provides essential structural support and tensile strength to tissues [27]. Collagen-based drug delivery systems (DDS) have been widely used for vascular application, with studies specifically targeting improved affinity of collagen scaffolds for ECs. By integrating diverse pro-angiogenic growth factors such as VEGF, researchers have achieved promising results in controlling the release of encapsulated molecules and promoting angiogenesis [28]. Moreover, implantation of biopolymer silk (Indian endemic non-mulberry silk) grafts with inherent proper mechanical and biological properties (e.g., arginine-glycine-aspartic acid (RGD) motifs) in abdominal aortic interposition for eight weeks showed neo-tissue formation, cell infiltration, and graft remodeling [29]. Due to their common porous structure and bioactivity, natural biomaterials have also been used for drug, cell, growth factor, and nutrition delivery [26].

1.5.2 Synthetic materials

Synthetic materials have easy availability and uniform diameter after processing; however, these materials have a higher risk of inflammation, infection, failure rate for grafts with diameter < 6 mm, and development of neointima [30]. Moreover, in

vessels with smaller diameters, synthetic graft failure is often attributed to a combination of atherosclerosis and anastomotic intimal hyperplasia [31]. However, synthetic materials can be processed to have the desired biocompatibility, biodegradability, mechanical strength, bioactivity, and biostability [30]. Synthetic polymers such as poly (lactic acid) have been widely used for organ and tissue replacement in the body [32]. Further, researchers have widely used synthetic materials in BBB models and cardiovascular systems. For example, PCL is a synthetic polymer used in TEVGs due to its proper degradation time, typically between 1-3 years, allowing extended presence of the scaffold and gradual development of robust structural tissue capable of withstanding physiological stresses [33]. Polyethylene glycol (PEG) hydrogels have been utilized as a delivery system for heparin to enhance vascularization via subcutaneous implantation in rodent models. The degradable PEG hydrogels with covalently heparinized showed significant vascularization and were replaced by tissue ingrowth after degradation [34].

1.6 Drug release profile

Drug delivery refers to administering therapeutic substances, such as medications or biologics, into the body to achieve a desired therapeutic effect. Drug delivery systems aim to deliver drugs to specific target sites within the body at the appropriate concentration and rate while minimizing side effects and maximizing therapeutic efficacy [35]. Drug delivery systems vary widely in complexity and design, ranging

from simple oral tablets to sophisticated nanoscale carriers. Drug delivery systems must be biocompatible, have high drug loading capacity, and be biodegradable.

The drug release profile refers to the rate at which the drug is released. There are various drug release profiles, including burst and sustained release, which understating their profile allows optimization of therapeutic outcomes. For example, sustained release rate in some TEVGs applications is essential to improve angiogenesis and endothelization. VEGF immobilization into heparinized PCL/Gel scaffolds has shown that the sustained release of VEGF has induced vascularization post-implantation in rodents compared to PCL constructs burst release [36].

Various materials have been used for local and controlled drug delivery, including porous materials, hydrogels, natural and synthetic polymers, and composite materials [37]. Hydrogels, for instance, are hydrophilic materials that are mostly water, and by changing their crosslinking, their properties alter and can affect their use in drug delivery. Covalent crosslinking, for example, reduces the dissolution and dispersion of the hydrogel for *in vivo* applications [38]. Additionally, hydrogels allow minimally invasive treatment by injectable cell delivery. However, hydrogels normally exhibit a burst release for up to 48 hours and are unsuitable for sustained release [39]. Researchers have been investigating different mechanisms to improve the local delivery of the drug with desired release profile.

1.7 Controlled drug delivery

Controlled drug delivery systems aim to maintain the administrated drug levels in a proper range without the need for multiple drug administration. They can also enhance patient compliance. Moreover, controlled drug release can reduce toxicities by minimizing the delivery of the drug to non-target tissues [37]. Drugs must have a minimum dosage to be effective in the body. However, many drugs have a short lifespan in the body, making it challenging to achieve a proper dose at the injury site. For this reason, researchers have been exploring various delivery methods to enhance drug loading and release efficiency including transdermal techniques, nano-and microparticles, and drug delivery via scaffold.

A transdermal or skin patch is a drug delivery method that delivers a specific drug dosage through the skin and to the bloodstream. Transdermal patches were first developed in 1970 and then received FDA approval in 1979. These noninvasive patches have various benefits, such as bioavailability, lower dosing frequency, longer release duration, and better plasma level. Although these skin patches provide many benefits, they cannot transfer bigger molecules, high dosages of drugs to the blood, or ionic drugs. Marwah et al. have shown that insulin can be delivered via transferosomal gel through the skin by minimizing the parental side effects. Moreover, researchers have tried to increase the efficacy of the drug release from microneedle skin patches. In this process, the water-soluble microneedles were mounted on an insoluble backbone, and because of immiscibility, the drug release from microneedles to the backbone was reduced significantly [40].

Drug delivery through implanted scaffolds is a smart alternative that provides better-controlled drug release in different targeted areas. Polymer scaffolds have been widely used to transfer proteins, ions, and drugs [41]. Polymer scaffolds (natural or synthetic) act as carriers and protect the drugs before releasing them into the body and can allow a controlled release in the target area [41]. Polymer scaffolds can keep the drug at a therapeutic level as they can release one or multiple compounds at a specific release rate.

Additionally, biocompatible polymer-based scaffolds, such as PCL, have enhanced cell attachment and proliferation by delivering active compounds. Wang et al. showed that PCL vascular grafts that were modified with a fusion protein VEGF–class 1 hydrophobin (HGFI) improved endothelialization and vascularization in rodents after one-month of implantation. Moreover, the implanted scaffold improves contractile smooth muscle cell (SMC) regeneration, suggesting the regenerative capacity of this graft [42].

Engineered micro-and nanomaterials are another delivery method that has shown significant improvement in disease diagnostics and treatment. Microparticles (MP) are designed for different pathologies with modifiable properties, including size, shape, charge, surface properties, and responsiveness [43]. Microparticles have high loading efficiency, facilitate the delivery of a wide range of compounds, enable targeted delivery through established pathological pathways, improve drug stability and availability, and can have sustained drug release. Moreover, using biocompatible and biodegradable material reduces the immune response risk from the body.

Considering microparticle fabrication is crucial for enhancing the effectiveness of these particles in delivering drugs to targeted diseased areas.

Microparticles have three main categories: lipid-based, inorganic, and polymeric. Different fabrication methods have been offered to enhance the MP's circulation time in the body [44]. Single emulsion, water/oil/water, and oil/water/oil emulsion techniques are commonly employed to fabricate microparticles for drug delivery. The double emulsion technique is widely employed for encapsulating hydrophilic drugs, including peptides and proteins, within polymeric microspheres to enhance drug loading efficiency [45]. The water/oil/water (W1/O/W2) double emulsion technique involves emulsifying an aqueous solution with therapeutic compounds in an organic solvent containing a polymer. The initial emulsion (W1/O) is then dispersed in a second aqueous phase (O/W2), forming solid microparticles upon removing the volatile organic solvent. This method is frequently used for hydrophilic drugs, utilizing an intermediary oil layer as a liquid membrane [46], [47]. For controlled and local drug delivery applications, it is essential to integrate diverse drug delivery techniques to enhance the effectiveness and lifespan of active compounds.

In this project, scaffolds and micro-carriers were employed for the targeted delivery of active compounds to diseased sites. PFC-based MB were utilized to deliver gasotransmitters to the BBB. Additionally, electrospun constructs and PLGA microparticles were utilized for the localized delivery of peptides, aiming to enhance endothelialization in small-diameter vascular grafts.

1.8 Drug delivery to blood brain barrier

1.8.1 Blood brain barrier

The nervous central system is uniquely vascularized by a specialized network of blood vessels known as the BBB [48]. This unique feature is crucial in maintaining the delicate balance of the brain's internal environment. The BBB is a remarkable mechanism that tightly regulates the selective transport of ions, molecules, and cells between the blood and the brain**.** This function is essential for maintaining brain homeostasis, ensuring proper neuronal function, and preventing transmitting pathogens and blood components [49]. The BBB, like other vessels, is primarily composed of ECs and mural cells.

Impairment of the BBB plays a significant role in a range of central nervous system (CNS) disorders, including stroke, brain tumors, neurodegenerative diseases, and HIV-associated dementia. BBB dysfunction is linked with several factors, including oxidative stress from reactive oxygen species (ROS) [50], the release or stimulation of matrix metalloproteinases (MMPs) [51], and angiogenic elements [52].

For example, elevation in BBB permeability is a main pathological characteristic shared by both ischemic and hemorrhagic strokes, often linked with poor prognosis. In stroke, BBB permeability leads to disruptions in transcytosis, specifically a shift from ligand-specific receptor-mediated transcytosis (RMT) to non-specific caveolar

transcytosis. This shift is influenced by the degeneration of pericytes, leading to calcification of the vasculature and damage and death of ECs. As a result, there is an increase in the number of endothelial caveolae, facilitating the non-selective passage of large molecules, including neurotoxic proteins like fibrinogen, across the BBB. This increased permeability contributes to neuroinflammation, exacerbating the dysfunction [53]. Moreover, in human immunodeficiency virus HIV-associated dementia, initial inflammation within the CNS, the presence of perivascular macrophages, and the infiltration of monocytes have been linked with the disruption of the BBB [54]. Additionally, in certain patients, the BBB damage linked to CNS disorders may not be reversible.

Disruption of the BBB system is often accompanied by the attack of free radicals and proteases on the ECs' membrane, leading to the degradation of the tight junctions and loss of ECs which often do not undergo automatic repair in many patients [55]. For this purpose, restoring and remodeling the function of the ECs is a crucial aspect of treating a compromised BBB.

1.8.2 Drug delivery through the BBB

Our research, unlike many pharmaceutical approaches that primarily aim to transfer active compounds through the BBB to address an existing disease, is not focused on enhancing the permeability of the BBB. Instead, we aim restoring ECs at the BBB to prevent various diseases such as vascular cognitive impairment. The current drug delivery strategies, including microspheres, microchips, and colloidal drug carrier systems, are designed to disrupt and transfer molecules through the BBB.

However, the goal of our approach is to promote and restore endothelialization by transferring active compounds to BBBs' ECs. For this purpose, several drug carriers have been utilized to enhance the efficiency of delivering active compounds and their release.

Microspheres are homogenous or heterogeneous structures of synthetic and natural materials. Microsphere particles can contain solid or liquid active pharmaceutical ingredients, and their diameter is typically 1– 1000 μm [56]. An example of solid particles is bio-adhesive chitosan microspheres that have been used to transport methotrexate drug to brain cells via nasal administration. According to this research, chitosan with higher molecular weight can entrap higher drug loading. It could improve the nose-to-brain transport of the drug due to its mucoadhesive properties [57]. However, it is important to note that this does not address repairing a damaged BBB, and instead will have the opposite effect.

Colloidal drug carrier systems include nano and micro-particle-sized systems such as nanoparticles, nanogels, liposomes, and micelles. These particles are usually between 1 nm to 1 μm. MBs have a gas core stabilizing the lipid, polymer, and protein shell. MBs are larger than lipid and polymer nano-carriers, ranging from 1–10 μm in diameter. MBs stay in the blood circulation system until they burst, dissolve, or are cleared by the phagocyte system [58]. Soft-shelled MBs comprise a thin shell material, increasing the MB's sensitivity to acoustic waves. These MBs burst in high ultrasound amplitude and release the drug [59].

Our current focus for this application is using colloidal drug carriers (MBs) to deliver active compounds to ECs to reduce vascular cognitive impairment risks.

1.8.3 Biomaterial choice for MBs

The first generation of MBs faced a short-term life span as the gas shell was unstable when it traveled in blood circulation [60]. The majority of these gas MBs were composed of nitrogen, PFCs, or sulfur hexafluoride. More recently, a lipid, protein, or polymer coating was integrated into the fabrication approaches of MBs to enhance the stability of the MBs system. These active coatings could be natural or synthetic. The lipid shell can be made of phospholipids such as dipalmitoyl phosphatidylcholine (DPPC), 2-distearoyl-sn-glycero-3-phosphoethanolamine-Poly (DSPE), and distearoylphosphatidylcholine (DSPC). These lipids enable the formation of a flexible shell, diminishing the sensitivity of MBs to factors such as temperature, pressure, and other physiological properties within the body. This flexibility contributes to an extended lifespan of the MBs in blood circulation. [60]. Utilizing polymers and proteins as coatings presents an alternative approach to enhance the MBs' efficacy. Polymer coatings, such as PCL and PEG, significantly improve the stability of MBs in blood circulation while concurrently reducing the body's immune response. These coatings can act as biocompatible barriers, contributing to an enhanced and more effective drug delivery system [61].

1.8.4 Ultrasound sensitive microparticles for drug delivery

A non-invasive method for delivering drugs to the brain, through the BBB, is through ultrasound sensitive MBs. This system allows the delivery of both imaging agents and therapeutics, such as antibodies [62]. However, in this study, ultrasound sensitive MBs were utilized for the targeted delivery of gasotransmitters to the BBB rather than attempting to transfer through the BBB into the brain tissue.

The MBs gas core allows the volumetric oscillation of the MBs in response to ultrasound waves. The gas core is usually fluorocarbons and nitrogen. Ultrasound-sensitive MBs can improve drug delivery via optimal ultrasound parameters with minimal cellular damage. In one study researchers developed MBs with a high capacity (around 68.01% ± 4.35%) for carrying 1,3-bis(2-chloroethyl)-1-nitrosourea (BCNU), a chemotherapy drug. When combined with focused ultrasound (FUS) at a frequency of 1 MHz, these BCNU-loaded MBs helped disrupt the BBB locally, while also releasing BCNU at the intended site, enhancing the drug's deposition at the target area. In animal models with brain tumors, the combined treatment of BCNU-loaded MBs and FUS effectively controlled tumor growth (reduced by 915.3% to 39.6%) and increased median survival (from 29 days to 32.5 days) [63]. Moreover, researchers used folate-inserted cationic MBs to load DNA and transfer through the BBB in rat models. After application of ultrasound to the targeted area, these MBs were broken down, and the DNA release increased the BBB permeability to transfer the folate ligands to the tumor cells and local gene therapy [64]. Several studies have

consistently aimed at enhancing the permeability of the BBB for the effective delivery of active compounds. However, our study seeks to transfer MBs to BBB tissue to enhance endothelialization at the site and mitigate vascular cognitive impairment by delivering specific gasotransmitters via MBs.

1.8.5 Gasotransmitters in drug delivery

Gasotransmitters are endogenously generated in mammalian cells, are involved in signaling pathways, and have specific cellular targets. Nitric oxide (NO), CO, and hydrogen sulfide (H2S) are among the gasotransmitters family [65]. Gasotransmitters are involved in intracellular and intercellular functions such as proliferation, apoptosis, and adenosine triphosphate (ATP) synthesis. The proper dosages of these gases have therapeutic effects in the body, such as apoptosis inhibition and cytoprotecting. A high dosage of these gasses is toxic for the organs and cells since binding to hemoglobin decreases the capacity of the hemoglobin to carry oxygen [66]. However, gasotransmittters have shown benefits in cardiovascular system such as improving the angiogenesis and cardio-protection at appropriate doses [67]. Due to their anti-inflammatory and anti-apoptotic benefits, the interest in this area has been growing.

1.8.6 Carbon monoxide benefits

CO is part of various physiological signaling pathways. Its production is a continuous process facilitated by heme oxygenase-2 and inducible heme oxygenase

1[68]. These metabolic enzymes significantly influence hemoprotein and heme molecules. While high doses of CO can be lethal, a specific concentration can be beneficial for cardiovascular diseases, inflammatory disorders, and organ transplantation. Researchers have shown that the proper dosage of CO would block vascular smooth muscle proliferation that can prevent intimal hyperplasia and improve endothelization. Sato et al. have demonstrated that in mouse-rat heart transplantation, the generation of CO in ECs not only prevented platelet aggregation and apoptosis but also suppressed graft rejection [69]. Similarly, Rodella et al. found that exogenous administration of CO in diabetic rat models, where ECs dysfunction is common, can prevent EC apoptosis and enhance EC proliferation by reducing oxidative stress [70]. Moreover, intro and *in vivo* studies show that CO has anti-inflammatory and antioxidant properties. Research on chronic obstructive pulmonary disease patients showed that inhalation of the low dosage of CO resulted in therapeutic effects and a decrease in eosinophil counts [71]. Overall, it is essential to investigate the proper dosage and carrier to achieve the therapeutic effects of CO for proper endothelization at the diseased site. The first objective of this project is to use MBs to deliver CO, improving endothelization at the BBB. Additionally, the secondary objective involves the administration of a novel peptide via TEVGs to enhance endothelization and mitigate intimal hyperplasia and early-stage thrombosis.

1.9 Drug delivery with cardiovascular grafts

1.9.1 Coronary artery diseases

Coronary artery diseases (CAD) are the leading cause of death worldwide, with more than 17 million deaths each year [72]. Most CADs mortalities occur due to heart stroke, and <20% of deaths occur because of aging. As a result of the development of technologies and science, the CAD mortality rate has declined; however, the risks and prevalence of these diseases are rapidly increasing globally. Atherosclerosis and intimal hyperplasia represent prevalent cardiovascular conditions wherein damage to ECs can lead to thrombus formation and excessive proliferation of vascular smooth muscle cells [72].

1.9.2 Atherosclerosis

Atherosclerosis is the leading cause of morbidity globally and is the most common coronary artery disease [73]. Atherosclerosis causes the blood vessels to narrow due to inflammation and plaque formation in the artery's inner layer [74]. This plaque consists of lipids, calcium, and macrophages and has different thicknesses throughout the plaque in the early stages of the disease [73]. Various risk factors such as obesity, diabetes, and low daily activity increase the atherosclerosis risk [75]. This disease is a cause of myocardial infarction and heart attack [76]

1.9.3 Intimal hyperplasia

Intimal hyperplasia in native vessels can be characterized as vascular smooth muscle cells (VSMC) migration and proliferation and deposition of ECM

components in the intimal layer of the vessels**,** which cause the thickening of the lumen [77]. Intimal hyperplasia can occur due to low/high blood shear stress, trauma, graft replacement, and vascular ECs injury [78]. Graft implantation damages the endothelium and exposes the medial layer, which increases the intimal hyperplasia risk in grafts [79]. Moreover, growth factors, macrophages, and various cell types cause the migration and proliferation of VSMC [80]. The vascular smooth muscle cells then release ECM components such as collagen, which thickens and narrows the lumen [77]. Intimal hyperplasia in native tissues is divided into eccentric intimal hyperplasia in the branched area and concentric hyperplasia in arteritis cells [81].

1.9.4 Treatments

Coronary artery diseases treatments vary from lifestyle improvements to pharmaceutical and surgical interventions [82]. Vascular surgeries involve endovascular procedures, including percutaneous coronary intervention, angioplasty, and stent insertion. Percutaneous coronary intervention procedures expand a high-pressure balloon to compress the plaque and increase the artery diameter [82]. In severe CADs, the occluded artery is replaced with a vascular graft. This procedure has been shown to have the optimal result for CADs patients [83].

While autologous and allografts have been widely used for vascular grafting due to their similar physiological properties to the tissue, they come with their own set of challenges. Donor morbidity, lack of availability, and invasive extraction are some of the limitations of these grafts [83]. Due to these limitations, synthetic grafts emerge as the third option for bypass surgery. However, they must meet specific

characteristics before implantation, including biocompatibility, non-thrombogenicity, biodegradability, proper mechanical strength, availability, and blood compatibility [84]. Synthetic grafts have shown proper compatibility in larger vessels, but the required properties are more challenging in vessels with lower blood flow rate (diameter <6mm) and need further research [85]. Non degradable synthetic grafts have shown thrombotic occlusions in the long term, which limits their applications for small diameter vessels [86]. TEVGs have received significant interest due to the limitations of current grafts. These grafts can be pre-seeded with cells or used as acellular grafts to recruit the cells at host tissue. TEVGs have enabled researchers to control graft's mechanical properties, biocompatibility, and biodegradability [87].

1.9.5 Scaffold fabrication process

Tissue-engineered scaffolds must have suitable cell attachment and migration properties and mimic aspects of the ECM structure [88]. Fabricating the vessel's conduits with biological and structural properties close to native tissue has always been challenging in tissue engineering [89]. The scaffold properties depend on both the inherent material composition and the processing procedure. Several processing techniques have been employed to produce desired scaffolds, including electrospinning, salt leaching, diffusion, and gas-forming methods.

1.9.6 Electrospinning

In 1990, the nanotechnology community received attention for the electrospinning technique due to the need to produce ultrafine polymeric fibers with

various diameter ranges [90]. Electrospinning is a cost-effective and simple method that has received significant attention in tissue engineering for fabricating scaffolds. Natural and synthetic polymers can be processed by electrospinning. This technique also offers an extremely high surface-to-volume ratio, low cost, easy to work, tunable porosity, and the ability to control the nanofiber composition to achieve the desired results from its properties and functionality [91].

The electrospinning device includes a high voltage supply, metal collecting tube, and a syringe pump. In this technique, polymeric fibers are produced by applying an electrostatic force and creating a Taylor cone by coupling the surface charge with the external electric field [92]. After overcoming the surface tension via applying a high voltage, the fluid is ejected from the cone on the collection device while the solvent in the polymer evaporates [91].

Solution concentration, applied voltage, needle gauge, solvent volatility, solution conductivity, and flow rate could affect the electrospinning procedure and the consistency of the achieved fibers [93]. Nozzle collector distance can also affect the morphology and structure of the electrospun fibers [91].

1.9.7 Drug delivery via tissue engineered vascular grafts

TEVGs have often aimed to mimic the physiological and biological structure of the native tissue from microstructure to macrostructure, including the protein, cells, and material present in the vessels [94]. TEVG improvements often involve investigating several approaches to transfer pharmaceutical substances such as small-

molecule drugs, growth factors, and other bioactive molecules to the targeted organ [95]. Currently, many researchers have focused on enhancing TEGFs endothelization via drug encapsulation and subsequent release of the drugs from the grafts [94].

In several studies, scientists have endeavored to improve drug delivery carriers by altering the surfaces of TEVGs to facilitate the transfer of active compounds. Researcher have shown that combining electrospun PCL constructs with decellularized rat aorta matrix, along with heparin and VEGF loading, has demonstrated minimal platelet adhesion in vitro. Furthermore, upon implantation into rat aortas, these grafts facilitate greater infiltration of ECs compared to pure PCL at 2- and 4-weeks post-implantation in rodents [96]. Moreover, hydrogel complex scaffolds fabricated via coating precursor solutions onto heparin-modified PCL (PCLH) scaffolds have reduced aneurysm incidence compared to hydrogel-free scaffolds post-implantation in rat abdominal aorta. Additionally, including heparin within the hydrogel enhanced vascular regeneration, suppressed calcification, and promoted the early emergence of contractile SMCs [97]. However, there is several limitations with delivery of heparin including the limited availability time [98].

Some research aims to extend the drug release profile by modifying the fabrication of the carrier. For this purpose, polymeric micro- and nanoparticles have received significant interest as they offer several benefits such as (i) protection of the encapsulated active agent from degradation, (ii) enabling precise regulation of the release rate of the incorporated drug, and (iii) providing convenient administration when injected. For example, Ma et al showed that delivering micro RNAs to

downregulate the inflamed ECs by using E-selectin-targeting multistage vector (ESTA-MSV) loaded microparticles could inhibit atherosclerosis. In vivo tests on mice fed a Western diet and treated biweekly with the miR-loaded particles showed that ESTA-MSV-mediated delivery reduced atherosclerotic plaque and can mitigate endothelial inflammation and atherosclerosis [99]. In another study, VEGF-loaded PLGA microparticles were locally administrated in a rat model of ischemia-reperfusion, resulting in extended release of the protein, increased angiogenesis and arteriogenesis, as well as positive remodeling of the heart [100]. However, this study aims to incorporate the microparticles within the scaffold for more controlled and local release of the active compound prior to arterial grafting.

The success of TEVGs relies not only on their ability to deliver therapeutic agents effectively but also on their interaction with the immune system upon implantation. Understanding the immune response to these biomaterials is crucial for ensuring their functionality and longevity within the body.

1.9.8 Immune response

Understanding the immune response to biomaterials and implants is crucial, as the effects of these devices are primarily linked to their interaction with the body and immune system. While all foreign body materials will inevitably encounter an immune response from the body, the adaptive immune response is a significant concern.

Immune response to the biomaterial happens due to tissue trauma during surgery, and the biomaterial's presence in the body is called a foreign body reaction (FBR). The body's inflammatory response to the biomaterial/implant can affect the biomaterial's structure, durability, drug release, and stability [101]. The degree of the FBR depends on the implant/biomaterial properties, including degradation rate, biocompatibility, size, porosity, and morphology [101].

After implantation, the blood from the damaged surrounding tissues covers and interacts with the implant/biomaterial [102]. This interaction normally determines both acute and chronic inflammation. Acute inflammation participates in wound cleaning and protein diffusion and lasts for hours to days [102]. Acute inflammation is based on neutrophils, the release of growth factors, and leukocyte to clean the injury site. If the stimuli of acute inflammation last for longer, chronic inflammation happens, and it is known with the presence of the mononuclear cells, including monocytes and macrophages. After the inflammation stage, granulation tissue forms which include macrophages, connective tissue, and blood vessels [103]. Presence of blood vessels for transferring nutrition and oxygen to the cells is necessary to restructure the damaged tissue [102]. The presence of the macrophages might lead to degradation of the biomaterial and its failure; however, recent studies have shown that macrophages have two types: M1, which is characterized for inflammation, and M2, which is involved in tissue regeneration and does not participate in the implant degradation procedure [103]. Also, these two phenotypes are different from each other. M1 macrophages are present in the initial steps of inflammation and can help

with biomaterial degradation. M2 macrophages release growth factors that can help with angiogenesis and healing. M2 macrophages produce needed enzymes for tissue generation the injury site including collagenases, elastases, and hyaluronidases [103].

1.9.9 Peptide delivery for cardiovascular diseases

Unlike the response in larger-diameter tissue-engineered vascular grafts, the patency of the small-diameter vascular graft is limited due to their high thrombogenicity in clinical applications [104]. Promoting rapid endothelialization is a promising approach to construct an anti-thrombogenic inner surface of the vascular graft [105]. The main challenges for rapid endothelialization are the adhesion, migration, and proliferation of the ECs on the small-diameter vascular graft [105]. Due to this, research has been developed to include the delivery of novel active compounds to promote endothelization on biomaterial surfaces.

Peptide delivery has shown advantages such as ECs adhesion in animal models. Peptides are smaller than proteins. They have shorter chain and better self-stabilization properties than proteins [106]. RGD, REDV, CAGs and various other peptides are currently used to treat scaffold surfaces. For example, Lei et al, have investigated the ECs attachment on polyethylene terephthalate (PET) surfaces treated with different peptides. That study showed that RGD peptides induced ECs adhesion more than the other type of groups [107].

Moreover, Nomura et al showed the recombinant Atrial Natriuretic Peptide, which has properties such as a diuretic, natriuretic, and vasodilative, has therapeutic

effect for treating acute heart failure [108]. Other research has been performed on cell-penetrating peptides which have high cellular uptake efficacy. These cell-penetrating peptides are pH sensitive, and their net charge increases in acidic environment and activate their cell penetration capacity [109]. Kumar and his colleagues demonstrated that α-Calcitonin gene-related peptide (α-CGRP), a regulatory neuropeptide widespread in the nervous system, can decrease the blood pressure in hypertensive and normotensive humans and rodent models and it can be used as a therapeutic agent for cardiovascular diseases [110], [111]

Much research has been done to reduce the immune response from the body and increase the peptides therapeutic half-lives [111]. Wang showed that the treatment of the hydrophobic polyester Poly (3-hydroxybutyrate-co-3-hydroxyvalerate) (PHBV) with ammonia plasma for increasing the hydrophilicity and using the poly (ethylene glycol) (PEG) as a crosslinker would allow RGD containing peptides to bind to the PHBV films covalently [112]. RGD containing peptides bind to the integrin on the cell surface and start signal transduction to induce cell proliferation, migration, and differentiation [112]. In another study, PCL grafts were coated with an RGD containing molecule. When implanted in rabbit carotid arteries for 2 and 4 weeks, all RGD-modified PCL grafts remained patent, while some non-modified PCL grafts became occluded due to thrombus formation. Additionally, result showed reduced platelet adhesion on the PCL-RGD surface, indicating improved hemocompatibility, enhanced cell infiltration and endothelial coverage [113].

Even considering several advantages of current peptides, specific challenges impede their clinical transition. While the treated surfaces can induce endothelization in TEVGs, they are not resistant to fouling from blood circulation. Biofouling increases the accumulation of other active compounds in the blood circulation, resulting in graft failure [114]. Consequently, researchers strive to integrate novel active compounds to enhance endothelization and mitigate these challenges.

1.9.10 UPI-Epsin mimetic peptide

Vasculogenesis primarily constructs the vascular framework of the heart and vascular plexus, while angiogenesis contributes to network expansion and tissue healing [115]. While vasculogenesis and angiogenesis are pivotal for establishing and expanding the vascular system, navigating the complex signaling pathways poses a formidable challenge. During angiogenesis, VEGF binding to its receptor VEGFR2 initiates a signaling cascade involving tyrosine phosphorylation. This cascade facilitates vessel proliferation, migration, and the transformation of ECs into mature blood vessels. However, disruption of ECs and the signaling pathways, has led to several pathological challenges. The UPI-Epsin mimetic peptide offers a precise approach to regulate VEGFR2 signaling, thereby impacting endothelial cell activity and the development of vascular networks.

Epsins are from the endocytic clathrin adaptors family. Epsins contain ubiquitin-interacting motifs (UIM), which are found at the epsin N-terminal homology (ENTH) domain of the epsin proteins and can advance the interaction with VEGFR2 and promote endocytosis by recognizing ubiquitinated plasma membrane proteins and

recruiting them to clathrin-coated pits [116]. Epsins bind to VEGFR2 and VEGFR3 and inhibit angiogenesis and diminish the proliferation of ECs crucial for vascularization [117]. Additionally, there has been recent evidence linking epsins to the promotion of atherosclerosis [118]. Epsin proteins are crucial for clatherin embryogenesis [119], angiogenesis vasculature [120], lymphangiogenesis [121], and cancer progression. Mammalians have three different types of epsins: epsin 1 and 2 are formed in abundance in the body, and epsin three is in the stomach and epidermis [122].

The UPI-epsin mimetic peptide that we use is a chemically synthesized peptide composed of internalizing RGD (iRGD), UIM, and a plasma membrane anchoring peptide and can modulate the VEGFR2 signaling [117]. The iRGD has a cyclic sequence structure, and the iRGD in the peptide structure can target the αvβ3 and αvβ5 integrin, which increase the endocytosis of the peptide via cells [123]. The plasma membrane anchoring peptide enhances the drug delivery efficacy by maintaining the peptide in the plasma membrane other than releasing it in the cytoplasm [116]. This peptide is formed from 36 amino acids and has a mass of 3967 Da, an isoelectric point of 6.34, and zero net charge.

Due to the UPI peptide's competitive nature, it binds to VEGFR2 and leaves an excessive amount of epsin in the cytoplasm. This process inhibits the epsin-VEGFR2 binding, leading to creating excess dysfunctional vessels in tumors and a decrease in tumor cells [116]. However, the mechanism is different in TEVGs due to the limited ECs present. Chen and her team have demonstrated that the UPI peptide specifically

targets VEGFR2 without affecting other angiogenic growth factors, such as epidermal growth factor, in cultured human umbilical vein ECs. Additionally, the core structure of the UPI peptide consists of 18 amino acids, with an additional short 10-amino acid segment preceding its core. This unique composition may contribute to its specificity towards VEGFR2. Furthermore, analysis of the three-dimensional structure of the UPI peptide reveals a closer alignment with the structure of VEGFR2 compared to other angiogenic growth factors [117]. One of the goals of this project is to utilize UPI peptide to improve VEGFR2 signaling via blockage of epsin-VEGFR2 signaling. We hypothesized that direct contact of UPI peptides with blood and its controlled release of our TEVG can improve EC proliferation and migration.

1.10 Experimental plan

The primary objective of this study was to evaluate endothelization using innovative carriers from the fields of tissue engineering and regenerative medicine. The central aim was to deliver active compounds that could enhance ECs function, migration, and attachment. To achieve this, the study introduced two novel methods: the use of PFC-based MBs to deliver CO to ECs at the BBB and the application of modified PCL-based constructs for the delivery of UPI peptide to the abdominal artery of rats. This study is divided into three main sections: the first section focuses on delivering CO to ECs at the BBB using PFC-based MBs and evaluating the effects *in vitro*. The second section examines the controlled release of UPI peptide via fibrin-coated PCL constructs, both *in vitro* and *in vivo*. The third section

incorporates the UPI peptide within PLGA-based microparticles and gelatin-coated constructs to assess the effects of extended release, both *in vitro* and *in vivo.*

In the first section, we aimed to enhance endothelialization at the BBB instead of transferring active compounds through the BBB. To achieve this, PFC-based MBs were fabricated using two PFCs with different boiling temperatures and loaded with CO. The biocompatibility of various CO dosages was assessed for both types of MBs. Additionally, the optimal ultrasound parameters were determined using 3-D phantoms, and the release of CO from MBs upon ultrasound application was evaluated using HUVECs. Lastly, the effects of a specified dosage of CO-loaded MBs with and without ultrasound on HUVECs were assessed using a gelatin-based phantom.

In the second section, we integrated UPI peptide within electrospun PCL constructs to evaluate early endothelialization in vitro and in vivo. Traditionally, most TEVGs have demonstrated endothelialization primarily at anastomotic sites rather than along the mid-graft region three to four weeks post-surgery. However, for successful clinical translation, it is imperative to enhance rapid endothelialization. We employed physical adsorption and fibrin coating techniques to determine the optimal release of UPI from the constructs. Furthermore, we investigated the effect of UPI peptide on ECs attachment on PCL meshes in vitro. Lastly, we evaluated two different dosages of UPI peptide and control conditions in arterial grafting experiments in rodents.

In the last section, we explored the effects of an extended-release of UPI peptide on endothelialization *in vitro*. Previously, we demonstrated a burst release of UPI peptide from a fibrin coating, which provided a sufficient release for endothelialization within the first week of arterial grafting. However, in this study, our goal was to enhance the prolonged release of UPI peptide. To achieve this, we incorporated the UPI peptide within PLGA-based microparticles. These particles were then embedded within UPI-loaded gelatin-coated PCL constructs. Additionally, we assessed the specificity of UPI peptide compared to a scrambled control peptide in vitro.

Reprinted from Changizi, Shirin, et al. *Journal of Biomedical Materials Research Part A* 112.4 (2024): 600-612.

Chapter 2: Carbon monoxide release from ultrasound sensitive microbubbles improve cell growth

Shirin Changizi[1], Isabel G. Marquette[1], Jennifer VanSant[1], Osamah Alghazwat[2], Adnan Elgattar[2], Yi Liao[2], Chris A. Bashur[1]

[1]Department of Biomedical Engineering, Florida Institute of Technology, Melbourne, FL 32901, USA

[2]Department of Chemical Engineering, Florida Institute of Technology, Melbourne, FL 32901, USA

Abstract

Carbon monoxide is a gasotransmitter that may be beneficial for vascular tissue engineering and regenerative medicine strategies because it can promote endothelial cell (EC) proliferation and migration by binding to heme-containing compounds within cells. For example, CO may be beneficial for vascular cognitive impairment and dementia because many patients' disrupted blood brain barriers do not heal naturally. However, control of the CO dose is critical, and new controlled delivery methods need to be developed. This study developed ultrasound-sensitive microbubbles with a carefully controlled precipitation technique, loaded them with CO, and assessed their ability to promote EC proliferation and function. Microbubbles fabricated with perfluoropentane exhibited good stability at room temperature, but they could still be ruptured and release CO in culture with

application of ultrasound. Microbubbles synthesized from the higher boiling point compound, perfluorohexane, were too stable at physiological temperature. The lower boiling point perfluoropentane microbubbles had good biocompatibility and appeared to improve VE-cadherin expression when CO was loaded in the bubbles. Finally, tissue phantoms were used to show that an imaging ultrasound probe can efficiently rupture the microbubbles and that the CO-loaded microbubbles can improve EC spreading and proliferation compared to control conditions without microbubbles as well as microbubbles without application of ultrasound. Overall, this study demonstrated the potential for use of these ultrasound-sensitive microbubbles for improving blood vessel endothelialization.

2.1 Introduction

Techniques to promote the regeneration of a functional endothelium are important for tissue engineered grafts and regenerative medicine approaches to treat vascular disease. Quiescent endothelial cells (ECs) maintain blood flow, prevent thrombosis, inhibit leukocyte adhesion, and modulate the phenotype of the surrounding smooth muscle cells (SMCs) [124]. However, activated ECs are typically found in diseased environments within the body [125]. A further complication is that many grafts (e.g., small diameter vascular grafts) and treatments for diseases (e.g., vascular cognitive impairment – VCID) require EC growth for restoration of a disrupted EC monolayer. For example, VCID is the deterioration of cognitive function as a result of the disruption of the blood brain barrier (BBB) through loss of brain capillary endothelial cells and tight junctions [126], [127]. This

allows diffusion of blood components through the BBB that have been linked to p-tau accumulation and inflammation[128]. Unfortunately, many patients with hypertension, diabetes, or hyperlipidemia have ECs that are not able to regenerate well enough by themselves to close the BBB and prevent further neurological damage [129].

Carbon monoxide delivery is one strategy that can potentially promote closure of a disrupted BBB. CO is produced naturally in the body as heme oxygenase 1 (HO-1) degrades heme [130], [131], and it is a gasotransmitter because it is involved in cell signaling when it binds to heme containing compounds within cells (e.g., guanidine cyclase and nitric oxide synthase)[132]. This signaling has been shown to result in many positive anti-inflammatory and anti-apoptotic responses [133],including protecting ECs from apoptosis [134], [135]. CO has also been shown to promote EC proliferation and migration at appropriate CO doses[68]. However, careful control of dose is very important because high doses can potentially lead to toxic effects, in part due to binding to hemoglobin, while lower doses may be ineffective[136].Thus, the development of new controlled release strategies for CO is important. Previous strategies to control delivery include CO releasing molecules (CORMs)[137], [138], synthetic nanoparticles[139], and micelles [140]. It is important that any release strategies be tailored to a specific application. We are investigating perfluorocarbon (PFC)-based, ultrasound-sensitive microbubbles for treatment of VCID.

PFC microbubbles are commonly used for imaging because of their low toxicity, and they have also been used for drug delivery purposes. For example, ultrasound-sensitive microbubbles have been used for sustained doxorubicin release to prevent tumor growth in a rodent model [141]. PFC microbubbles are also used for VCID. However, the current strategies involve high-intensity focused ultrasound to temporary open the BBB[142], which is the opposite of our strategy. Our goal is to develop a strategy to close the BBB. With our overall strategy, the bubbles would be ruptured with a regular imaging ultrasound machine at the internal carotid artery, which is close enough to the BBB barrier to deliver the CO but far enough away to avoid cavitation and BBB disruption. Our recent computationally study based upon blood hemodynamics and kinetics of CO binding supported the hypothesis that enough CO should be able to reach the brain capillary endothelial cells [143]. However, more research is needed to determine if these PFC microbubbles can deliver an appropriate dose of CO to improve EC function and the impacts of different levels of CO.

This study developed CO-loaded PFC microbubbles with a carefully controlled precipitation technique and assessed their ability to promote EC proliferation and function. Unlike typical emulsion-based techniques, this method can allow improved microbubble stability and CO loading. Ultrasound sensitive microbubbles were synthesized with both higher (i.e., perfluorohexane) and lower (i.e., perfluoropentane) boiling point PFCs, and their size and stability were quantified over time. The microbubbles were saturated with CO and their

biocompatibility was investigated with human umbilical vein endothelial cells (HUVECs) in culture. The impact of different ultrasound parameters (e.g., intensity and frequency) on microbubble rupture and the corresponding EC response was investigated in well plates and in tissue phantoms. Finally, the ability for the microbubbles to be endocytosed by HUVECs was investigated with time-lapse imaging using confocal microscopy.

2.2 Material and methods

2.2.1 Materials

All disposables, chemicals, and biological supplies were purchased from Thermo Fisher Scientific (Pittsburgh, PA) unless specified otherwise. Perfluorohexane and perfluoropentane were purchased from SynQuest (Alachua, FL). 1,2-Distearoyl-*sn*-glycero-3-phosphoethanolamine-polyethylene glycol (DSPE-PEG) was purchased from Sunbright (Tokoyo, Japan). Dipalmitoyl phosphatidylcholine (DPPC) was from Echelon Biosciences (Salt Lake City, UT). All primary antibodies were purchased from Abcam (Cambridge, MA), and the secondary antibody was from Thermo Fisher.

2.2.2 Microbubble synthesis

Microbubbles were synthesized with a PFC core and lipid shell with a method adapted from Li et al [144]. This is a controlled precipitation process based upon the ouzo effect that can provide more stability than the emulsion-based processes typically used to create PFC microbubbles. The steps to make the microbubbles are

illustrated in Supplemental Figure 1. Perfluorohexane and perfluoropentane at 0.10 and 0.15 mL, respectively, were slowly added into a 4.5 mL lipid and ethanol solution. This solution contained 84.5 mg DPPC, 15.5 mg DSPE-PEG, and 100 mL of ethanol. The mixture was stirred at 150 rpm for 30 min, and then the solution was diluted further in 13.5 mL of the lipid and ethanol solution. An aqueous solution containing DI water, propylene glycol, and glycerol (volume ratio of 7:2:1) was mixed with the PFC solution. The nucleation occurred instantaneously upon mixing the solutions. After bubble nucleation and growth, the microbubble solution was centrifuged three times at 2,700 rpm to remove the ethanol. The temperature was kept below the boiling point of the perfluoropentane (i.e., 29ºC) during the synthesis by keeping the solution in an ice bath. Microbubble solutions were stored in the refrigerator until use or CO loading.

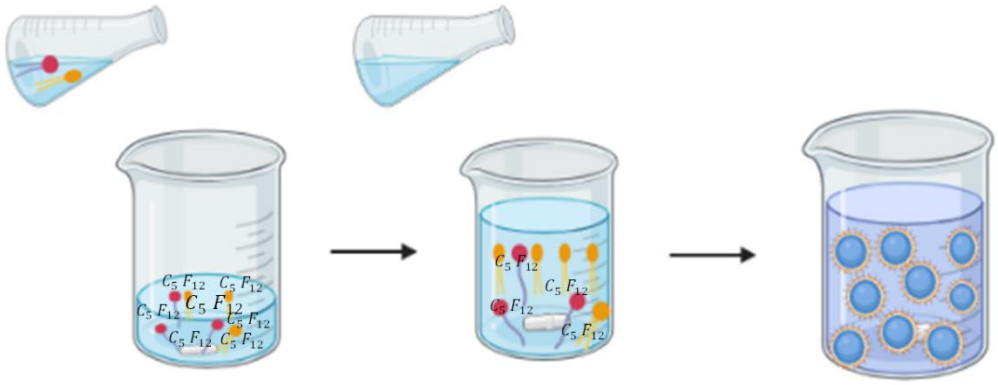

Supplemental Figure 2.1. Illustration of the steps in the microbubble preparation through a precipitation technique.

Reprinted from Changizi, Shirin, et al. *Journal of Biomedical Materials Research Part A* 112.4 (2024): 600-612.

2.2.3 CO loading

CO-loaded microbubbles were prepared by slowly passing CO gas through the microbubble solution using a balloon. This allowed the CO to dissolve within the PFC at the saturation limit. CO-loaded microbubble solutions were stored in the refrigerator until use. Prior to use, the CO-saturated solution was centrifuged and washed two times to remove excess CO from the water surrounding the bubbles.

CO loading was confirmed with a fluorescent probe (FL-CO) that was synthesized following a method reported in the literature [145]. Briefly, fluorescein was dissolved in 20 mL dry tetrahydrofuran under nitrogen, and then triethylamine was added with constant stirring for 10 min. Afterward, the mixture was cooled in an ice bath, allyl chloroformate was added dropwise. The reaction mixture was stirred overnight at room temperature and then the precipitate formed was filtered and dried *in vacuo*. The crude product was purified using column chromatography, and the composition was verified with ^{1}H NMR.

For CO assessment, the FL-CO probe was mixed 1:1 with palladium acetate and added to the CO-loaded microbubble solution for a final solution concentration of 10 μM. The fluorescence was assessed at 490 / 525 nm (excitation / emission) after either application of ultrasound or a corresponding time of incubation. A calibration curve was prepared with a serial dilution of DI water saturated with CO and mixed with the probe as described for the microbubble conditions.

Reprinted from Changizi, Shirin, et al. *Journal of Biomedical Materials Research Part A* 112.4 (2024): 600-612.

2.2.4 Microbubble Characterization

2.2.4.1 Size

The size of the microbubbles synthesized from both perfluoropentane and perfluorohexane were assessed by brightfield microscopy using a Zeiss Axio Observer A.1 fluorescent microscope (Carl Zeiss Microscopy, Thornwood, NY). The average microbubble diameter was quantified on high magnification 100x images using ImagePro software (Media Cybernetics, Rockville, MD - n=3 samples / condition). The diameter was measured over 5 days, with the samples kept in an incubator between time points to maintain the physiological 37 °C temperature. The initial microbubble diameter was also analyzed using dynamic light scatter (DLS) on a Horiba nanoPartica system (Irvine, CA). For DLS, a standard cuvette was used for measurement of the particle size distribution as reported by the mean peak diameter. The values are reported as the average of at least 5 individual measurements.

2.2.4.2 Stability

To assess stability, the microbubbles were diluted in DI water, and absorbance was measured at 570 nm (n=3 samples / condition). The microbubble diameter and stability were measured over 5 days, with the samples kept in the incubator at 37 °C between the time points. Separately, the stability of microbubbles stored in the refrigerator at 2 °C was also characterized.

Reprinted from Changizi, Shirin, et al. *Journal of Biomedical Materials Research Part A* 112.4 (2024): 600-612.

2.2.5 Ultrasound characterization

2.2.5.1 Application in 2D with therapeutic ultrasound

Initial optimization of ultrasound parameters was performed with a Physio Sound UT therapeutic ultrasound machine with intensity ranging from 1-3 W/cm^2 and frequencies ranging from 1-3 MHz. The intensity, frequency, and time of application were varied, with the focus on assessing the impact of frequency on microbubble rupture. A 1:40 dilution of the microbubbles mixed with DI water in a well plate was used to test the different ultrasound parameters. To minimize temperature increases in the well, a water gap was placed between the well plate containing the microbubbles and the ultrasound transducer. Phase contrast images were taken before and after application of ultrasound to determine changes in the number of bubbles. The sample size was n = 6 samples / condition.

2.2.5.2 Application in 3D with imaging ultrasound

The effects of ultrasound on microbubbles were also assessed in a 3D phantom using a low intensity Vevo 3100 (VisualSonics, Bothell, WA) imaging ultrasound machine with a 21 MHz transducer. To fabricate the 3D phantom, a polypropylene tube was embedded ~ 8 mm deep within a 4% agarose hydrogel. The ends were still accessible for perfusion. The microbubble suspension was introduced through a parafilm seal, and ultrasound was administered to the static system with microbubbles within the tube. Initial imaging was performed in contrast mode with 10% of the maximum intensity prior to performing burst sequences. Different

ultrasound routines were applied to assess the impact of rupturing the bubbles. Short pulses were provided by 1 s burst sequences at 100% intensity (i.e., approximately 1 W/cm^2) that were repeated up to 4 times. This intensity is within the range (i.e., 0.5-3 W/cm^2) that has previously been shown to avoid destructive heating [146]. Continuous ultrasound was also applied for a longer time frame of 5 min at 100% intensity. Finally, the low frequency therapeutic ultrasound was also tested (i.e., 3 W/cm^2 and 3 MHz) with the 3D phantom as a control for comparison. For the therapeutic ultrasound control, ultrasound was applied at 1-, 2-, and 5-min durations. The sample size was n=3 samples / condition.

2.2.6 2 D Cell culture

2.2.6.1 Microbubble biocompatibility

Human umbilical vein endothelial cells (HUVECs) were cultured on tissue culture polystyrene (TCPS) to determine the effects of microbubbles on cells biocompatibility. The cells were cultured in endothelial growth media with the media supplement (Promocell, Heidelberg, Germany) and 1% antibiotic, and they were passaged at 10,000 cells/cm^2. After reaching confluence, the cells were seeded into 24 well plates at 10,000 cells/cm^2. After 1 day, microbubbles suspensions were added to the cells at 1:1000, 1:40, and 1:20 dilutions in growth media. This corresponds to 3.4, 87, and 170 µg/mL total PFC in the media. Microbubbles synthesized from perfluoropentane were tested for conditions with and without CO loading. No ultrasound was applied. Cells without any microbubbles were considered as the

control condition. Culture media was changed every two days up to 7 days. Cell number, viability, morphology, and function were characterized at days 3 and 7.

2.2.6.2 Cellular impacts of ultrasound in 2D

Ultrasound was applied to HUVECs cultured in well plates to determine the impact of CO-loaded microbubbles on their phenotype. HUVECs were cultured and seeded as described in Section 2.5.1. Only the 1:1000 dilution of the low boiling point microbubbles was added to the wells. Instead, the tested conditions were with and without ultrasound and with and without CO-loading. A 3-kHz transducer was used with an intensity of 3 W/cm^2 and an exposure time of 15 min. The ultrasound was applied 1 day after the microbubbles were added to the well. To minimize temperature changes from the ultrasound probe, the water gap was added between the cells and the ultrasound transducer. EC response was analyzed with fluorescence staining 1 day after ultrasound was provided (i.e., 3 days after seeding the cells).

2.2.7 Fluorescence imaging

HUVECs were fixed in 4% paraformaldehyde, permeabilized with 0.1% Triton X, and then blocked with 5% goat serum. Alexa 488-phalloidin was used to stain the F-actin and the cytoskeleton. EC phenotype was investigated by staining the cells with VE-cadherin. Samples were incubated with the primary antibody at a 1:100 dilution in a cold room overnight. The secondary antibody anti-rabbit Alexa 633 was added at a 1:1000 dilution. The samples were then mounted with DAPI-

containing mounting media and imaged. The contrast and brightness of the images were adjusted equally for all samples. The number of cell nuclei stained with DAPI and the intensity of VE-cadherin expression were quantified in each image with ImagePro software. For VE-cadherin quantification, background subtraction was performed and then the average intensity was quantified for each image. Analysis was performed on three images / sample and n=6 samples / condition. Cell viability was determined via live/dead staining according to the manufacturer's protocol (Thermo Fisher, Pittsburgh, PA). After imaging, the live and dead cells were counted with ImagePro software and reported as either percent live or percent dead cells.

2.2.8 Analysis of endocytosis

Both HUVECs and green fluorescent protein $(GFP)^+$-HUVECs (Angio-proteomie, Boston, MA) were seeded in well plates to investigate cell endocytosis of low boiling point microbubbles. Cell culture was performed as described in Section 2.5, except the HUVECs were incubated with 15 µg/mL of DiO stain for 20 min prior to seeding. GFP^+ HUVECs did not have an additional fluorophore added. Low boiling point microbubbles without CO-loading (1:1000 dilution) were incubated with 10 µg/mL DiI stain for 10 min. The microbubble suspension was added to the cells, and after 20 min, imaging was performed with a Nikon 4 Laser Line Solid State Confocal microscope (Melville, NY). An environmental chamber was used to mimic physiological conditions – e.g., 37℃ and 5% CO_2. DiO stained HUVECs were

imaged with time-lapse, and z-stacks were acquired for up to 2 h. GFP^+ HUVECs were only imaged at one z-plane to enable faster sampling.

2.2.9 Ultrasound activation with ECs on a tissue phantom

GFP^+ HUVECs were seeded on gelatin hydrogels within a mold to enable application of ultrasound without disrupting the cells. Gelatin was cast at 0.05 g/mL and then crosslinked with 1-ethyl-3-(3-dimethylaminopropyl) carbodiimide (EDC) and N-hydroxysulfosuccinimide (NHS) chemistry. Briefly, the samples were immersed in 0.5 M 2-(N-morpholino) ethanesulfonic acid (MES) buffer for 30 min, and then 10 mM EDC and 5mM NHS were added to the samples for 4 h. Samples were washed two times with anhydrous dibasic sodium phosphate (Na_2HPO_4) for one h each and then washed three times with PBS for 15 min. The cross-linked hydrogel surface was coated with 5µg/mL fibronectin before cell seeding. These steps to prepare the gelatin hydrogel were performed in sterile conditions. The cells were seeded at 12,500 cells/cm^2, and the microbubbles (1:50 dilution in media) were added 1 day after seeding. Ultrasound was applied 30 min after the bubbles were added, and then the media with any unruptured bubbles was removed after 20 min. Control conditions were cells only without microbubbles or ultrasound and CO-loaded microbubbles without ultrasound. The cell number and morphology were investigated at 4 and 24 h using fluorescent microscopy. VE-cadherin staining was performed 1 day after application of ultrasound (i.e., 2 days after seeding the cells).

Reprinted from Changizi, Shirin, et al. *Journal of Biomedical Materials Research Part A* 112.4 (2024): 600-612.

2.2.10 Statistics

Results are presented as the mean ± standard deviation. Statistical analysis was performed using JMP software, and statistical significance was determined using either two-way or three-way ANOVA with Tukey posthoc comparisons ($p \leq 0.05$).

2.3 Results

2.3.1 Microbubble stability and CO loading

The microbubbles synthesized from high and low boiling point PFCs were prepared by precipitation when the aqueous solvent was added. High magnification images showed that there was a distribution of microbubble diameters that appeared to be similar for both high and low boiling point PFCs (**Figure. 2.1A-B**). Quantification of the diameters from these images indicated that the initial average diameters were 1.16 ± 0.34 and 1.30 ± 0.40 μm for microbubbles from high and low boiling point PFCs, respectively. The average peak diameter from DLS results were slightly higher at 1.5 ± 0.42 and 1.7 ± 0.35 μm for microbubbles made with perfluorohexane and perfluoropentane, respectively. The average diameter of the microbubbles was comparable throughout the 3 days tested in this study (**Figure. 2.1C**). Most of the microbubbles were between 0.8 to 1.5 μm in diameter at the day 0 timepoint (**Figure. 2.1D-E**).

Reprinted from Changizi, Shirin, et al. *Journal of Biomedical Materials Research Part A* 112.4 (2024): 600-612.

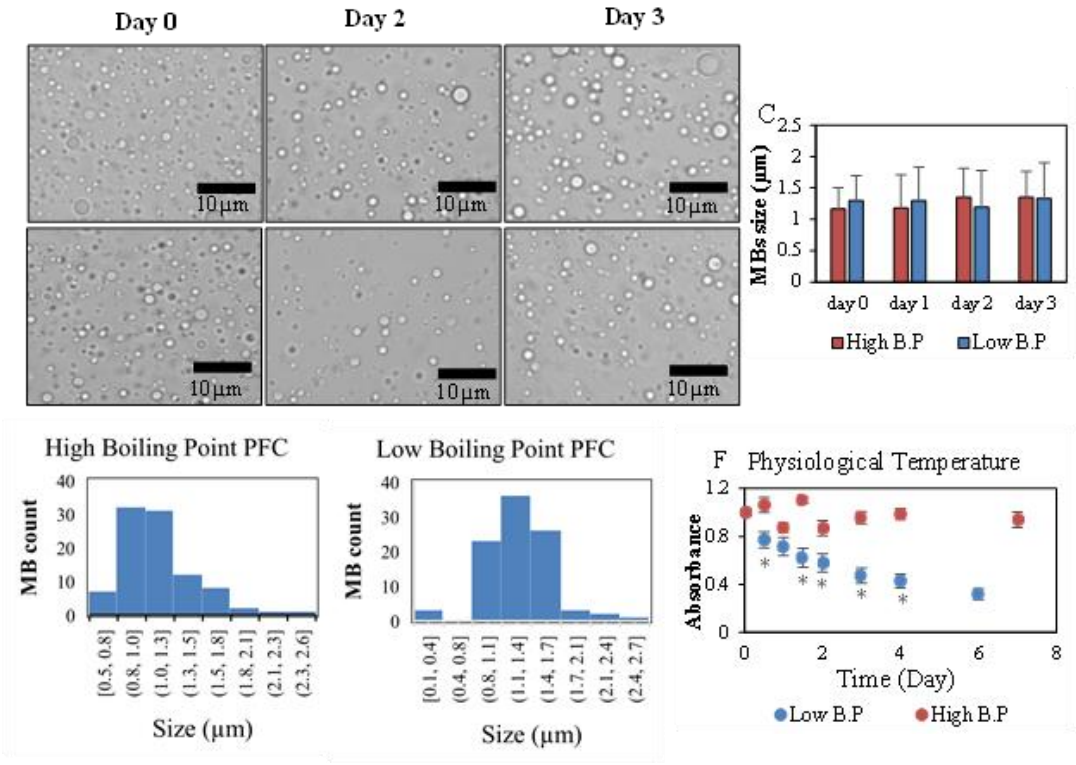

Figure 2.1. Microbubble characterization. Representative phase contrast images of high (A) and low (B) boiling point (B.P.) microbubbles (MBs) over time. Quantified results for microbubble diameter are shown (C). Histograms for microbubble diameter are shown at day 0 for high (D) and low (E) boiling point microbubbles. Absorbance readings show stability of the microbubbles at 37 °C over time (F). (*) statistical differences from corresponding high B.P. condition. *n*=3 samples / condition.

Absorbance readings were used to indicate the concentration of intact microbubbles (**Figure. 2.1F**). The results showed that the high boiling point microbubbles were more stable for up the 1 week at 37 °C than the low boiling point microbubbles. The low boiling point microbubbles lost >20% absorbance within 12 h and >50% within 3 days. When a 3-way ANOVA was performed, both time (p<0.0001) and temperature (p<0.0001) had significant impacts on the absorbance

readings. Individual comparisons showed that the high boiling point microbubbles had higher absorbances than low boiling point microbubbles starting at the 0.5-day time point (p<0.0001), as shown in the graph. The stability of the bubbles was also assessed at storage temperature in the refrigerator (**Supplemental Figure. 2.2**). Both high and low boiling point microbubbles had good stability at 2 °C.

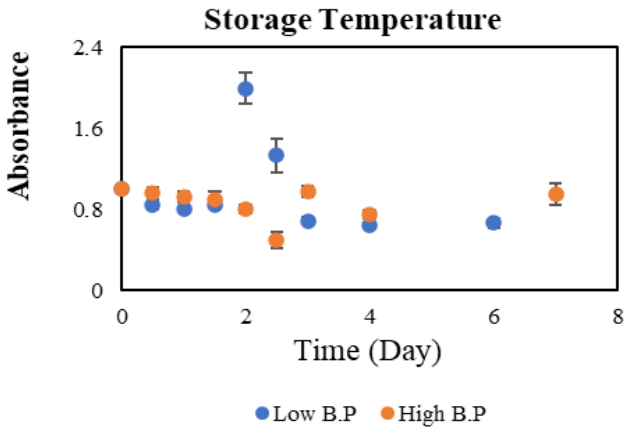

Supplemental Figure 2.2. Absorbance readings show stability of the high and low boiling point (B.P.) microbubbles at 2 °C over time. (n=3 samples / condition).

Ultrasound was applied on microbubbles both with and without CO to assess the impact of ultrasound on the efficiency of rupturing the bubbles. As expected, the high boiling point microbubbles exhibited limited ability to be ruptured with the ultrasound frequencies up to 3 MHz applied for 15 minutes (**Supplemental Figure. 2.3**). The low boiling point microbubbles could be partially ruptured with ultrasound applied for 15 minutes, especially for the highest intensity (3 W/cm^2) and highest frequency setting (3 MHz) (**Supplemental Figure. 2.4**). There was variability in

efficiency between individual samples, and the rupture was especially noticeable with the microbubbles >1 μm in diameter and not for the smaller ones.

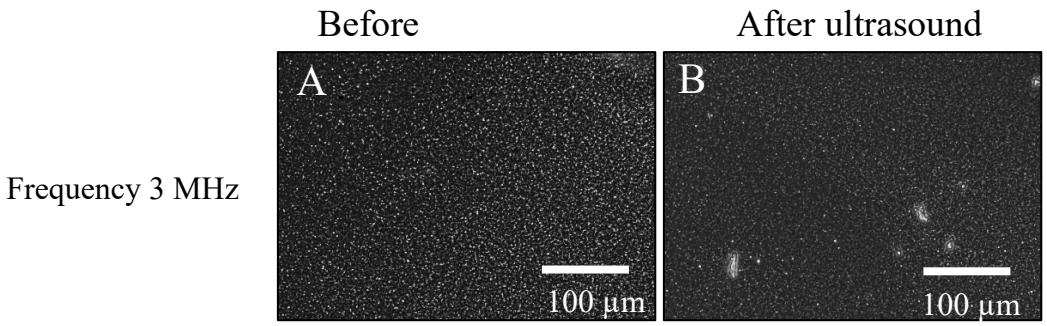

Supplemental Figure 2.3. Impact of low-frequency ultrasound on high boiling point microbubbles in 2D. Shown are 10x phase contrast images of microbubbles without application of ultrasound (A) and with the application of ultrasound at 3 MHz (B).

Reprinted from Changizi, Shirin, et al. *Journal of Biomedical Materials Research Part A* 112.4 (2024): 600-612.

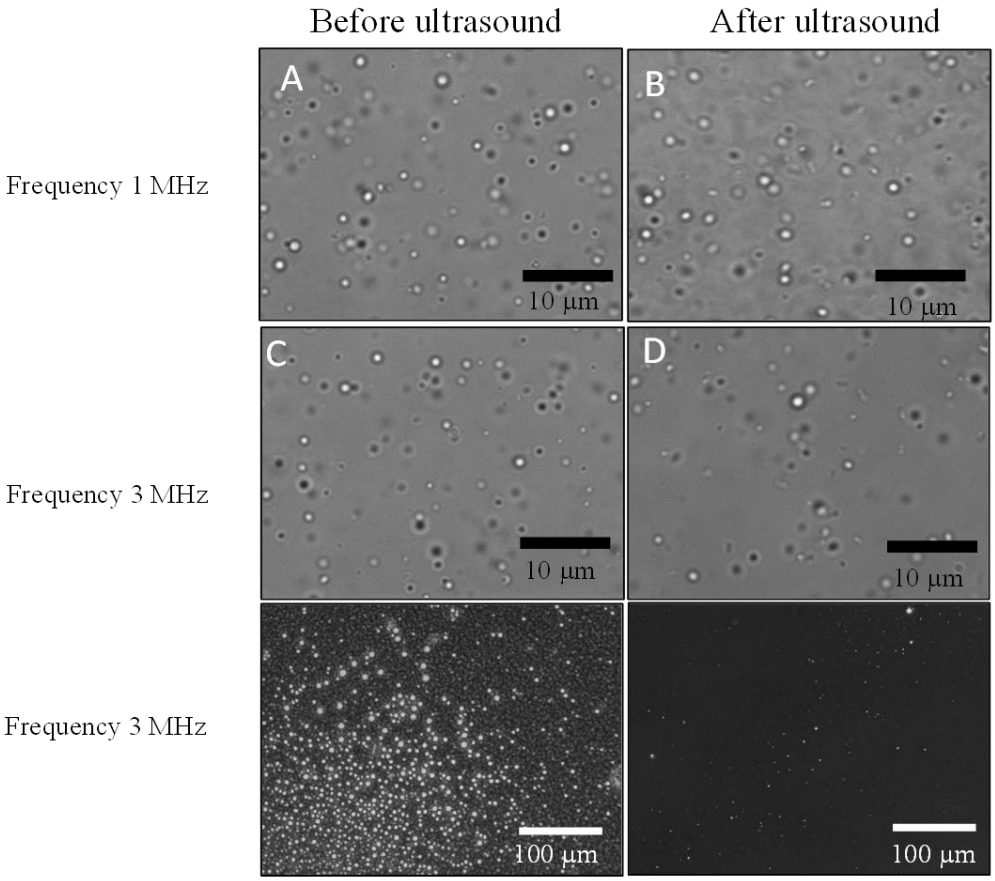

Supplemental Figure 2.4. Impact of low frequency ultrasound on low boiling point microbubbles in 2D. Shown are 100x brightfield images of microbubbles without application of ultrasound (A, C) and with application of ultrasound at 1 MHz (B) and 3 MHz (D) for 15 mins. Low magnification phase contrast images are also shown for one spot before and after application of 3 MHz ultrasound. (*n*=6 samples / condition).

CO loading was verified with the FL-CO probe and palladium acetate. We demonstrated that the fluorescent probe works with CO gas (**Supplemental Figure. 2.5**). Further, a higher amount CO was released from CO-loaded microbubbles (1:20 dilution) after the application of ultrasound for 10 min than with a control sample incubated for 10 min without ultrasound. There was some residual CO that was left after the centrifuging and washing step that was subtracted for a calculation of the

CO concentrations. With the calibration curve and the CO solubility in water, there were an estimated 58 µM and 6 µM concentrations of ultrasound and no ultrasound conditions, respectively. This is only a semi-quantitative analysis, and further optimization of the probe is needed for a more detailed analysis of CO stability within the microbubbles.

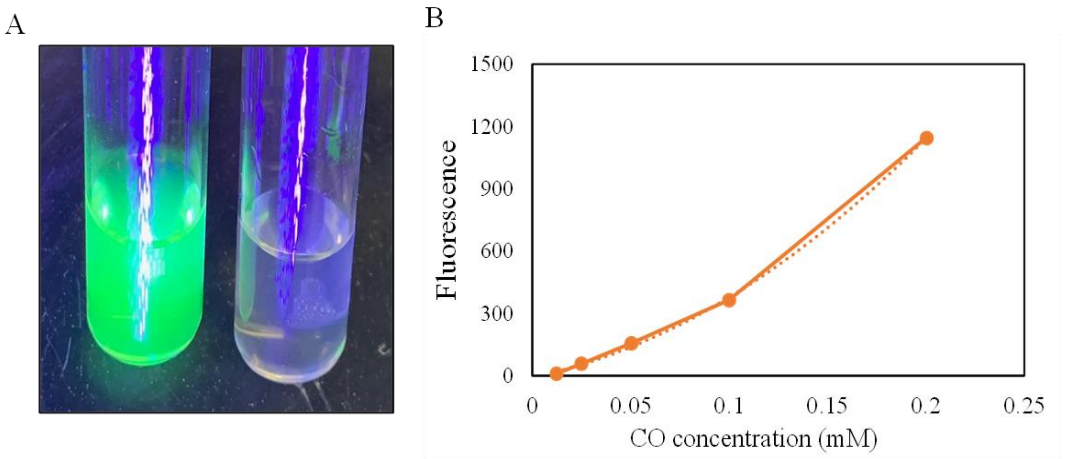

Supplemental Figure 2.5. Demonstration that the FL-CO probe can be used for semi-quantitative analysis of CO release. Saturated CO in DI water (left) and DI water without CO (right) after application of a UV light. Shown is a calibration curve for the FL-CO probe with a serial dilution of CO in DI water.

2.3.2 Biocompatibility and cellular response on TCPS

The microbubbles were initially added to the cells with different dilutions, but without the application of ultrasound, to assess biocompatibility. Only the low boiling point microbubbles were tested because the high boiling point microbubbles could not be efficiently ruptured with application of ultrasound. HUVECs cultured on tissue culture polystyrene without any microbubbles were included as a control. Cell attachment and spreading were still supported 2 days after adding microbubbles

(i.e., day 3 of culture) (**Figure. 2.2A-H**). Only the highest concentration (i.e., 1:20 dilution) appeared to show a reduction in cell density at day 3 of culture. This reduction in cell density also appeared to be prevented when CO was loaded within the microbubbles, although the differences were not statistically significant (p=0.23 for the effect of CO-loading from 2-way ANOVA). The expression of VE-cadherin (i.e., a functional EC marker) was observed at the boundaries between some, but not all, of the cells. It visually appeared that CO-loading within the low boiling point microbubbles increased the HUVEC expression of VE-cadherin compared to microbubbles without CO and the control without microbubbles. However, quantified results were not statistically different because of high variability (**Figure. 2.2I**).

Live dead staining was also performed at day 3 of culture, with a high percentage of live cells observed for most conditions (**Figure. 2.3A-G**). Like the cell nuclei analysis, the 1:20 dilution without CO-loading showed the lowest number of live cells per image. A quantitative analysis indicated that both the 1:20 and 1:40 dilutions without CO-loading had significantly lower number of live cells than the cells only condition (p<0.0034 - **Figure. 2.3H**). However, the dilutions with CO-loading did not have a significantly lower number of live cells than the cells only condition. More importantly, there were a significantly higher number of live cells for the 1:40 and 1:20 dilutions with CO-loading compared to the corresponding conditions without CO-loading (p<0.017). When the dead cells were considered, only the 1:20 dilution without CO had a significantly lower percentage of live cells

than the cells only condition (p<0.0003) and the 1:20 dilution with CO-loading (p<0.0002 - **Figure. 2.3I**). Interestingly, all of the other conditions had comparable percentages of live cells.

The results from day 7 of culture for cell nuclei showed smaller differences between samples because most samples were confluent, but the highest 1:20 microbubble dilution without CO-loading still appeared to reduce biocompatibility **(Supplemental Figure. 2.6)**. Further, CO-loading appeared to still improve biocompatibility. There were no statistical differences in VE-cadherin expression at day 7 between condition.

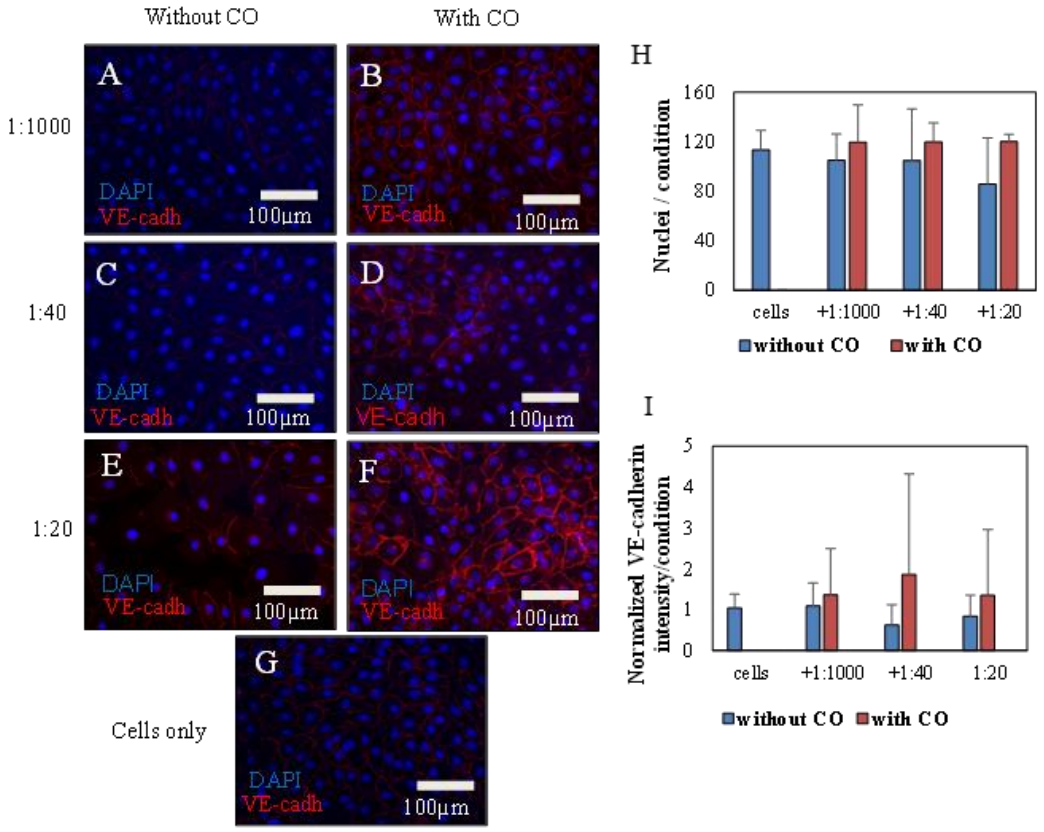

Figure 2.2. Low boiling point microbubble biocompatibility. Representative VE-cadherin stained images of HUVECs cultured with the microbubbles. The concentration was varied with dilutions at 1:1000 (A, B), 1:40 (C, D), and 1:20 (E, F). The microbubbles provided to the cells were either without (A, C, E) or with (B, D, F) CO-loading. A cell only control is also shown (G). Nuclei are also stained with DAPI (blue). Quantitative results for the number of nuclei / image (H) provide an estimate of cell density (*n*=3 samples / condition). Semi-quantitative results are also shown for the normalized VE-cadherin expression (*n*=6 samples / condition).

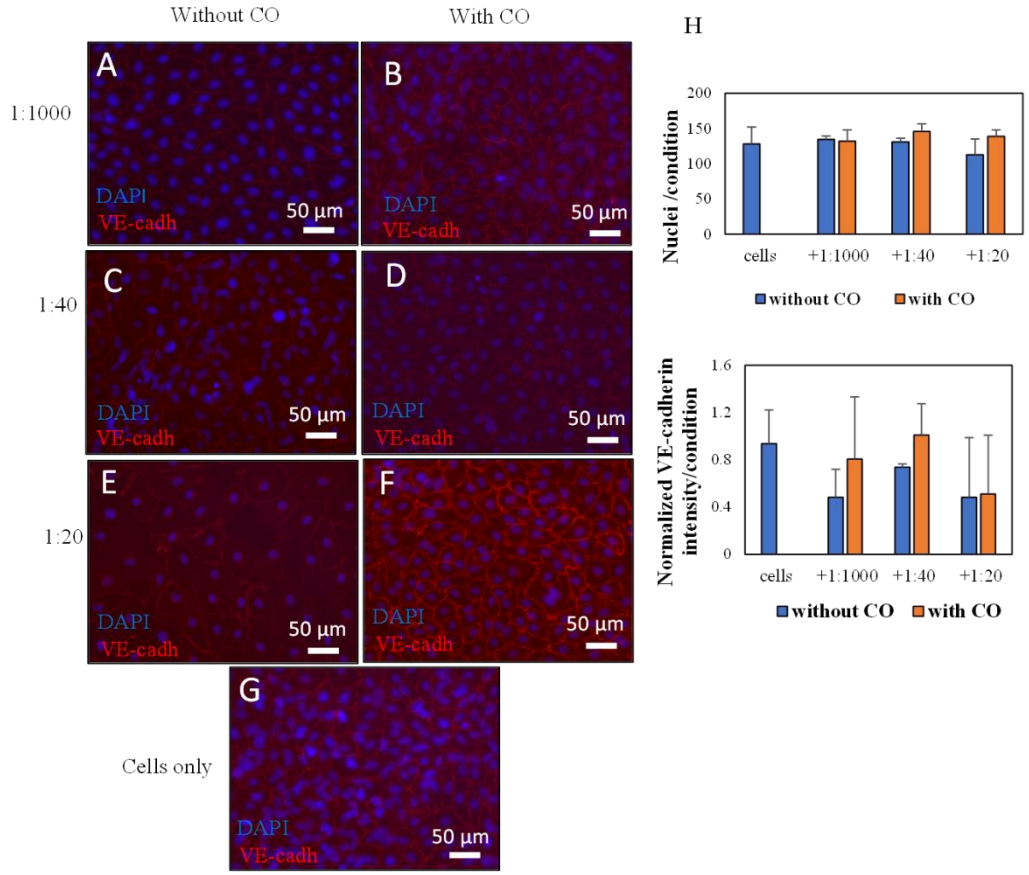

Supplemental Figure 2.6. Low boiling point microbubble biocompatibility at 7 days. Representative VE-cadherin stained images of HUVECs cultured with the microbubbles. The concentration was varied with dilutions at 1:1000 (A, B), 1:40 (C, D), and 1:20 (E, F). The microbubbles provided to the cells were either without (A, C, E) or with (B, D, F) CO-loading. A cell only control is also shown (G). Nuclei are also stained with DAPI (blue). (*n*=3 samples / condition). Quantitative results for the number of nuclei / image (H) provide an estimate of cell density (*n*=3 samples / condition). Semi-quantitative results are also shown for the normalized VE-cadherin expression (*n*=3 samples / condition).

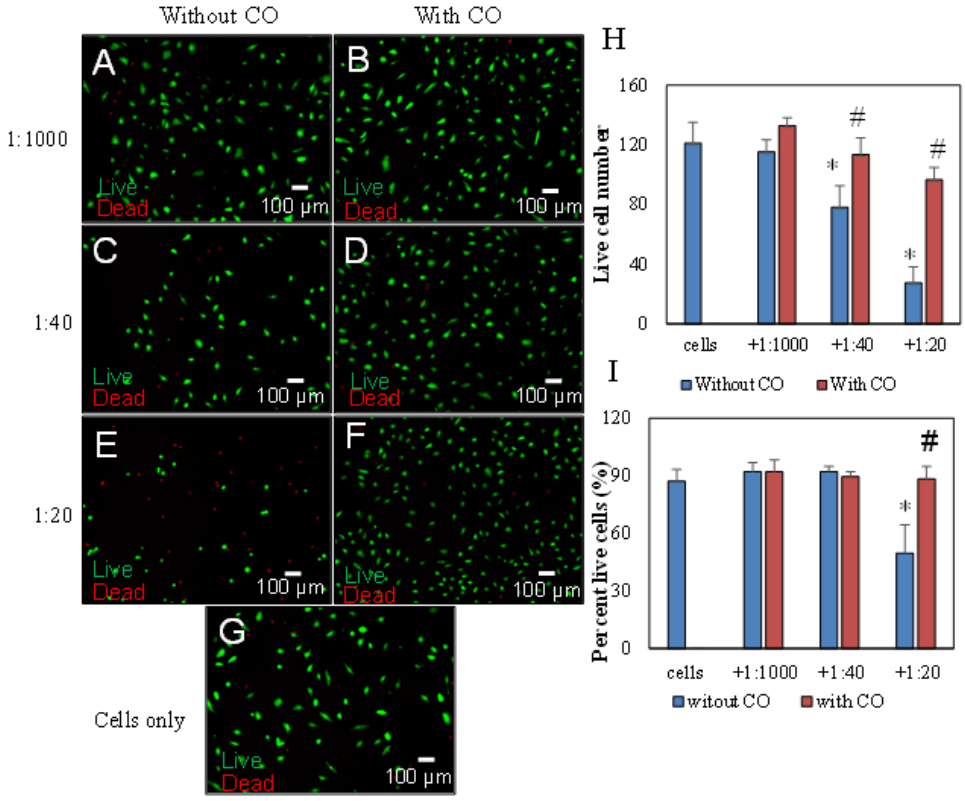

Figure 2.3. Live/dead assay for HUVECs cultured with microbubbles. The concentration was varied with dilutions at 1:1000 (A, B), 1:40 (C, D), and 1:20 (E, F). The microbubbles provided to the cells were either without (A, C, E) or with (B, D, F) CO-loading. A cell only control is also shown (G). Quantitative results for the number of live cells/image (H) and the percent live cells (I) are shown. (*n*=3 samples / condition). (*) indicates significant difference from cells only. (#) indicates significant difference from the corresponding condition without CO-loading.

The impact of ultrasound on HUVECs was only investigated for the low boiling point microbubbles, and for the lowest concentration of microbubbles (i.e., the 1:1000 dilution). The therapeutic 3 MHz ultrasound applied for 15 min both to the CO-loaded microbubbles and to cells only (**Figure. 2.4**). There appeared to be

higher VE-cadherin expression when CO-loaded microbubbles were present than cells only as was also observed in the biocompatibility tests. Surprisingly, there was no clear impact of applying ultrasound on cell number or VE-cadherin expression. Quantitative analysis of cell nuclei did not show any differences in cell number (**Figure 2.4I**). Further, quantitative analysis of VE-cadherin showed slightly higher expression with the 1:1000 dilution of CO loaded microbubbles after application of the ultrasound compared to cells only without ultrasound (**Figure 2.4J and Supplemental Figure. 2.7**). However, the results were not statistically different due to high variability between samples. Phalloidin staining did suggest that an extended 15 min of exposure to ultrasound resulted in more intense actin fibers within the cytoskeleton independent of the presence of the CO-loaded bubbles.

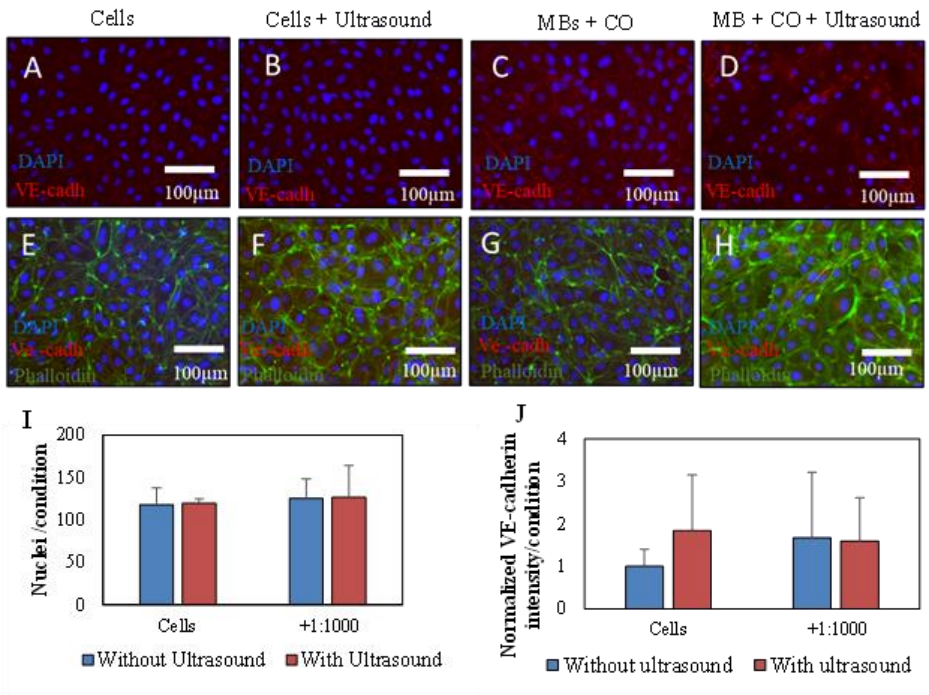

Figure 2.4. Low frequency ultrasound on HUVECs culture on TCPS. Representative VE-cadherin-stained images of HUVECs without (A-B) and with (C-D) a 1:1000 dilution of low boiling point microbubbles. Phalloidin staining is also shown for HUVECs without (E-F) and with (G-H) microbubbles. Ultrasound was applied to both cells only (B, F) and to cells with microbubbles (D, H). Nuclei are also stained with DAPI (blue). *n*=6 samples / condition. Quantitative results for number of nuclei/image (I) and VE-cadherin intensity (J). (*n*=6 samples / condition).

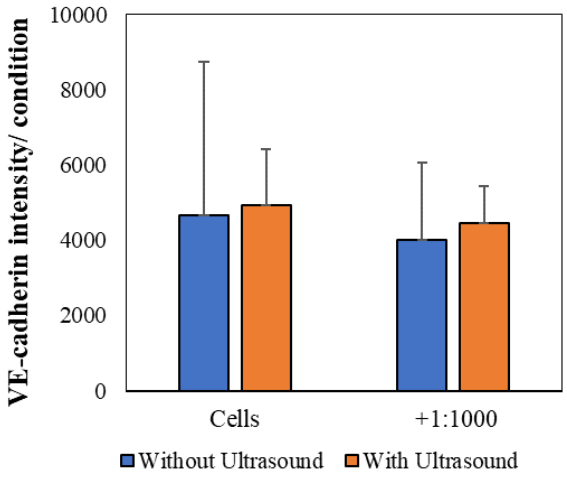

Supplemental Figure 2.7. Semi-quantitative analysis of VE-cadherin expression after application of low-frequency ultrasound without normalization. Shown are condition both with and without CO-loaded microbubbles for HUVECs cultured on TCPS (*n*=6 samples/condition).

2.3.3 Potential for endocytosis by HUVECs

The CO released from the microbubbles has the potential to impact ECs through a couple of routes, including free CO within the culture media after rupture and rupture of the CO-loaded microbubbles while within the cell. To consider the potential of this second route, we investigated the ability of HUVECs to endocytose the low boiling point microbubbles under physiological conditions. Z-stacks in combination with time lapse imaging showed rapid movement of the bubbles on the millisecond time scale, and both smaller and larger bubbles can be distinguished (**Figure. 2.5** and **Supplemental Video 1**). There also appeared to be periodic rupture

of the bubbles with time observed from the confocal images. Further, it was clear that several of the bubbles slowed their movement and were co-localized over time with DiO stained HUVECs, indicating internalization. These appeared to be within the size range of our microbubbles that we have observed in **Figure. 2.1**. It is also possible that some of the internalized material was debris from ruptured bubbles, but further analysis would be necessary to confirm. Even if some of internalized material was debris, **Figure. 2.3** showed a clear impact of the CO-loaded microbubbles after rupture with ultrasound and CO release. Most of the microbubbles that were internalized were smaller microbubbles, and the number of internalized microbubbles increased over the 2 h of imaging. In addition, some of the HUVECs were more efficient at endocytosing microbubbles than others.

Reprinted from Changizi, Shirin, et al. *Journal of Biomedical Materials Research Part A* 112.4 (2024): 600-612.

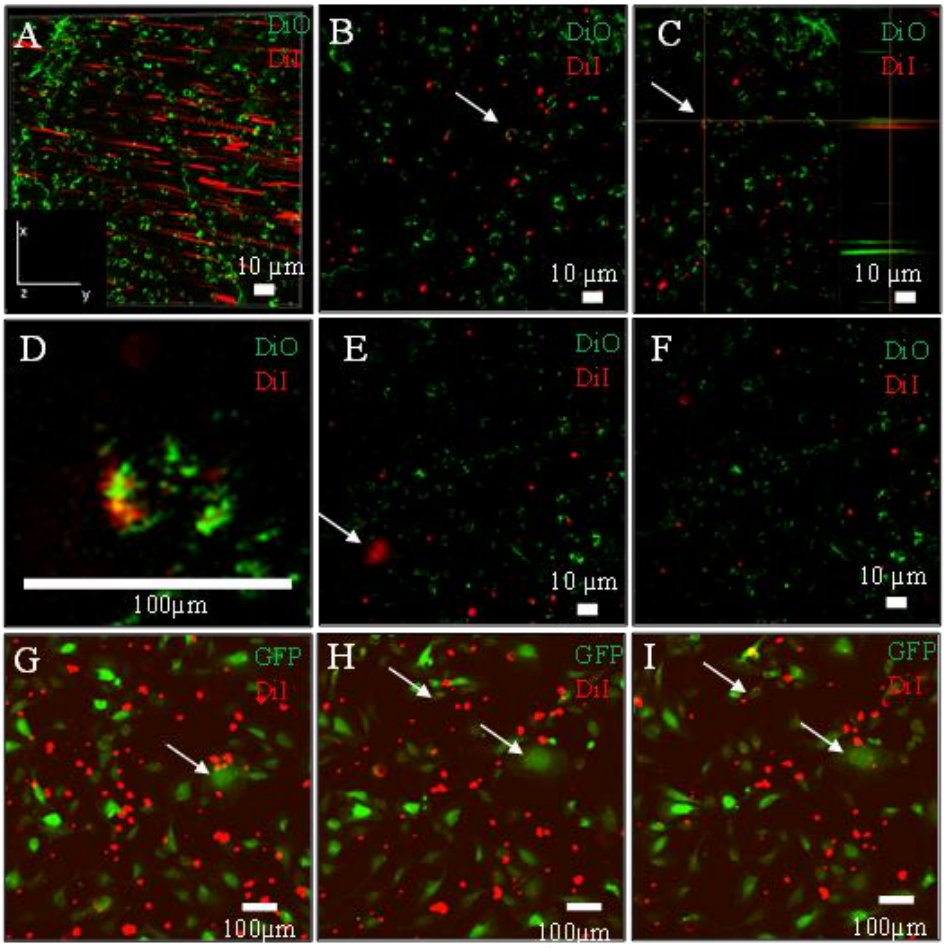

Figure 2.5. Assessment of microbubble endocytosis by confocal microscopy. A 3D volume shows DiI-stained low boiling point microbubbles (red) and their rapid movement during the time to create a z-stack (A). DiO-stained HUVECs (green) are also shown. 2D x-y (B) and y-z (C) slices, and a high magnification x-y image (D), show an accumulation of microbubbles within a cell. Periodic rupture of bubbles can also be observed (E-F). Endocytosis of microbubbles can also be seen with 2D x-y images over time with GFP^+ HUVECs (green) (G-I).

Reprinted from Changizi, Shirin, et al. *Journal of Biomedical Materials Research Part A* 112.4 (2024): 600-612.

2.3.4 Ultrasound impacts in 3D phantoms

After verifying the initial cellular responses in the simplified TCPS environment, the impact of CO-loaded, low-boiling point microbubbles was assessed using more realistic tissue phantoms. First, rupture of microbubbles without CO-loading was tested within a tubular construct using a higher frequency imaging ultrasound (**Figure. 2.6**). Unlike application of the lower frequency ultrasound in **Supplemental Figure. 2.4**, the intensity of the signal decreased for the microbubbles in the images and some of the microbubbles ruptured after only 1 s of application of a burst sequence. After 4 burst sequences (i.e., 4 s of ultrasound total), large decreases in microbubble intensity and rupture were observed. Finally, almost all of the bubbles were ruptured after 5 min of high frequency ultrasound. We also confirmed that high frequency ultrasound made a difference because application of the low-frequency ultrasound showed negligible microbubble rupture up to 2 min, and it required 5 min for partial rupture of the bubbles. These results indicated that the microbubbles can be controllably ruptured and are expected to release CO.

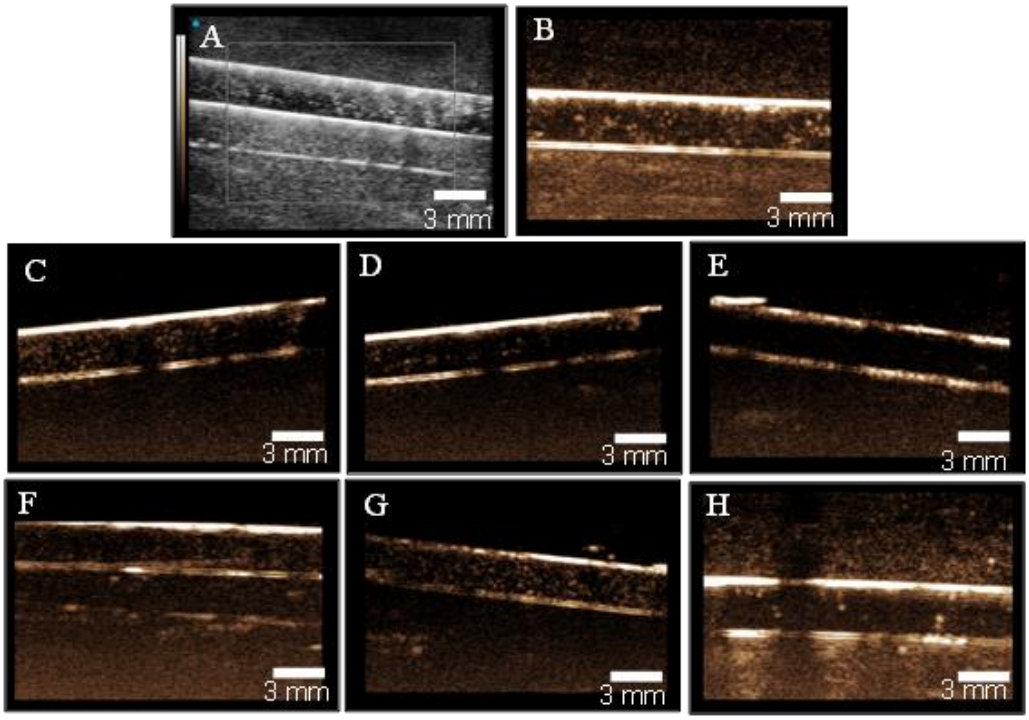

Figure 2.6. Rupture of low boiling point microbubbles in a static 3D tubular phantom. The microbubbles can initially be seen in the tube with B-mode (A) and contrast mode (B). Contrast mode shows changes in the microbubbles after 1 s (C), 4 s (D), and 5 min (E) of high frequency ultrasound at 100% intensity. Contrast mode images are also shown with application of low frequency therapeutic ultrasound for 1 (F), 2 (G) and 5 (H) min. *n*=3 samples / condition.

The impact of rupture of the CO-loaded microbubbles with the imaging ultrasound machine was tested using GFP^+ HUVECs and a gelatin-based tissue phantom where slower cell growth is expected than with a TCPS well. Application of ultrasound using a 1:50 microbubble dilution resulted in much clearer differences than were observed with the 2D TCPS results (**Figure. 2.7**). The cells on the fibronectin-coated gelatin surfaces were attached with only localized colonies with high-cell densities, and the coverage was heterogenous and variable. Interestingly,

providing this higher concentration of CO-loaded microbubbles without the application of ultrasound resulted in significantly more rounded cells. Similarly, rounded cells were also observed for application of the ultrasound without incorporation of CO loaded microbubbles. However, when ultrasound was applied to CO-loaded microbubbles for only 1 min, the HUVECs were more spread, had a higher density, and were more consistent through individual samples than the control without microbubbles. This was consistent for all 6 samples / condition. This can be even more clearly visualized with 2D confocal projections (**Supplemental Figure. 2.8**).

Quantitative analysis showed that application of ultrasound on CO loaded microbubbles resulted in significantly higher cell numbers than without ultrasound (p=0.029). Further, the result showed that the application of ultrasound to CO-loaded microbubbles results in a significantly higher cell density than with ultrasound applied to cells only (p=0.019).

Reprinted from Changizi, Shirin, et al. *Journal of Biomedical Materials Research Part A* 112.4 (2024): 600-612.

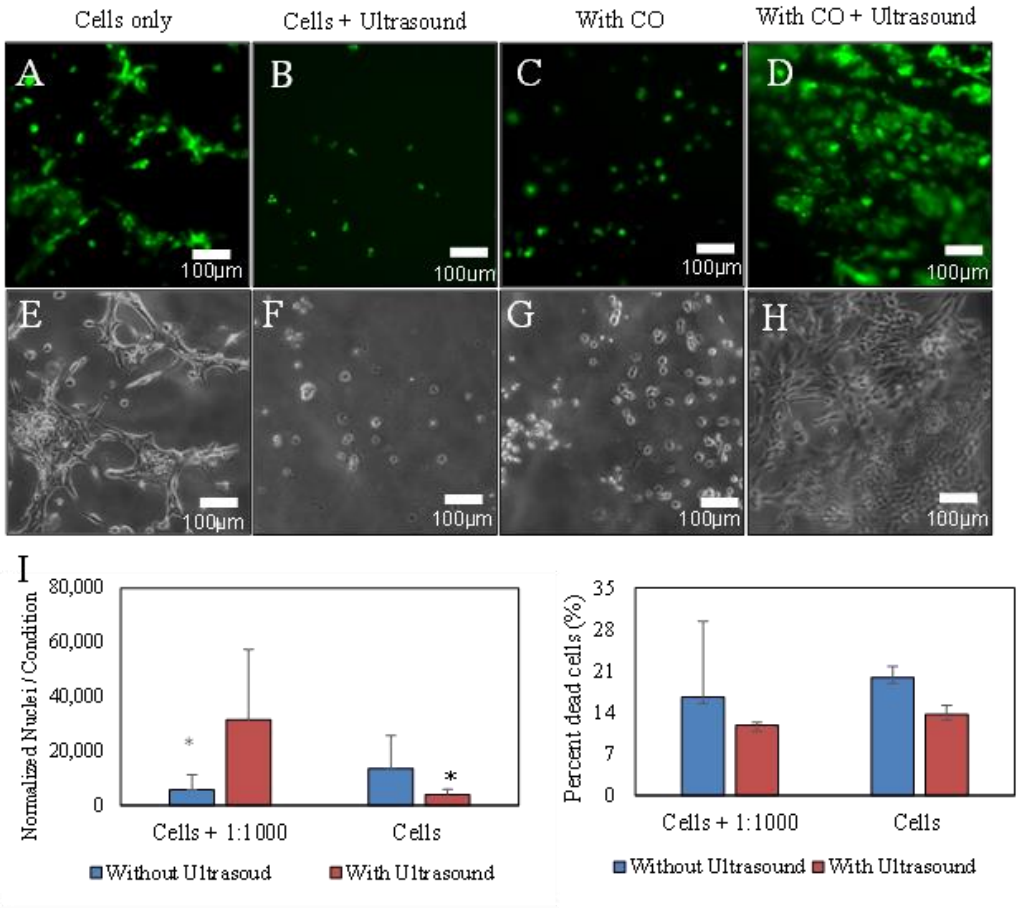

Figure 2.7 Cellular impacts of high frequency ultrasound with a gelatin-based phantom. Shown are representative fluorescence images of GFP^+ HUVECs with cells only both without (A) and with (B) application of ultrasound as well as cells with CO-loaded microbubbles both without (C) and with (D) application of ultrasound. Phase contrast images are also shown for cells only both without (E) and with (F) application of ultrasound as well as cells with CO-loaded microbubbles both without (G) and with (H) application of ultrasound. (*n*=3 samples / condition). (*) indicates significant difference from CO-loaded microbubbles after application of ultrasound.

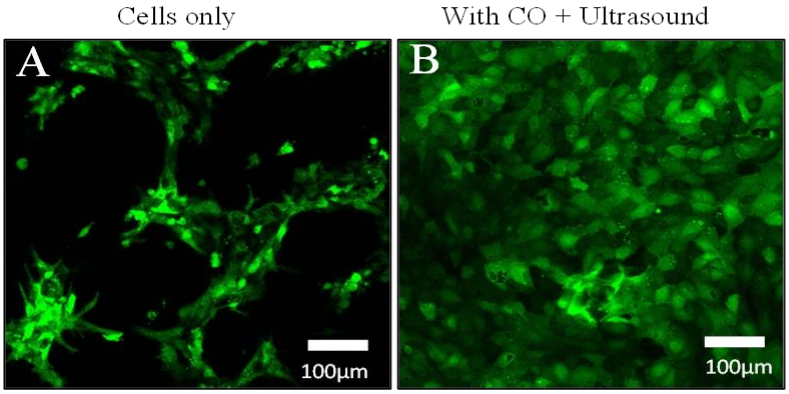

Supplemental Figure 2.8. Cellular impacts of high frequency ultrasound with a gelatin-based phantom. Shown are representative confocal 2D projections of GFP^+ HUVECs for cells only (A) and for CO-loaded microbubbles with the application of ultrasound (B).

2.4 Discussion

Regeneration of a functional endothelium is critical for both vascular grafts and regenerative strategies for treating vascular disease. This includes the need to develop strategies to repair the disrupted BBB for many VCID patients. We are investigating a different approach to use of ultrasound-sensitive PFC microbubbles as a carrier to more controllable deliver the gasotransmitter CO to the BBB. We propose that this drug delivery system can provide a high enough dose of CO that can positively impact EC growth and can be applied controllably in the body with the application of low intensity ultrasound. In this study, we demonstrated that the boiling point of PFC impacts its stability and ultrasound-sensitivity, with lower boiling point, perfluoropentane-based microbubbles especially showing promise. We also demonstrated that application of ultrasound at the appropriate frequency can lead to rapid microbubble rupture and improved EC growth. To our knowledge, only

one other study by Guo et al. included gasotransmitters within microbubbles, and they investigated the impact of CO loaded microbubbles on tumor cell apoptosis [147].There are important differences in tumor cell response to CO and different microbubble fabrication strategies were used in that study [148].

Several different types of PFC microbubbles are commercially available and have been tested in clinical trials [149]. However, these PFC microbubbles typically have limited stability that require them to be reconstituted close to the time of use [150]. This complicates the ability to controllably load CO or other gasotransmitters within the microbubbles. In this study, we developed microbubbles through a controlled precipitation process that also allowed for us to load CO into the microbubbles. CO has an affinity for PFCs and a higher solubility than in the surrounding water. These microbubbles maintained high stability when refrigerated for storage over 7 days. The stability was lower at physiological temperature, but this is also important for the microbubbles to be ultrasound sensitive. The low boiling point PFC (i.e., perfluoropentane – boiling point of 28 °C) maintained some stability out to 4 days at 37 °, which is higher than values reported for other PFC-based microbubbles [151]. However, the perfluoropentane microbubbles could still be efficiently ruptured with ultrasound. The boiling point and the stability of the perfluoropentane microbubbles suggests that they are mostly in the gas phase at physiological conditions. The higher boiling point perfluorohexane (boiling point 56 °C) microbubbles were unfortunately too stable to be used for ultrasound bubble rupture and release of the loaded CO.

Microbubbles created from volatile PFCs are considered to have a good safety profile in the body because they evaporate and can be rapidly cleared from the blood [151], [152]. Conversely, more important safety concerns have been discussed for the use of high frequency ultrasound to disrupt the BBB [142].However, biocompatibility is something that we also need for our microbubbles. The biocompatibility for low boiling point microbubbles without CO-loading appeared to only be reduced for the 1:20 dilution, or 170 µg/mL of total PFC when counting cell nuclei. Live/dead staining indicated this even more clearly, with the 1:20 dilution without CO-loading condition providing fewer live cells. Interestingly, the 1:40 dilution without CO-loading also had fewer cells per image, but the live/dead ratio was not decreased. For the gelatin phantom, there was not a significant decrease in cell number with the 1:50 dilution of microbubbles tested, but the cells were more rounded. Overall, these data suggest that a 1:40 dilution negatively impacts cells growth but only a higher concentration of perfluoropentane microbubbles (i.e., 1:20 dilution) noticeably decreases cell viability. For contrast imaging, concentrated microbubbles are typically injected. This includes up to 250 µL, or ~2.8×10^8 microbubbles, for a typical injection in a human patient.

One observation was that the loading of CO in the microbubbles reduced any toxicity concerns from the PFC component of the microbubbles. This was observed through higher cell densities in the biocompatibility studies with CO-loading within the low boiling point microbubbles. This is interesting because no ultrasound was applied to rupture the bubbles and release the CO in these studies. This is likely due to the

volatility of these microbubbles. Our stability data showed that some of low boiling point microbubbles can rupture over time without the application of ultrasound. The improvement in biocompatibility with the addition of CO was more clearly confirmed with the test of HUVEC growth on a gelatin phantom. A high (1:50) concentration of microbubbles caused noticeable toxicity when ultrasound was not applied, but the opposite result was observed when ultrasound was applied and CO was released from the microbubbles. With the high solubility of CO within PFCs, we expect that relatively low concentrations of microbubbles will be needed to provide EC benefits. Further, results with the gelatin phantom demonstrated that there were no biocompatibility concerns for CO-loaded microbubbles, and instead they provided a significant benefit for ECs.

CO-loading within the microbubbles also appeared to impact HUVEC function, especially for the low boiling point microbubbles where there appeared to be higher VE-cadherin expression with CO-loading. This is likely due to the fact that the low boiling point bubbles will rupture over time and release CO without the application of ultrasound. This is likely also one reason why application of low frequency ultrasound resulted in comparable VE-cadherin expression for CO-loaded low boiling point microbubbles with and without application of ultrasound. However, the low frequency ultrasound was still shown to impact the ECs through an increase in expression of F-actin in the cell cytoskeletons. This occurred even without any microbubbles being present. Hauser et al. showed that low-intensity pulsed ultrasound by itself can lead to increased actin stress fibers within a SAOS-2

osteoblast-like cell line [153].The 15 min of ultrasound is our study is an extended time, and less noticeable impacts on the ECs are expected for the shorter times of ultrasound activation that would likely be applied in the body.

This study showed the importance of carefully controlling the ultrasound parameters. Our results are consistent with the literature that shows that the size of microbubbles impacts their ultrasound sensitivity [154]. This is in agreement with the resonance frequency for the different sized bubbles. Smaller bubbles have a higher resonance frequency for interacting with ultrasound waves. In our study, 3 MHz was also not enough to consistently rupture the smaller microbubble, but 21 MHz ruptured these microbubbles efficiently. While frequencies in between were not tested, it is likely that traditional ultrasound transducers used clinically (e.g., 7 MHz commonly used for children and neck application [155]) would still be able to rupture the bubbles based upon the literature [156]. Further, the fact that the microbubbles can be ruptured in our 3D phantom suggest that bubble rupture and CO release can occur at a timeframe that is relevant clinically. High intensity ultrasound is often provided for 3-5 min for disrupting the BBB [157], and low intensity ultrasound is safe for an extended time of application.

The large improvement in EC density and homogeneity with application of high frequency ultrasound in our study shows that CO-loaded perfluoropentane microbubbles can provide therapeutic benefits. However, careful control of dose is important for the anti-inflammatory and pro-angiogenic properties because CO has a biphasic effect depending on dose [68]. Low doses of delivered CO can often have

negligible effects in cell culture without controlled delivery because it can escape the system as a gas, and in the body binding of delivered CO to hemoglobin will reduce the potential benefit to ECs[95]. In essence, this would reduce the CO that can bind to nitric oxide synthase (NOS) and other heme containing targets within the cell. Of course, doses that are too high, or too extended, can also lead to pro-inflammatory properties. In this study, the 1:40 dilution provided a clear benefit when ultrasound was provided shortly after adding the microbubbles to HUVECs in culture. However, it is likely that lower dilutions could also have a benefit. While additional studies are needed to determine the impact of gasotransmitters dose within microbubbles on cell proliferation, CO with concentrations as low as 1.1×10^{-5} mol/m^3 have been shown to positively benefit ECs when delivered through other means [158], [159]. The determination of appropriate CO doses is further complicated by that fact that CORM byproducts after releasing CO can also impact cells. The ability to separate the effect of CO from the CORM molecules is another benefit of the CO-loaded microbubbles. Finally, it is also important to note that our study only applied ultrasound to rupture the bubbles one time. The potential benefit of repeated rupture of a percentage of the microbubbles over a more extended time frame is something that still needs to be investigated.

Another important area of future study is how effective the CO is when the bubbles are ruptured outside the cells vs. when they are endocytosed. CO can enter the cell membrane through passive diffusion, but mass transport of this gas may limit the concentration of free CO that enters the cells. In this study, we showed that the

microbubbles can be endocytosed, and in particular the smaller particles. This is consistent with previous studies that have shown lower uptake of 10 μm compared to 1 μm particles [160], [161]. We also showed variability in endocytic activity for individual cells that may be due to a combination of the physiological activity of the cells, if the cells are actively proliferating, and the structural complexity of their vesicles and endosomes [162], [163].The impact of free CO diffusion and release after endocytosis should be considered for future experimental and computational studies. This could be another route of release of CO to provide a therapeutic benefit. Overall, this study provides initial support for the potential therapeutic use of CO-loaded microbubbles as a non-invasive way to treat the BBB for VCID patients.

2.5 Conclusion

This study demonstrated that microbubbles of similar sizes can be prepared with lower and higher boiling point perfluorocarbons, but their promise for ultrasound-sensitive drug delivery are different. The lower boiling point perfluoropentane-based microbubbles showed promise with better stability than current emulsion-based PFC microbubbles and yet also exhibited the ability to be ruptured with ultrasound and release CO. This study confirms that the microbubbles, especially the low boiling point ones, have good biocompatibility, and that noticeable toxicity was only observed at high microbubble concentrations. Interestingly, the inclusion of CO within the microbubbles appeared to maintain biocompatibility of HUVECs when the microbubbles were added at higher concentrations using traditional TCPS culture and significantly improved cell growth in a gelatin-based

tissue phantom. This study also showed that proper ultrasound parameters are needed to efficiently rupture the microbubbles and elicit EC benefits. This was clearly shown with the gelatin phantom where application of ultrasound from an imaging ultrasound machine led to important increases in HUVEC spreading and growth after only a one-time application of ultrasound and CO release. Overall, this study demonstrated the potential for use of these perfluoropentane ultrasound-sensitive microbubbles to be used for improving blood vessel endothelialization.

Acknowledgments

This work was supported by the National Science Foundation under Grant No. CBET 1510003. The work was also supported by a Brevard Foundation Medical Research grant.

Reprinted from Changizi, Shirin, et al. *Macromolecular Bioscience* 23.9 (2023): 2300073.

Chapter 3: Epsin mimetic UPI peptide delivery strategies to improve endothelization of vascular grafts

Shirin Changizi [1, a], *Mahyar Sameti* [1,a], *Gabby Bazemore* [1], *Hong Chen* [2], *Chris A. Bashur* [1, *]

[1]Department of Biomedical Engineering, Florida Institute of Technology, Melbourne, FL 32901, USA

[2] Vascular Biology Program, Boston Children's Hospital, Harvard Medical School, Boston, MA 02115, USA

[a] indicates joint first author.

Abstract

Endothelialization of engineered vascular grafts for replacement of small-diameter coronary arteries remains a critical challenge. The ability for an acellular vascular graft to promote endothelial cell (EC) recruitment in the body would be very beneficial. This study investigated epsins as a target since they are involved in internalization of vascular endothelial growth factor receptor 2. Specifically, epsin-mimetic UPI peptides are delivered locally from vascular grafts to block epsin activity and promote endothelialization. The peptide delivery from fibrin coatings allowed for controlled loading and provided a significant improvement in EC

attachment, migration, and growth in vitro. The peptides have even more important impacts after grafting into rat abdominal aortae. The peptides prevented graft thrombosis and failure that is observed with a fibrin coating alone. They also modulated the in vivo remodeling. The grafts are able to remodel without the formation of a thick fibrous capsule on the adventitia with the 100 μg mL^{-1} peptide-loaded condition, and this condition enabled the formation of a functional EC monolayer in the graft lumen after only 1 week. Overall, this study demonstrated that the local delivery of UPI peptides is a promising strategy to improve the performance of vascular grafts.

3.1 Introduction

Autologous vessels (e.g., saphenous veins) are the gold standard for treating atherosclerotic occlusions in coronary arteries but are unavailable in greater than 30% of patients due to systemic vascular disease [164]. Tissue engineered vascular grafts (TEVGs) offer a promising alternative with a few strategies that have been tested in clinical trials, but still with the need to develop new approaches that can balance the concerns of graft stenosis and aneurysmal dilation [165]. Most approaches consider the necessity of an endothelial cell (EC) pre-seeding step to prevent early-stage thrombosis and graft failure [166]. However, groups are also investigating approaches with an acellular graft that would recruit ECs in the body after implantation [167], [168]. For example, biomaterial modifications including adding heparin [5,6], collagen type IV [171], and fibrin [172] have been used to improve endothelialization in culture and in animal models. The benefits of pursuing

an acellular strategy include providing an off-the-shelf graft and simplifying the FDA approval process.

Any approach involving an acellular vascular graft needs to be able to promote rapid endothelialization in the lumen. Cell signaling from these ECs has been shown to reduce long-term intimal hyperplasia within a graft in addition to preventing early-stage thrombosis [173]. Assessing the potential for endothelialization in the clinical environment is challenging since rodent models will typically endothelialize over time unlike human patients [174]. However, few of the TEVG studies report the presence of functional ECs earlier than 3 or 4 weeks after grafting [175], [176], [177]. For example, a study by Pektok et al. showed that electrospun poly(ε-caprolactone) (PCL) meshes reached a confluent EC coverage by 18 weeks post-surgery [178]. Further, it has also been noted that migration of ECs to the graft near the anastomosis can occur quickly, but rapid endothelialization in the mid graft is more challenging [179], [180]. In one of the few exceptions where early endothelialization occurred, Kuwabara et al. showed an improvement in the percent endothelialization with the inclusion of CAG peptides to reach 64.4% coverage [181]. However, the development of drug delivery-based strategies to further promote early endothelialization *in vivo* has the potential to prevent early-stage thrombosis and benefit not just TEVGs but also non-degradable vascular grafts and stent-grafts as well.

Epsins represent an interesting and new target for promoting graft endothelialization. They are a family endocytic clathrin adaptors [182], and they

contain ubiquitin-interacting motifs (UIM) that are capable of recognizing ubiquitinated plasma membrane proteins and recruiting them to clathrin-coated pits for internalization [183]. This regulation of endocytosis includes promoting the internalization of vascular endothelial growth factor (VEGF) receptor 2 [184], which would reduce the potential for EC proliferation through VEGF signaling. This mechanism is illustrated in more details in our prior publication [117]. Further, epsins have recently been linked to promotion of atherosclerosis [185]. Thus, blocking epsin signaling will likely have several benefits for long-term vascular graft viability. We have previously developed an endothelium-targeting chimeric peptide (UPI peptide) with UIM, plasma membrane anchoring, and iRGD homing sequences that has been shown to block epsin signaling and promote rapid EC proliferation and angiogenesis when injected systemically into rodents [123], [186]. The iRGD region of UPI makes the peptide more specific by targeting the $\alpha_v\beta_3$ integrins found on ECs, where it can then be uptaken and block VEGFR2 internalization. Thus, we postulate that these peptides also offer the potential for promoting endothelialization of vascular grafts with local delivery of the peptides from the graft.

A variety of drug delivery techniques have been used for local delivery from tissue engineered grafts that lead to different release profiles and considerations for drug stability. These include physical adsorption [187], incorporation within a scaffold [188], heparin incorporation [189], delivery from microparticles [190], and the use of a drug-containing coating [191]. One technique that has been used for vascular grafts that can allow high drug loadings is the use of fibrin or fibrin glue as

a carrier [192]. Further, fibrin can provide benefits for endothelialization [193], and fibrin coatings have been shown to be non-thrombogenic [194]. However, the inclusion of a fibrin coating by itself has not been successful to improve the patency rates [195], [196], confirming the importance of combining with a bioactive compound.

In this study, epsin-mimetic UPI peptides were incorporated within a fibrin coating to improve EC proliferation *in vitro* and graft endothelialization *in vivo*. The coating was applied to PCL-based electrospun conduits that are commonly used in vascular graft studies. Electrospinning of both pure PCL and 10% blends of collagen/PCL (w/w) was performed to determine the impact of the base scaffold on the coating process. Physical adsorption and other control conditions were included to compare the release profile and cellular responses with the fibrin coating process. UPI peptide impacts on cell attachment, migration, and proliferation were assessed with human umbilical vein ECs (HUVECs). Finally, the endothelialization and remodeling response was assessed after grafting into a rat abdominal aorta. Arterial grafting was performed for one week to enable detection of rapid endothelization and comparison between conditions.

3.2 Materials and methods

3.2.1 Materials

All disposables, chemicals, and biological supplies were purchased from Thermo Fisher Scientific (Pittsburgh, PA) unless specified otherwise. Polycaprolactone

(PCL) with inherent viscosity of 1.2 dL/g in chloroform was from Lactel Absorbable Polymers (Pelham, AL). Lyophilized collagen type 1 from calf skin was from Elastin Products Company (Owensville, MO). Bovine fibrinogen was purchased from Alfa Aesar. Bovine thrombin was purchased from Millipore Sigma. UPI peptide was synthesized by a solid phase fluorenylmethyloxycarbonyl (FMOC) method as described elsewhere [123]. All primary antibodies were purchased from Abcam (Cambridge, MA), and all secondary antibodies were from Thermo Fisher. Polydimethylsiloxane (PDMS) was purchased from Ellsworth adhesives (Germantown, WI).

3.2.2 Electrospinning and characterization

Conduits and meshes were prepared by electrospinning 0% and 10% blends of collagen/PCL (w/w) onto a 1.6 mm stainless steel mandrel and drum, respectively. The electrospun sheets were used for more controlled cell culture analysis, and the conduits were used for the release profile and for grafting. Solutions were prepared at 13 wt. % by dissolving in 1, 1, 1, 3, 3, 3-hexafluoro-2-propanol (HFIP). Electrospinning was performed using a 22-gauge needle, 15 kV voltage gradient, a throw distance of 10 cm, and a flow rate of 0.8 mL/h. Consistent thickness and the random orientation of the fibers were achieved via lateral movement and slow rotation of the mandrel (<100rpm). The conduits were removed from the rod by using ethanol, segmented into 2 cm long sections, and stored in a desiccator. Scanning electron microscopy (SEM) was used to characterize the fiber diameter (n = 3 samples / condition, n>100 measurements/sample). Cross-sections were also

prepared with cryo-fracture for thickness measurements (n = 3 samples / condition). The electrospun meshes and conduits were mounted, sputter-coated with gold, and then imaged. ImagePro Plus® software was used to analyze the SEM images.

3.2.3 Peptide incorporation via physical adsorption and fibrin coating

Conduits were sterilized via ethylene oxide and all the coating steps were performed in sterile conditions. Conduits and meshes were coated with UPI peptide through both physical adsorption and the fibrin coating method (**Supplemental Figure 1**). The peptide was dissolved in phosphate buffer saline (PBS). Conduits were wetted by immersing in ethanol for 5 seconds prior to soaking in PBS. For physical adsorption, the PCL conduits were soaked in different concentrations of UPI peptides overnight and then dried in a desiccator prior to use. For fibrin coating, the PCL conduits were soaked in 50 mg/mL of fibrinogen and different concentrations of UPI peptide in the fibrinogen solution overnight. The coated conduits were then collected, dipped into a 10:1 solution of 5 U/mL thrombin for 30 s to crosslink the fibrinogen retained within the conduits, and then transferred to an empty tube. To characterize the fibrin infiltration throughout the wall, the conduits were mounted in optimal cutting temperature compound (OCT) and 8 μm cross-sections were prepared. The sections were stained with an anti-fibrinogen primary antibody and an Alexa 633 secondary antibody. PCL sections without a primary antibody were used as a control. The sections were imaged using a Zeiss Axio Observer A.1 fluorescent microscope (Carl Zeiss Microscopy, Thornwood, NY) with a ProgRes® SpeedXT core 3 CCD camera (Jenoptik, Jupiter, FL). The sample size was n = 3 condition.

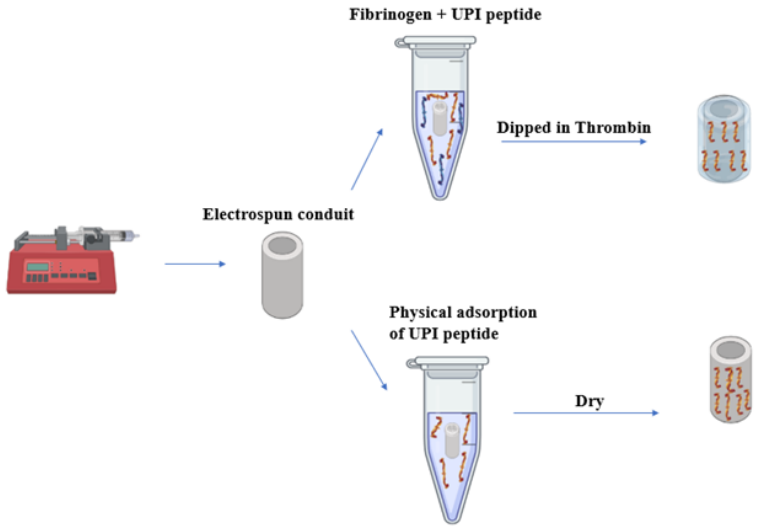

Supplemental Figure 3.1. Illustration of the processes for incorporating the UPI peptide via fibrin coating and physical adsorption.

3.2.4 Suture retention test

A suture retention test was performed on PCL conduits with different thicknesses and with and without fibrin hydrogel incorporation. No UPI peptides were included for suture retention testing. One side of the conduit was clamped to the grip and the other side was sutured with a 9-0 nylon suture placed 2 mm from the edge of conduit. This is the same suture used for the rodent surgeries. The suture was then connected to the top clamp of an Instron E3000 test frame. Samples were stretched at 50 mm/min until fracture and the maximum load was reported as suture retention strength (n=6 per condition).

3.2.5 Platelet adhesion assay for fibrin coating

Blood was collected from healthy rats following an IACUC approved procedure in collection tubes containing 3.2% sodium citrate. The fresh blood was centrifuged

for 15 minutes at 300 g, and then the platelet-rich plasma was collected and stored in the refrigerator. Meshes electrospun with pure PCL and 10% collagen/PCL (w/w) were tested both with and without fibrin and UPI peptide coating. Meshes were incubated in platelet-rich plasma for 5 hours, rinsed with 0.9% saline solution to remove unadhered platelets, and then fixed overnight in 2.5% paraformaldehyde at 4° C. Meshes were gradually dehydrated in ethanol and then placed in a vacuum desiccator to dry the samples to maintain the PCL structure and cell shape. Critical point drying was not performed since supercritical CO_2 is a partial solvent for PCL. Cover glass and polytetrafluoroethylene (PTFE) mesh were used as positive controls. The samples were imaged via SEM with n = 3 samples per condition.

3.2.6 UPI peptide release profile

Conduits loaded with UPI peptides were immersed in PBS on an orbital shaker at room temperature. The PBS solution was collected and replaced with fresh PBS at multiple time points up to 7 days. The Pierce Bicinchoninic acid (BCA) assay was used to assess the total UPI peptide release following the manufacturer's protocol, except UPI peptides were used for the standard curve instead of the provided bovine serum albumen. The results are reported as the total accumulation of the protein (μg) through 7 days. A sample size of n = 3 was used for physical adsorption and n = 4 was used for the fibrin coating conditions.

3.2.7 Cell culture

HUVECs were seeded on electrospun meshes to determine the effects of UPI Peptide. The cells were cultured in endothelial growth media with the media supplement and 1% antibiotic, and they were passaged at 15,000 cells/cm^2. PDMS was utilized to hold the pure PCL sheets in place as described previously [197]. Meshes were wetted with ethanol and soaked in PBS prior to culture. HUVECS were seeded on the electrospun meshes and controls at a density of 5,000 cells/cm^2 and were exposed to different UPI peptide concentrations and coating methods. A PCL control mesh without peptides or a coating was included. An exogenous peptide in media control was also included, with 42 µg/mL of the peptide added to the media to match the release observed from the high peptide condition (i.e., fibrin + 500 µg/mL peptide solution coated on PCL conduits) after 30 min. Cultural media was changed every other day for 7 days prior to analysis with fluorescence imaging.

3.2.7.1 Fluorescence imaging

Meshes from the *in vitro* study were fixed in 4% paraformaldehyde, permeabilized with 0.1% Triton X, blocked with 5% goat serum, and mounted with DAPI mounting media. Alexa 488- Phalloidin was used to stain the F-actin in the cytoskeleton. After imaging, the contrast and brightness of the images were adjusted similarly for all samples (n = 4). The images of cell nuclei stained with DAPI were used with Image Pro software to quantify the number of cells per image (3 images per sample).

3.2.7.2 Cell migration assay

HUVECS were passaged onto 24 well plates at 15,000 cells/cm^2 to assess the effects of UPI on cell migration. After reaching confluency, the cells in the center were removed by scratching with a sterile pipette tip and the medium was changed immediately afterwards. Endothelial growth media containing UPI peptides with concentrations of 100 µg/ml and 0 µg/ml (control) were added to the wells. The wells were imaged at 0, 8, and 18 h time points via an all-in-one fluorescence Keyence BZ-800 microscope (Itasca, IL). The width of the gap was measured with at least 4 images per sample and n=3 samples / condition.

3.2.8 Arterial grafting

Sprague-Dawley rats (226-250g, male) were anesthetized with 2–3% isoflurane and 1–2 L/min of oxygen. All the surgical procedures were approved by the IACUC committee located at the University of Central Florida. Conduits were grafted into the abdominal aorta. Briefly, the abdominal aorta was separated from the vena cava and two vascular clams were placed on the arterial distal and proximal sites. The aorta was cut, and suturing was performed on both sides with a 9-0 nylon suture. After suturing, the clamps were removed and blood flow through the graft was verified. After confirming blood flow, the incision was closed, muscle suturing was performed, the skin was stapled, and analgesic was delivered. The animals were euthanized after 1 week of grafting, which represents an early time point to assess graft endothelialization. We chose an early time point (i.e., 1 week) in this study because most studies do not show graft endothelialization until at least 3 or 4 weeks

after grafting. There were n = 3 grafts per condition for the *in vivo* analysis, with the exception of the fibrin only condition that had n = 5 due to occluded grafts.

3.2.9 Ultrasound imaging

Ultrasound imaging was performed one-week post-surgery prior to euthanasia using a Vevo 31000 ultrasound machine. B mode was used to evaluate the graft position, and color Doppler and pulse wave Doppler were used to assess the blood flow and graft patency.

3.2.10 Histology

The conduits were harvested and mounted in OCT. Cyrosectioning was used to prepare 8 μm thick cross-sections. Staining was performed after fixing the sections with 4% paraformaldehyde for 10 minutes. H&E staining was performed to assess the cell infiltration within the scaffold wall and construct remodeling after grafting. The samples were stained following the manufacturer procedure. Masson trichrome staining was performed to assess construct remodeling and collagen fiber formation. The slides were submerged in Bouin's solution at 56℃ for 1 h. To differentiate the nuclei, the samples were immersed in Wiegert's hematoxylin and washed with tapping water. The samples were submerged in aniline blue to stain the collagen fibers and treated with 1% acetic acid solution, and slides were dehydrated with graded ethanol prior to mounting. After staining, all samples were mounted using coverslips and limonene as a mounting medium. Imaging was performed using the

Zeiss Axio Observer A.1 fluorescent microscope. Images of these sections were also used to measure wall thickness and luminal diameter for the different conditions.

3.2.11 Immunofluorescence staining

Ex vivo tissue sections and were fixed in 4% paraformaldehyde, permeabilized with 0.1% Triton X, blocked with 5% goat serum, and mounted with DAPI mounting media. Endothelial cell phenotype was investigated by staining the tissues with primary antibodies for CD31, von Willebrand Factor (vWF), and VE-cadherin. Alexa 633 secondary antibodies were used to detect the stains. Alexa 488-Phalloidin was used to stain the cytoskeleton. All conditions had a negative control that did not have a primary antibody added. After imaging, the contrast and brightness of the images were adjusted similarly for all samples. At least three images were taken per sample. A semi-quantitative analysis of the percent surface coverage was performed in ImagePro for the images. The length of the lumen covered by phalloidin, or VE-cadherin positive cells was divided by the total length of the lumen and multiplied by 100.

3.2.12 Statistics

Results are presented as mean ± standard deviation. For the total release profile, standard deviation was calculated using propagation of error. Statistical analysis was performed using JMP software. The statistical significance was determined using one-way ANOVA with Tukey multiple comparisons and a significance criterion of $p \leq 0.05$.

3.3 Result

3.3.1 Conduit characterization

The electrospun sheets and conduits were fabricated via electrospinning of pure PCL and a 10% collagen/PCL (w/w) blend onto a drum and 1.6 mm mandrel, respectively. SEM images showed that the fibers were randomly oriented, and the average fiber diameter fiber was 0.91 ± 0.21 μm for pure PCL and 0.67 ± 0.16 μm for the collagen/PCL blend conditions (**Figure 3.1**). For these conduits, the wall thickness was 242 ± 29 μm and 240 ± 8 μm for pure PCL and collagen/PCL, respectively. The conduits were also imaged after fibrin coating. SEM images showed the presence of a coating covering regions of the lumen of the conduit, but also with areas where the underlying electrospun fibers were visible. An anti-fibrinogen antibody confirmed the presence of fibrin within the conduit as well as its distribution. The densest fibrin was on the edges, but fibrin was also present throughout the conduit wall. Images showed that the coating was consistent on the adventitia and throughout the wall. Finally, the collagen-containing samples exhibited a higher expression of fibrin within the conduit wall. Control images demonstrated that that no significant non-specific binding or autofluorescence occurred.

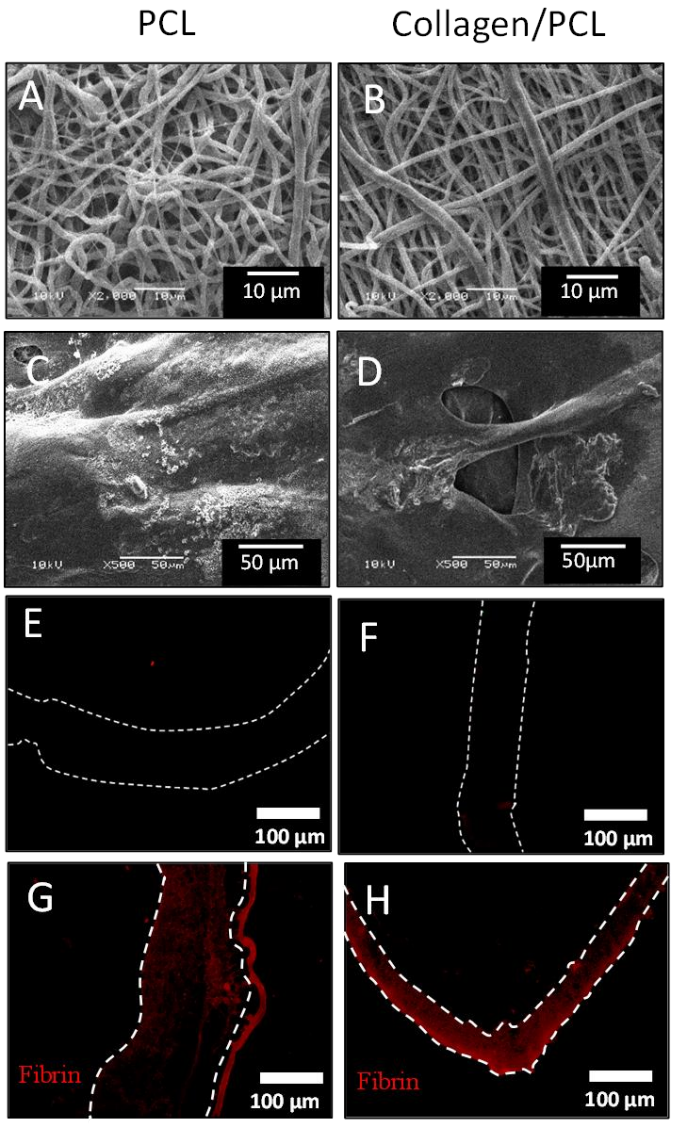

Figure 3.1. Fabricated scaffolds with fibrin coatings. Representative SEM images of electrospun fibers showing pure PCL (A) and 10% collagen/PCL (B) at the 2kx magnification. Images of the electrsopun lumen covered with a fibrin layer for pure PCL (C) and collagen/PCL (D) at 500x magnification. Immunofluorescence images on conduit cross sections before coating with fibrin for pure PCL (E) and collagen/PCL (F), and after coating for PCL (G) and collagen/PCL (H). n=3 samples / condition.

The ability of the samples both with and without UPI peptides to reduce platelet adhesion was assessed (Figure 3.2). SEM images showed negligible platelet adhesion for all experimental conditions: the uncoated mesh, mesh with a fibrin only coating, and mesh with both fibrin and peptide. SEM images also showed no platelet adhesion on areas where there was a gap in the fibrin hydrogel coating and the underlying electrospun fibers were exposed (Figure 3.2C; Figure S2, Supporting Information). The supplemental figure shows areas where there was a gap in fibrin coating, which occurred both with and without peptide incorporation. A higher magnification image also shows that the small fibrin fibers are present within the hydrogel coating. Finally, the glass and polytetrafluoroethylene (PTFE) control surfaces demonstrated that these platelets had the ability to attach and become activated.

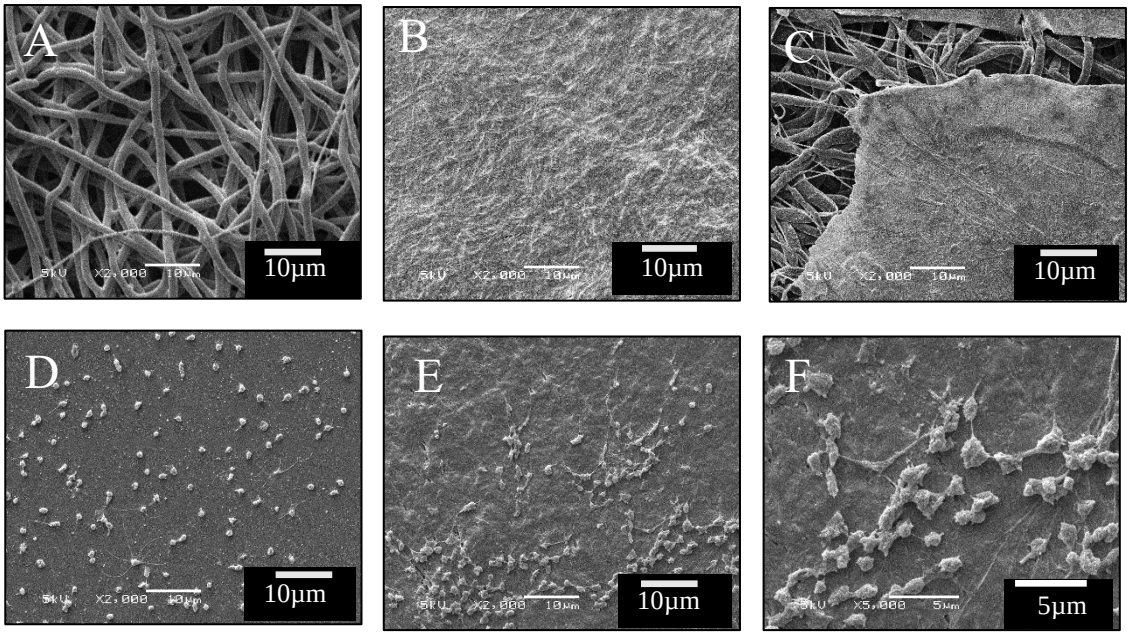

Figure 3.2. Assessment of platelet adhesion. Representative SEM images of samples exposed to platelet rich plasma to assess platelet adhesion. Pure PCL (A), fibrin only coating (B), and peptide with fibrin coating (C) samples are shown. The glass (D) and PTFE (E,F) controls are also shown. All images are at 2,000x magnification, except for (F) that is included at 5,000x to show platelet activation on the control surface. n=3 samples / condition.

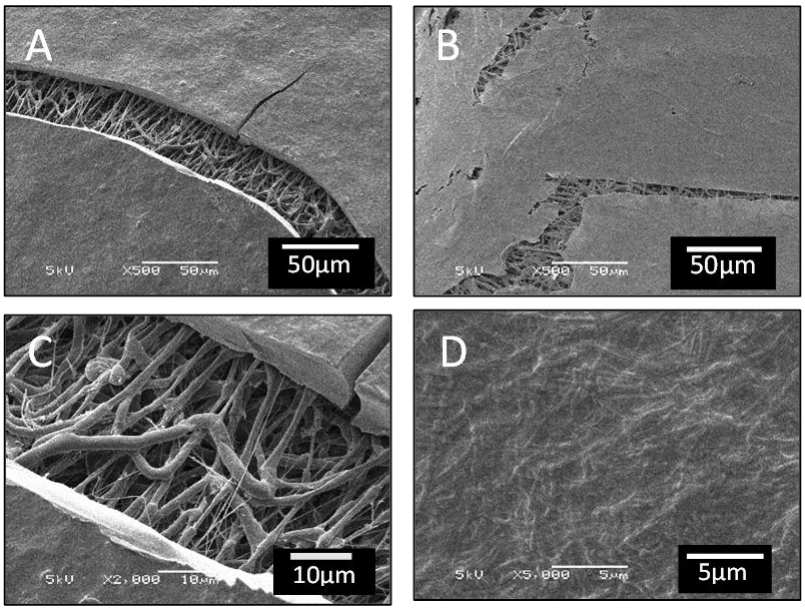

Supplemental Figure 3.2. Magnified images showing the fibrin coatings. Representative SEM images of samples exposed to platelet-rich plasma to assess platelet adhesion. Fibrin-only coating (A-C), and peptide with fibrin coating (B) samples at 500x magnification are shown. Fibrin-only coating (C, D) at 2000x and 5000x magnification, respectively, are included with the higher magnification showing the fibrin fibers. These images show some areas of PCL fibers that are covered by fibrin hydrogel. n=3 samples / condition.

3.3.2 UPI peptide release study

The ability for the coated conduits to release UPI peptides was assessed with 10, 25, 50, 100, 250, and 500 µg/mL of the peptide within the fibrinogen loading solution (**Figure 3.3**). PCL conduits with UPI peptides via physical adsorption were also tested. At the highest loading concentration (500 µg/mL), 6.4 times lower number of peptides were loaded and released with physical adsorption compared with the corresponding fibrin condition. Less of an impact of increasing the concentration of the loading solution was also observed with physical adsorption, except for the 500

µg/mL condition. However, most of the readings were at the limit of detection for the assay. For fibrin coating-based peptide delivery, there was a systematic increase in loading and release with increasing concentration of the peptide solutions. With a 500 µg/mL loading solution, 208 µg of the peptide was released from the fibrin coating. For both delivery methods, a burst release was observed. For example, the fibrin coating samples exhibited greater than 90% of the release after 4 h. The fibrin coating on 10% collagen / PCL conduits surprisingly provided lower peptide release than the coated PCL conduits, with released doses more like the samples with physical adsorption. For this reason, only pure PCL conduits were used for cell studies. The higher concentration peptide loading solution was used for *in vitro* studies to determine if the delivery method impacts EC response.

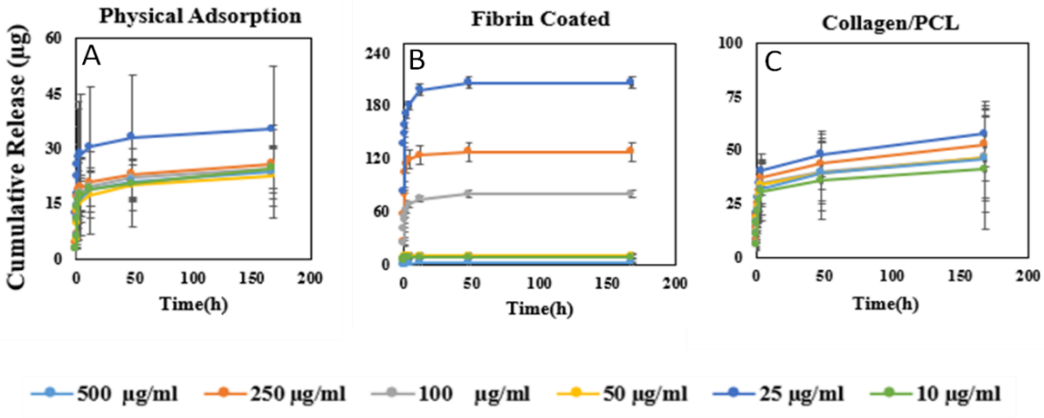

Figure 3.3. Cumulative UPI peptide release through 7 days in PBS. Different concentrations of the peptide in the loading solution are shown for physical adsorption (A), fibrin coating on pure PCL (B), and fibrin coating on collagen/ PCL (C) conduits. The error bars are larger due to the propagation of error method. n=3-4 samples / condition.

3.3.3 Effects on HUVECS *in vitro*

The PCL sheets were coated with a fibrin layer with/without UPI peptide to assess EC response. Other conditions tested included physically adsorbed peptide, peptide injected in media similar to prior studies, and a control electrospun mesh without fibrin or peptides (defined as PCL). According to the fluorescent images, the EC attachment was very limited on the PCL meshes in the absence of the peptide or a coating and for the peptide in the media (**Figure 3.4**). Adding the peptide through physical adsorption improved cell attachment and spreading in some locations, but the majority of the locations still exhibited limited cell attachment. The addition of a fibrin coating appeared to improve EC attachment as expected. However, the inclusion of peptides from a 500 μg/mL loading solution appeared to further increase cell adhesion and proliferation and resulted in more consistent cell adhesion between images for the same sample. A semi-quantitative analysis indicated that the fibrin + peptide condition had a significantly higher number of cells than the pure PCL condition ($p < 0.05$). The fibrin + peptide condition also appeared to have a higher cell number than the peptide in media condition, although the results were not statistically different ($p = 0.11$). Finally, samples that have peptides or a fibrin coating show F-actin staining primarily on periphery of the cell. Cortical actin filaments are typically observed with functional ECs. Finally, the ability for the peptide to impact EC migration was assessed with a scratch assay (**Supplemental Figure 3.3**). After 18 h, the ECs migrated significantly further when the peptides

were added exogenously to the media at 100 µg/mL compared to standard growth media (p=0.048) (**Figure 3.4H**).

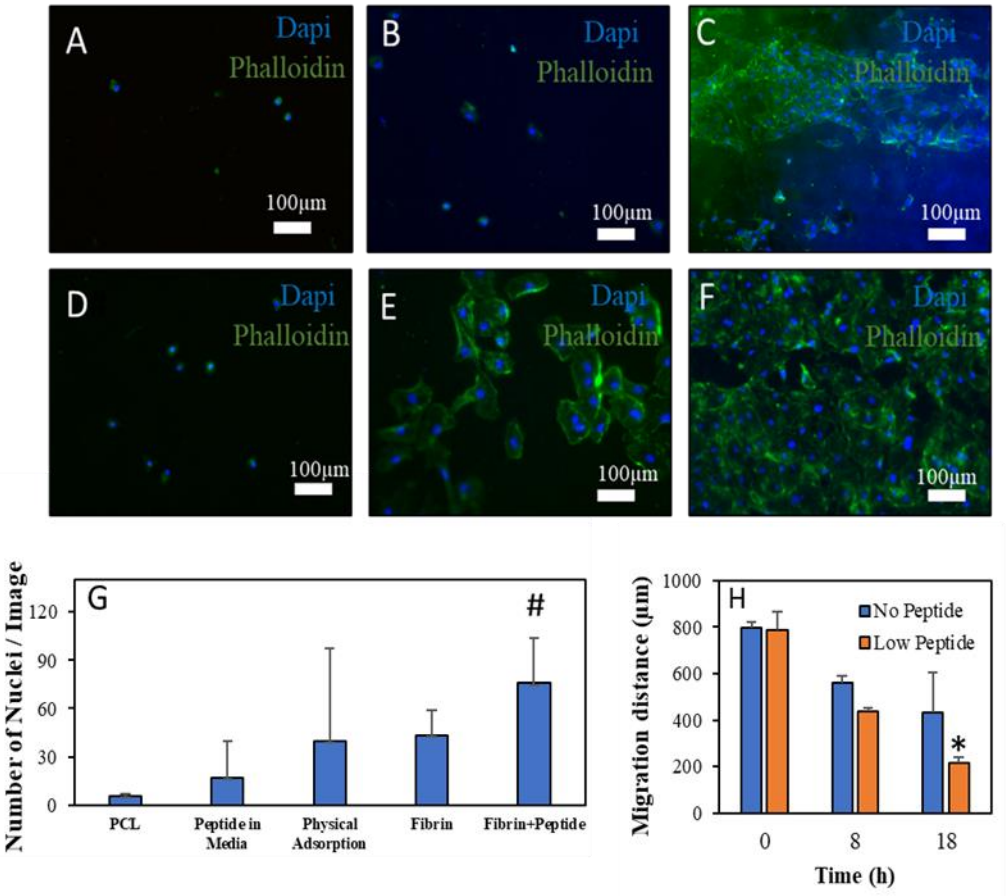

Figure 3.4. *In vitro* analysis of UPI peptides. Representative fluorescence images of the *in vitro* study on HUVECs. HUVECS were cultured on PCL meshes without peptide (A), peptide in media (B), physical adsorption (C, D), fibrin coating (E), and fibrin coating with peptides (F) after 7 days of culture. Includes phalloidin staining for actin structure and DAPI for cell nuclei. Physical adsorption showed more variability in cell density within a sample (C, D). # indicates statistical difference from the pure PCL condition. Quantified results for HUVEC migration over time with and without UPI peptide. Significance from (*) without UPI peptide. n=3 samples / condition.

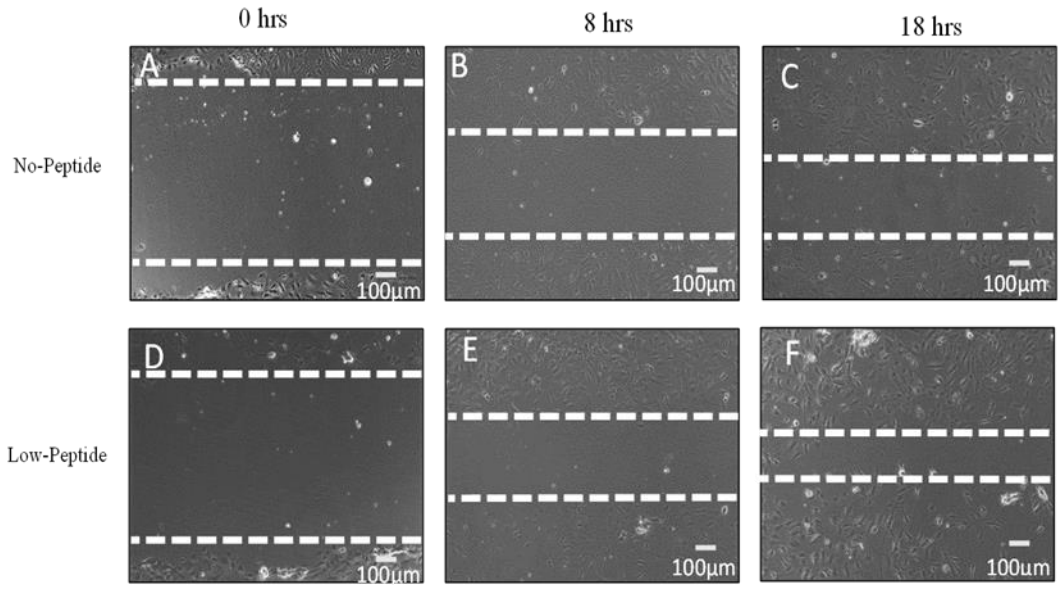

Supplemental Figure 3.3. Images for the cell migration test. Representative phase contrast images of HUVECs with and without UPI peptide over time. Shown are HUVEC right after scratching with no peptide (A, D), 8 hours after (B, E), and 18 hours after (C, D) with and without peptide. n=3 samples / condition.

3.3.4 Aortic grafting

The ability of the electrospun grafts with different wall thicknesses to hold sutures was assessed prior to grafting using conduits without UPI peptides (**Figure 3.5**). The thickness of the tested conduits was 117 ± 26.08 µm (low), 157 ± 17.95 µm (medium), and 407 ± 67.13 µm (high). For PCL conduits without a fibrin coating, a significant improvement in suture retention strength was observed by increasing the wall thickness from 117 to 157 µm. The suture retention strength did not significantly increase further by increasing the wall thickness to 407 µm (p = 0.52). A similar trend with conduit wall thickness was observed with inclusion of a

fibrin coating, but the suture retention strength was lower than the corresponding non-coated conduit for the medium wall thickness ($p < 0.05$). As a result, PCL conduits with a thickness in between the medium and high wall thickness conditions (i.e., 240 μm) were chosen because they were suturable and they were closer to the thickness of the native rat artery wall.

The *in vivo* response for electrospun conduits was assessed with the fibrin coating delivery method as well as pure PCL control conduits. Two different coating solution concentrations were tested: the 500 μg/mL that showed benefits *in vitro* and 100 μg/mL that provided a lower dose. All of the grafting conditions were able to hold the structures, although the fibrin only conditions were harder to handle during surgery. The graft viability was 100% within the rat abdominal aorta for the PCL control conduits and for the conduits coated with fibrin with the UPI peptides, indicating that early thrombosis after 1 week was not a concern for these grafts (**Figure 3.5**). However, only 40% of the fibrin only conduits remained patent and viable, with two failed grafts resulting in graft occlusion prior to the 1 week endpoint. The viable grafts from all conditions were imaged with ultrasound at 1 week prior to excision and analysis of the grafts. B-mode analysis confirmed the presences of the viable grafts without apparent stenosis or aneurysmal dilation. Color Doppler analysis verified graft patency and blood flow through the grafts.

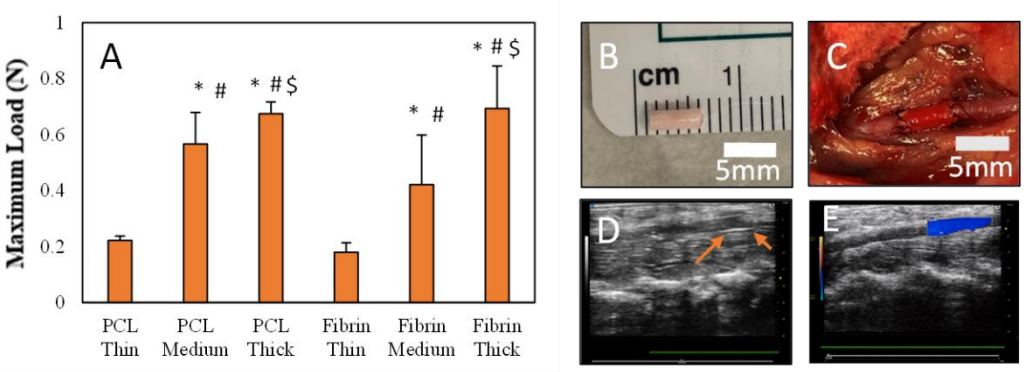

Figure 3.5. Suture retention and graft patency of PCL-based conduits. The result shows the suture retention strength for different thicknesses of PCL conduits with and without fibrin coating (A). n=3 samples / condition. Representative images of the graft and ultrasound analysis are also shown. Images of a fibrin + low peptide graft prior to implantation (B) and after suturing (C). Shown are ultrasound B-mode (D) and color Doppler (E) images of the grafted conduit. Arrows in the B-mode image show the location of the graft. Significance from (*) fibrin thin, (#) PCL thin, and ($) fibrin medium.

3.3.5 *In vivo* impact of UPI peptides

Histological staining showed different responses between conditions after 1 week of grafting. All conditions showed some cell infiltration and tissue deposition with H&E staining (**Figure 3.6**). Adventitial tissue deposition was the highest for fibrin and high peptide (i.e., 500 µg/mL loading solution) conditions, but this was also noticeable for the PCL only condition. These conditions exhibited collagen deposition after only 1 week, especially in the adventitia, as observed with Masson's trichrome staining (**Supplemental Figure 3.4**). However, the remodeling response between these conditions was noticeably different. The PCL samples exhibited cells and tissue throughout the thickness of the graft wall. The fibrin only samples

exhibited cells and tissues throughout most of the graft wall, but with a few areas that did not remodel. Interestingly, the inclusion of the high peptide concentration within the fibrin coating prevented cell infiltration and tissue remodeling near the lumen. The light pink areas show unremodeled fibrin coating that are also clearly visible in the fibrin only grafts that failed within the first couple of days (**Figure 3.6E**). Evidence of minor thrombosis at the mid-graft was shown for all conditions, although none of the PCL, high peptide, or low peptide grafts failed. One of the three fibrin + high peptide grafts had more extensive thrombosis, but the rat survived and there was still blood flow through the graft at the 1 week timepoint. Semi-quantitative analysis of the histology images further suggested that the fibrin only and high peptide conditions had the thickest graft walls due to the thick adventitial layer (**Supplemental Figure 3.5**). However, the results were not statistically significant due to high variability between samples. There was no significant difference in luminal diameter in the mid graft between conditions.

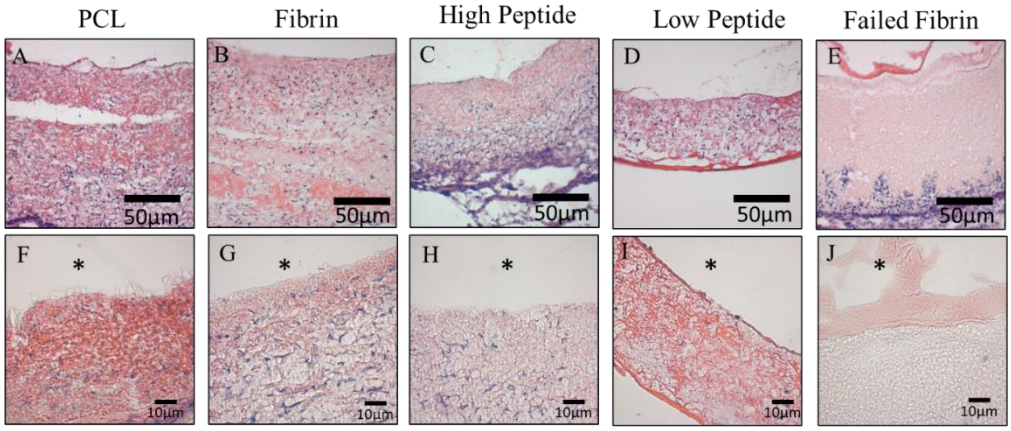

Figure 3.6. Histology results after grafting. Representative H&E images (A-E) at 20x and (F-J) at 40x magnifications. Shown are pure PCL (A,F), fibrin only (B,G), and fibrin with high (C,H) and low (D,I) peptide concentrations. One of the failed fibrin only grafts with limited remodeling is also shown (E,J). The graft lumen is on the top for all samples. * Indicates the lumen of the grafts. n=3 samples / condition.

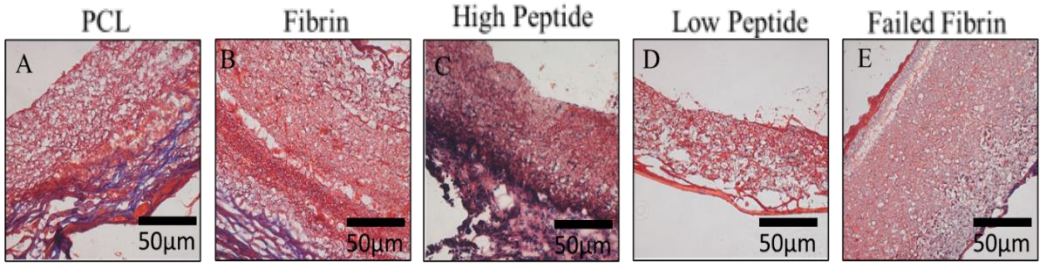

Supplemental Figure 3.4. Masson Trichrome images after grafting. Shown are pure PCL (A), fibrin only (B), fibrin with high (C) and low (D) peptide concentrations. One of the failed fibrin only grafts with limited remodeling is also shown (E) at 20x magnification. The graft lumen is on the top for all samples. * indicates the lumen of the grafts. n=3 samples / condition.

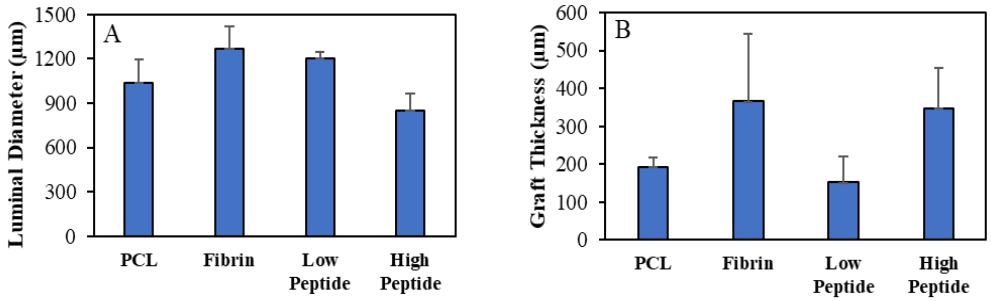

Supplemental Figure 3.5. Quantitative analysis of histology samples. Luminal diameter (A) and wall thickness (B) are shown. n=3 samples / condition.

3.3.6 Endothelialization i*n vivo*

Fluorescence imaging showed the extent of endothelialization after only 1 week for the different conditions (**Figure 3.7**). Phalloidin staining showed a partial layer of cells with stained cytoskeletons within in the lumen for the PCL and fibrin only conditions, but a complete monolayer for the low peptide condition. This was confirmed with a semi-quantitative analysis that showed that there was a significantly higher percent surface coverage when a low concentration of the UPI peptide was present (p = 0.047). The high peptide condition is not shown, but negligible cells were found in the lumen. It was also noticeable that only the fibrin without peptides condition had cells with intense phalloidin staining at the interface between the outside of the graft and new adventitial tissue. vWF staining was observed for all conditions on both the adventitial and luminal sides, but the staining was most intense at the lumen for both the fibrin only and low peptide conditions. Expression of the EC marker VE-cadherin was observed in the lumen for all of these conditions, indicating the presence of functional endothelial cells. Quantification of

the images appeared to show that percent coverage of VE-cadherin positive cells at the lumen was higher for the low peptide compared to fibrin only condition. However, the results were not statistically different due to high variability. No primary antibody control sections confirmed that the immunofluorescence results were not from autofluorescence background (**Supplemental Figure 3.6**).

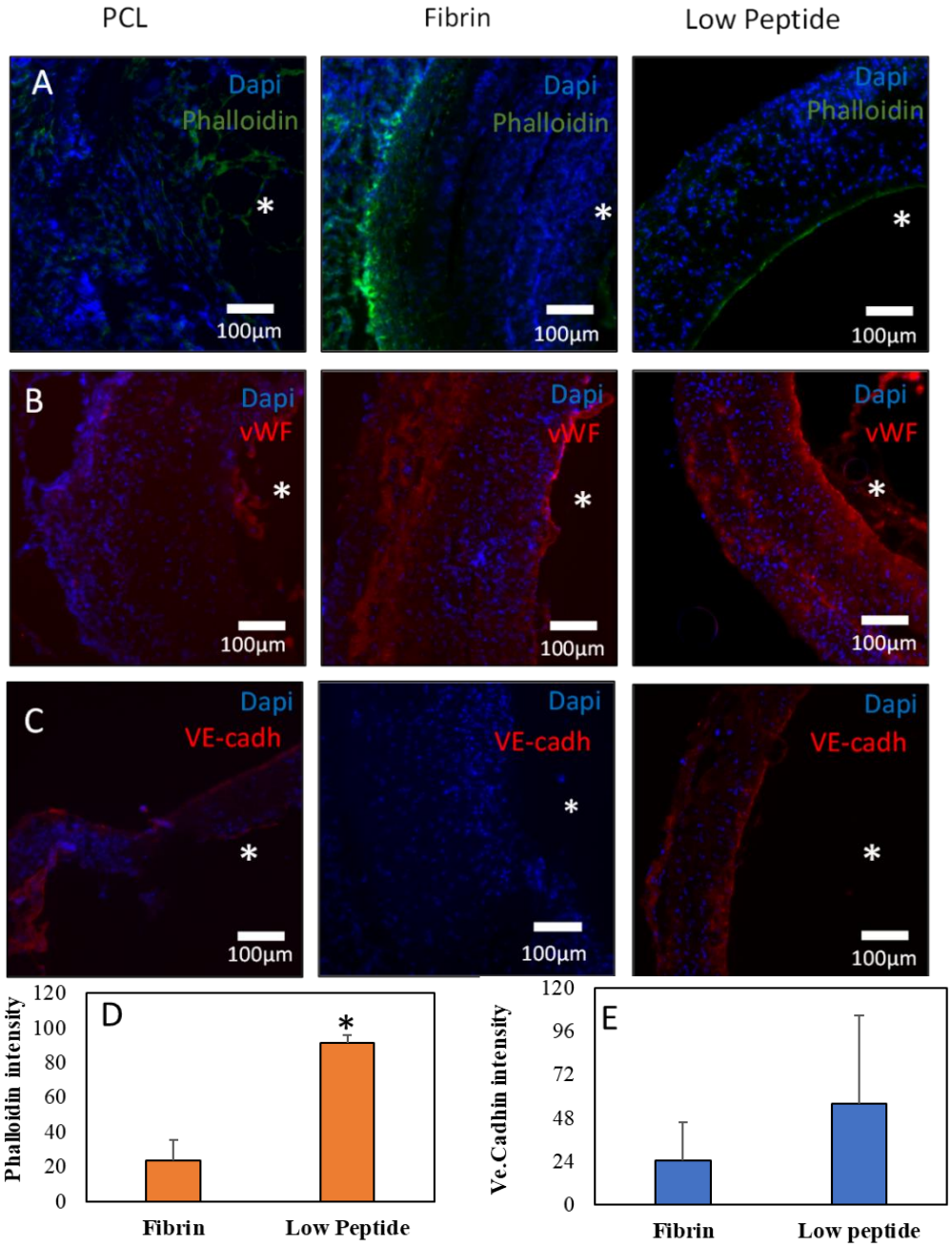

Figure 3.7. Immunofluorescence staining of grafts and controls for endothelial cell markers. Representative images 1 week after grafting for pure PCL, fibrin only, and fibrin + low peptide conditions. The samples are stained for the cytoskeleton using phalloidin (A), vWF (B), and VE-cadherin (C). Nuclei are stained with DAPI. * indicates the lumen of the grafts. Phalloidin (D), and VE-cadherin (E) quantification are shown for fibrin only and low peptide conditions. Significant difference (*) from the fibrin only condition. n=3 samples / condition.

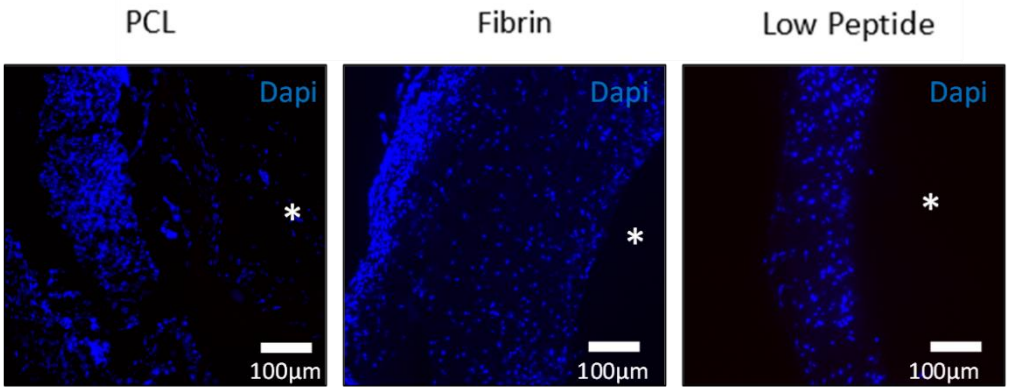

Supplemental Fig 3.6. No primary antibody controls for immunofluorescence staining. The results are shown for the PCL, fibrin only, and low peptide conditions.

3.4 Discussion

Endothelialization of vascular grafts remains a critical challenge for the field and is important to prevent thrombosis and graft occlusion. Most studies focus on adding a pre-seeding step with ECs, but that also can have challenges for cell retention after grafting and adds to the complexity for FDA approval. Our group and others are investigating materials and methods to graft acellular constructs and promote endothelialization in the body. UPI peptides are a promising approach to modulate ECs, and in this study we applied these peptides to vascular grafts and delivered them locally from the graft for the first time. We demonstrated that a fibrin coating technique can provide controlled doses of UPI peptides that impact endothelial cells both *in vitro* and *in vivo*. We also demonstrated that response and required dose was different between cell culture and in the rodent model.

This study provided a local release of the peptides from our graft instead of the systemic injection that has been used previously for these UPI peptides. These peptides were designed with D-isomers in the UIM region to improve stability while circulating in the blood [117], but local delivery can help to further improve peptide stability as well as provide a high local concentration near the ECs of interest. A variety of coating methods have been used for drug delivery from biomaterial scaffolds (e.g., fibrin coating and covalent binding to the scaffold), with goals including controlling the overall dose and the time of release. For example, this study showed the ability to deliver peptides via physical absorption onto electrospun PCL scaffolds, but with a burst release and, more importantly, low peptide loading. This is consistent with the literature for peptides adsorbed on a variety of types of surfaces [35,36]. Delivery of UPI peptides encapsulated within a thin fibrin coating in this study also primarily provided a burst release profile, but with up to six times higher loading and release than physical adsorption. We also noted that the chemistry of the electrospun scaffold that the coating was applied to impacted the loading and/or release, with much lower release in PBS when coating the collagen/PCL scaffolds. This is likely partially related to lower loading from a thinner or less consistent fibrin coating on the inside and outside of the grafts than with pure PCL. However, the fact that the peptide can better adsorb on the less hydrophobic surface when collagen is included suggests that some of the peptide may release at a later time [197]. This is important since one of the challenges for endothelialization of vascular grafts in the clinic is promoting EC migration from the anastomosis. Overall, the fibrin and

peptide coated PCL scaffold provided high doses of the peptide that can be released, and can be endocytosed enabling the peptides to block internalization of VEGFR2 by native epsins [116]. Importantly, even though this technique provides a burst release, this was enough to positively impact both ECs *in vitro* and remodeling and endothelialization *in vivo*.

Both the coating with UPI peptides and the coating with only fibrin appeared to improve EC attachment to the electrospun surfaces *in vitro*. The fibrin was expected to improve EC attachment due to increased hydrophilicity compared to the hydrophobic PCL fibers that typically exhibit limited cell attachment without a coating [200], [201]. The results also suggest that the UPI peptides promoted cell attachment to the surface, as shown with physical absorption as well as cell attachment when including peptides in the coating compared to fibrin alone. Although verifying the mechanism is beyond the scope of this study, our prior analyses have investigated the mechanism of UPI peptide impacts on ECs when delivered exogenously and verified the specificity of this particular peptide with controls (e.g., scrambled control peptides) [116]. The primary impact of peptides in these *in vitro* studies appears to be due to improvement in cell binding since the peptide in media condition exhibited limited attachment and rounded cells like the PCL only control. The peptides delivered exogenously in media would be expected to impact ECs that were able to bind to a biomaterial surface, based upon prior cell culture studies [117]. However, this cell culture result emphasizes the potential benefits of inclusion of peptides within the local scaffold on both cell attachment and

the ability for these cells to spread with the cytoskeleton at the periphery like quiescent ECs [202]. *In vivo* studies were still necessary though to fully assess the potential benefits of including UPI peptides within tissue engineered vascular grafts.

In this study we performed grafting for 1 week into a rat abdominal aorta. The initial optimization of graft wall thickness was important to balance suture retention strength with prevention of a large mismatch in size between the graft and the surrounding artery at the anastomoses. Suturability of electrospun PCL grafts has not been a concern in our prior studies, but this study surprisingly showed that the inclusion of a fibrin coating may reduce suture retention strength. The reason for this is not clear, but it may be related to the crack propagation mechanism of failure that occurs with a suture retention test. It has been reported that the initial defect created by the needle during suturing dominates initial failure [203]. Individual fibers within highly-porous electrospun meshes can typically move, minimizing damage from the needle, but the inclusion of a continuous coating layer may limit movement of the electrospun fibers as the needle is inserted. Further, adding a fibrin component is not expected to substantially improve suture retention because of the much lower mechanical properties of hydrated fibrin fibers [204].

Our results showed that the PCL and low peptide-containing grafts were all viable, but many of the fibrin only grafts failed due to graft occlusion. This was initially surprising since fibrin by itself has been shown to not promote thrombosis [194], and fibrin based grafts have been used successfully for vascular tissue engineering [205], [206]. However, there are other studies that suggest that fibrin

coatings can promote platelet adhesion [194], [207]. It appears that differences such as free fibrinogen vs. crosslinked fibrin within a coating may provide different results [208]. In this study, our results showed that neither the PCL mesh nor the fibrin coating promoted platelet adhesion *in vitro*. We have shown previously that fibrous meshes made from PCL exhibit negligible platelet adhesion [197]. It was observed that these fibrin only grafts were more difficult to handle during surgery and exhibited a thick graft wall after 1 week in the rat. The grafts were initially patent at the time of surgery and the mid graft region did not exhibit significant stenosis compared to the other conditions after 1 week, but these fibrin grafts appeared to fail from thrombosis at the anastomoses. It is likely that the hemodynamics was disrupted contributing to thrombosis and narrowing at the anastomoses. It is also possible that uncrosslinked fibrinogen and extra thrombin in the graft may have also contributed to graft thrombosis [209]. Either way, it is important to note that the inclusion of UPI peptides within the fibrin coating provided high graft viability. The fibrin coating technique was a useful strategy for this study because it allowed an assessment of clear endpoints (i.e., viability) that is typically not possible within healthy rodent models. Future development of the graft could consider either a fibrin coating or another coating material to deliver the UPI peptides.

One of challenges with animal models is making sure that they are relevant for the clinical situation. For example, grafts in rodent models will typically endothelialize by several months [210]. Further, our prior study showed that graft endothelization correlated with the presence of intimal hyperplasia instead of the

type of graft, unlike what we observed for inflammatory and remodeling responses [211]. Finally, we had observed complete endothelialization after longer grafting times (e.g., 10 months) [212]. Thus, we chose an early time point (i.e., 1 week) in this study to better compare the potential for endothelialization because most studies do not show graft endothelialization before 3 or 4 weeks after grafting. With a shorter time point, this study showed that partial endothelialization occurred by 1 week for the PCL and fibrin only control conditions, but only the condition with a low concentration of the peptides provided a complete monolayer of endothelial cells in the mid graft. This suggests both the importance of adding the peptides as well as the importance of controlling the dose.

Major differences in remodeling were also observed between the different conditions. For example, fibrin promoted the production of additional tissue. This is consistent with prior studies using fibrin-based biomaterials that showed significant benefits on their remodeling and the production of collagenous tissue [213] . The inclusion of UPI peptides within the graft changed the *in vivo* response and modulated the cell ingrowth and tissue deposition. Since epsins are endocytic clathrin adaptor proteins that recruit plasma membrane proteins to clathrin-coated pits, adding epsin mimetic peptides can block receptor internalization and subsequent degradation by the native epsin protein [123]. The ability to prevent internalization of VEGF receptor 2 and enable longer-term VEGF signaling can explain why low doses (i.e., 100 μg/mL in the loading solution) of the peptide are able to promote the formation of the monolayer of ECs in the lumen of the graft. The function of the

epsin mimetic peptides may also explain why the inclusion of a high peptide dose can prevent cell infiltration and remodeling. Clathrin-mediated endocytosis is important for a variety molecules and for cell functions in addition to internalization of the VEGF receptor [183]. Large-scale blocking of endocytosis with very high levels of these peptides may interfere with these other cellular functions [214], [215]. It is also possible that the iRGD region of the peptide can impact cell adhesion at a high dose. However, if this would increase or decrease adhesion is not currently clear since released cell-adhesive peptides not bound to a surface have been shown to decrease cell attachment [216], but cross-talk has also been shown between $\alpha_v\beta_3$ integrin activation and VEGFR2 in angiogenesis [217]. While this may be possible locally within the graft where there is a high peptide concentration, negative systemic effects are not expected. Our prior studies demonstrated a broad therapeutic window with injection of peptides at high dose (up to 50 mg/kg of UPI peptides or 1,250 µg equivalent amount when consider the mass of the mouse) exhibiting limited systemic side effects and the glucose and lipid metabolism remaining normal [117]. Additionally, the µg of UPI peptides we are releasing in this study represent a low dose in circulation when it is diluted throughout the blood and distributed throughout the body. Finally, it is important to perform *in vivo* optimization of peptide dose since the *in vitro* loading that worked well did not work as well *in vivo*. Overall, this study demonstrates that a proper dose of epsin mimetic peptides can lead to multiple beneficial responses, with the promotion of graft endothelialization being only one

of them. The specific mechanism for these responses will be investigated in future studies.

The low dose UPI peptide condition in this study showed promise as part of a vascular graft. The *in vitro* release profile indicates that the released amount of peptide in this study (80 µg) was lower than the equivalent amount used systemically in prior studies (i.e., 20 mg/kg or 500 µg equivalent when considering the mass of the mouse), but it was delivered locally from the surface of the graft that the ECs would attach to [123]. The low dose of UPI peptides appeared to enable cell infiltration and remodeling throughout the graft wall that is desirable for tissue engineering, and simultaneously prevent the formation of thick tissue observed with the fibrin only coating graft. This difference is clearly observed with the adventitial layer, where the fibrin and PCL only conditions show a thicker, collagen-rich fibrous capsule but the low peptide condition shows only a thin non-collagenous layer on the adventitial side. While fibrous capsules can remodel around vascular grafts, studies often focus on ways to reduce or prevent them [218], [219]. This study only analyzed an early time point for fibrous capsule formation and fibrous capsules still may form at later time points [220]. However, the results suggest that there is a decrease in the rate of fibrous capsule formation with incorporation of a low concentration of peptides. Even more importantly, the low peptide grafts enabled complete endothelialization of the mid graft. This is important for preventing initial thrombosis and early graft failure that can occur within the first month in patients [221]. Future studies with longer grafting times will be needed to assess the impact

of the UPI peptides and the resulting EC monolayer on intimal hyperplasia. Finally, while this study showed important benefits of UPI peptides released from a graft within 1 day, different coatings and extended release methods may be able to provide further benefits.

3.5 Conclusions

In conclusion, this study demonstrated that epsin-mimetic UPI peptides delivered locally from electrospun vascular grafts were able to promote EC attachment and proliferation in cell culture and promote endothelialization and positive graft outcomes *in vivo*. The fibrin coating technique results in a burst release, but provides a high enough peptide loading to provide a positive benefit on ECs. The delivery of the peptides within a fibrin coating provided a significant improvement for EC attachment, migration, and growth *in vitro*. The inclusion of peptides also prevented graft thrombosis and failure that was observed for grafts with a fibrin coating alone. Further, it is noteworthy that the impact of these peptides is dependent on dose. Importantly, aortic grafts with lower dose (i.e., 100 μg/mL) provided a unique response *in vivo* compared to fibrin only and higher dose conditions, and provided combined beneficial impacts not observed with these other graft conditions. This included a consistent monolayer of functional ECs after only 1 week of grafting as well as prevention of thick adventitial tissue deposition. This can allow the formation of a functional endothelial monolayer within a vascular graft that is important to address the clinical concerns with thrombosis and graft occlusion.

3.6 Declaration of competing interest

Dr. Hong Chen has patent #US11084852B2 related to the epsin mimetic peptides. The authors declare that do not have any other competing financial interests or personal relationships that could have appeared to influence the work reported in this paper.

Acknowledgement

This study was supported by an American Heart Association grant (18AIREA33960390https://www-sciencedirect com.portal.lib.fit.edu/science/article/pii/S1742706117306220) awarded to C.A. Bashur

Chapter 4: Extended release of epsin mimetic UPI peptide on endothelization of vascular grafts

4.1 Introduction

Coronary artery diseases are the leading causes of global mortality, responsible for over 17 million deaths annually. Small-diameter vascular grafts, with a diameter < 6mm, encounter numerous challenges, including lower graft patency and higher early-stage thrombosis risk, necessitating further modifications [222]. Tissue-engineered vascular grafts (TEVGs), utilizing various fabrication methods have gained significant interest. Pre-seeding techniques have some promising results for mitigating early-stage thrombosis in such grafts. However, FDA approval for pre-seeded TEVGs remains challenging [166]. For this purpose, researchers have recruited acellular grafts to reduce long-term intimal hyperplasia and induce endothelization within the TEVGs.

In rodent models, acellular TEVGs have typically demonstrated endothelialization within three to four weeks post-surgery and full endothelization is different depending on the material used in TEVGs. Additionally, in most cases observed in rat models, rapid endothelialization primarily occurs at the graft's anastomosis sites rather than in the midsection [223]. For instance, implanting a nanofibrous PCL scaffold within the rat aorta showed endothelialization at the anastomosis site ten days post-implantation, leaving the central portion of the graft without morphologically differentiated endothelium [224]. However, ensuring rapid and consistent endothelialization across the entire graft is crucial for the clinical

advancement of these grafts. To address this challenge, researchers are exploring various modifications, including novel surface treatments, the integration of active compounds to induce endothelialization, and enhancements in the controlled local release of these compounds.

Various techniques have been employed to enhance endothelialization and graft remodeling in TEVGs. One approach involves peptide delivery to improve ECs attachment and proliferation. For instance, incorporating RGD peptides onto PET polymer surfaces enhances endothelial cell adhesion. In addition to RGD peptides, other peptide sequences have also been explored to facilitate EC attachment. The REDV sequence, derived from fibronectin [225], has been utilized on synthetic surfaces and have shown EC attachment and migration, and preventing smooth muscle cells proliferation [226]. However, the existing peptides encounter obstacles such as biofouling, where the treated surface absorbs other active compounds from the bloodstream, ultimately resulting in graft failure over time [227]. Additionally, some of these peptides have induced platelet adhesion on the graft surface, leading to graft failure. These challenges have hindered the progression of these peptides into clinical applications. Thus, there remains a pressing need to develop grafts that facilitate early-stage endothelialization.

Epsins are from family endocytic clathrin adaptors containing ubiquitin-interacting motifs (UIM). UIM promotes the internalization of VEGFR2 to clathrin-coated pits, thereby attenuating EC proliferation via VEGF signaling. This mechanism suggests that blocking epsin signaling could benefit long-term vascular

graft viability, particularly in atherosclerosis prevention [228]. In our previous work, we used UPI peptide that consisted of UIM, plasma membrane anchoring, and internalizing RGD (iRGD) homing sequences. The iRGD component enhances specificity by targeting αvβ3 integrins on ECs, facilitating blocking VEGFR2 internalization. In our previous study, we investigated the effects of incorporating the UPI peptide within a fibrin-coated scaffold and examined its impact on endothelialization both in vitro and in vivo. Additionally, we observed enhanced cell attachment on a hydrophilic surface in vitro. Furthermore, endothelial cell markers indicated functional endothelialization, cell infiltration, and graft remodeling *in vivo* one-week post-surgery. While these results demonstrate the beneficial impact of the initial burst release of the UPI peptide from the fibrin coating on promoting rapid endothelialization of the grafts, we hypothesized that a more sustained release is necessary for achieving functional vascular graft.

In this research, UPI peptides were incorporated into microparticles made from PLGA using a double emulsion method for more sustained release. These microparticles were further included within a gelatin coating and then embedded into electrospun PCL conduits. Water loaded microparticles were included as a control to evaluate UPI peptide release from the microparticles. The effects of UPI peptide on cell specificity, attachment, migration, and proliferation were evaluated using HUVECs *in vitro*.

4.2 Material and method

4.2.1 Materials

All disposables, chemicals, and biological supplies were purchased from Thermo Fisher Scientific (Pittsburgh, PA) unless specified otherwise. Polycaprolactone (PCL) with inherent viscosity of 1.2 dL/g in chloroform was from Lactel Absorbable Polymers (Pelham, AL). Gelatin was purchased from Sigma (Burlington, MA). PLGA with inherent viscosity of 0.65 dL/g in 1, 1, 1, 3, 3, 3-hexafluoro-2-propanol was purchased from Lactel Absorbable Polymer. UPI peptide was synthesized by a solid phase fluorenylmethyloxycarbonyl (FMOC) method as described elsewhere [123]. All primary antibodies were purchased from Abcam (Cambridge, MA), and all secondary antibodies were from Thermo Fisher. Polydimethylsiloxane (PDMS) was purchased from Ellsworth adhesives (Germantown, WI).

4.2.2 Scaffold fabrication

4.2.2.1 Electrospinning and characterization

Conduits were fabricated by electrospinning 13% PCL (w/w) onto a stainless-steel mandrel with a diameter of 1.6 mm. The solution was prepared at 13 wt. % by dissolving in 1, 1, 1, 3, 3, 3-hexafluoro-2-propanol (HFIP). Electrospinning was performed using a 22-gauge needle, 15 kV voltage gradient, a throw distance of 10 cm, and a flow rate of 0.8 mL/h. Consistent thickness and the random orientation of the fibers were achieved via lateral movement and slow rotation of the mandrel (<100 rpm). The conduits were removed from the rod by using ethanol, segmented into 2

cm long sections, and stored in a desiccator. Scanning electron microscopy (SEM) was used to characterize the fiber diameter (n = 3 samples / condition, n>100 measurements/sample). Cross-sections were also prepared with cryo-fracture for thickness measurements (n = 3 samples / condition). The electrospun conduits were mounted, sputter-coated with gold, and then imaged. ImagePro Plus® software was used to analyze the SEM images.

4.2.2.2 Preparation of PLGA microparticles

The fabrication of PLGA microspheres was adopted from literature with modifications in the water-in-oil-in-water (w/o/w) double emulsion method [229]. In brief, 150 mg of PLGA was dissolved in 3 mL of methylene dichloride, and peptide surrogate protein in deionized water and water was introduced to the organic phase, followed by emulsification using a homogenizer for 80 seconds at 10,000 rpm. The resulting single emulsion (w/o) was transferred into a 10 mL solution of aqueous polyvinyl alcohol (PVA) as well as PVA and NaCl (2% w/v and 5% w/v, respectively) and stirred at 700 rpm for 5 minutes. The solution was then further diluted in 5% NaCl. The resulting solution was stirred at 700 rpm for 6 hours to facilitate the evaporation of the organic solvent. The microparticles were washed three times with distilled water, collected by centrifugation at 2700 rpm for 5 min, and lyophilized. Further, to optimize the fabrication process, UPI peptides in deionized water and water as control was introduced to the organic phase, followed by emulsification. The resulting single emulsion (w/o) underwent the same procedure described above, including transfer into the aqueous PVA solution with

NaCl, stirring, dilution, and further emulsification. After the solvent evaporation step, the microparticles were washed three times with distilled water, collected by centrifugation at 2700 rpm for 5 minutes, and then lyophilized. The microparticles were further hydrated and lyophilized to remove the extra PVA. The microspheres were imaged before and after lyophilization using scanning electron microscopy (SEM). The samples were mounted, sputter-coated with gold, and then imaged at 10 KV accelerating voltage. ImagePro Plus® software was utilized to analyze the microspheres' diameters.

4.2.2.3 Gelatin - microparticle coated PCL conduits

A 3D-printed construct with a diameter of 1.4 mm was utilized to integrate a gelatin coating within the lumen of PCL conduits. The PCL conduits were dipped in DI water and wetted with ethanol prior to gelatin coating. The samples were then positioned on the 3D printed construct, and a 5% gelatin solution was applied to coat both the lumen and periphery. The conduits were allowed to rest overnight to facilitate the drying process of the hydrogel, after which they were gently removed via tweezers and then stored in desiccator. The samples were cut longitudinally and mounted on SEM holder for characterization.

4.2.3 UPI peptide release profile

Microparticles containing UPI peptides were placed in deionized water (DI) on an orbital shaker at room temperature. The DI water was periodically collected and substituted with fresh DI water at different time intervals for up to 28 days. Total UPI peptide release was assessed using the Pierce Bicinchoninic Acid (BCA) assay.

4.2.4 Cell study in vitro

4.2.4.1 Cell migration

HUVECS were passaged onto 24 well plates at 15,000 cells/cm^2 to assess the effects of UPI on cell migration. After reaching confluency, cell population in the center were removed by scratching with a sterile 200 µl pipette tip and the medium was changed immediately afterwards. Endothelial growth media containing UPI peptides and scramble peptide with concentrations of 100 µg/ml and 37 µg/ml were added to the wells. A control condition was established with cells only, without any peptide (0 µg/ml concentration). The wells were imaged at 0,3,8, and 18 h time points via an all-in-one fluorescence Keyence BZ-800 microscope (Itasca, IL). The width of the gap was measured and analyzed over time.

4.2.4.2 Cell attachment

GFP+ HUVECS and HUVECs were passaged on 5% spin coated PCL at 15000 cells/cm^2 to assess the effects of UPI peptide on cell attachment. Right after passaging the cells, UPI peptide and scramble peptide at concentration of 100 µg/ml were added to the wells. Cells only condition with 0 µg/ml peptide was established as control condition. The cells were imaged via the Keyence microscope 3 days post culture.

4.2.5 Statistical analysis

Results are presented as mean ± standard deviation. For the total release profile, standard deviation was calculated using propagation of error. Statistical

analysis was performed using JMP software. The statistical significance was determined using one-way ANOVA with Tukey multiple comparisons and a significance criterion of $p \leq 0.05$.

4.3 Results and discussion

4.3.1 PLGA microparticles fabrication

PLGA microparticles in this study were prepared using w/o/w double emulsion technique. The SEM results showed that the biodegradable microparticles were spherical and exhibited a smooth surface morphology with some porosity. Moreover, addition of NaCl showed a reduction in microparticles porosity and enhancement of the stability of microparticles (figure 4.1). Incorporating NaCl into the aqueous phase elevates osmotic pressure, forming more compact microparticle internal structures, reducing the protein diffusion to this external aqueous phase and consequently increasing both encapsulation efficiency and protein loading. Furthermore, the implementation of an additional homogenization step prior to incorporation led to a notable reduction in the average microparticle size [230], reducing microparticles diameter from 13.15 ± 2.26 to 6.62 ± 4.07.

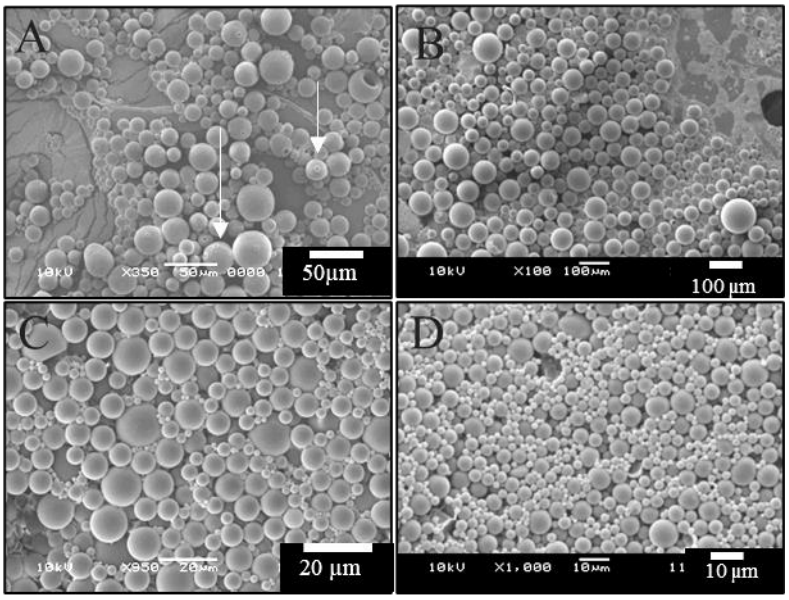

Figure 4.1. SEM images of Albumin loaded PLGA microparticles before and after addition of NaCl in the double emulsion after lyophilization (A, B). SEM images of UPI peptide loaded PLGA microparticles before and after addition of extra homogenization step after lyophilization (C, D).

4.3.2 Scaffold fabrication

The conduits were electospun using pure PCL blend onto a 1.6 mm mandrel. SEM images showed that the fibers were randomly oriented. For these conduits, the wall thickness was 217 ± 15.06 µm for pure PCL. The conduits were also imaged after gelatin coating. SEM images showed the presence of a gelatin coating covering regions of the lumen of the conduit, but also with areas where the underlying electrospun fibers were visible (figure 4.2). The gelatin coating was mostly consistent throughout the conduits. Control microparticles were also blended within the gelatin coating. SEM images showed the presence of PLGA microparticles within

the gelatin coating. However, the microparticles' distribution was not consistent throughout the coating and needs further investigation to determine the consistency of gelatin coating and microparticles within the coating.

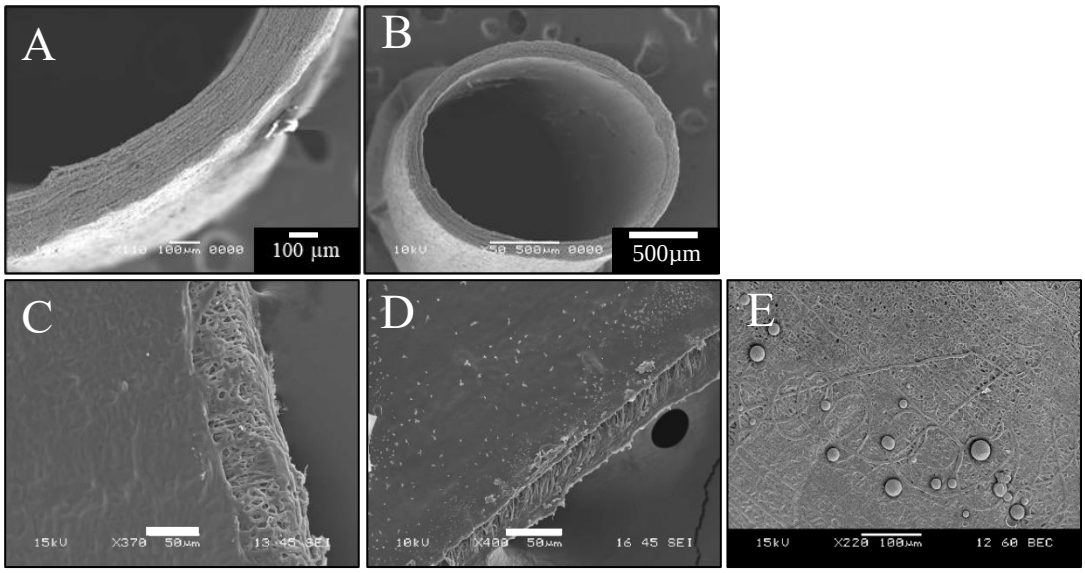

Figure 4.2. SEM images of cross-section of PCL constructs. SEM images of PCL cross section (A, B), PCL constructs with gelatin coating (C, D), and gelatin coated constructs with PLGA microparticles (E).

4.3.3 UPI peptide release

The *in vitro* release of 100 µg/mL UPI peptides was assessed within PLGA microparticles in DI water at room temperature for 28 days. UPI peptide appeared to have a sustained release with almost 20% release of the total UPI peptide loaded within the microparticles, assuming no loss of the peptide in the process within 28 days. (figure 4.3). Furthermore, the release has not yet reached a plateau, and the extended-release study is still ongoing. The UPI peptide release study is currently

limited to a sample size of n=1, indicating a need for further investigation to obtain more comprehensive results.

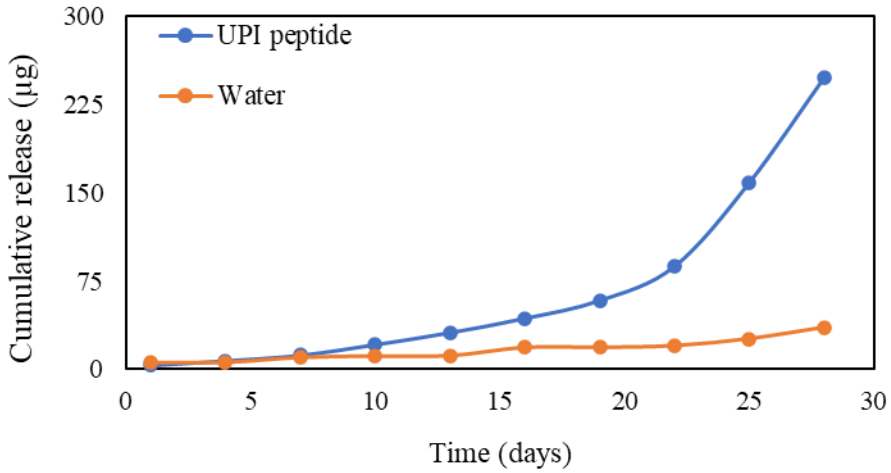

Figure 4.3. Cumulative UPI peptide release in 28 days in DI water. 100 µg/ml of UPI peptide and water as a control sample in PLGA microparticles. (n=1)

4.3.4 Cell migration and attachment

The ability of UPI and scramble peptide concentrations to impact EC migration was assessed with a scratch assay *in vitro*. After 18 h, the ECs migrated significantly further when the UPI peptide with the concentration of 100 µg/ml was added exogenously to the media compared to the presence of 100 and 37 µg/ml scramble peptide (p=0.0007, p=004) (Figure 4.4). It also appeared that UPI peptide incorporation at 100 µg/ml improved EC migration compared to the standard medium (p=0005). The result also suggested that ECs migrated further when UPI peptide at a lower concentration (37 µg/ml) was present compared to higher scramble peptide concentration (p=0.049).

GFP+ HUVECs morphology on spin-coated PCL meshes was assessed after three days of culture using the higher concentration of UPI and scramble peptides. Cells only with the standard medium were also considered as controls. The results suggested that GFP+ HUVECs showed more elongated morphology with proper cytoskeleton dispersion in the presence of UPI peptide. However, GFP+ HUVECS were round in shape in the presence of scrambled peptides (Figure 4.5). Furthermore, the 2D culture of GFP+ HUVECs revealed that the inclusion of UPI peptide exhibited promising organization of ECs. Finally, HUVECs attachment on spin-coated PCL meshes was assessed after three days of culture. Semi-quantitative analysis of ECs nuclei showed higher cells attachment in presence of UPI peptide compared to scrambled peptide and control conditions. However, the results were not statistically different due to high variability between samples (Figure 4.5).

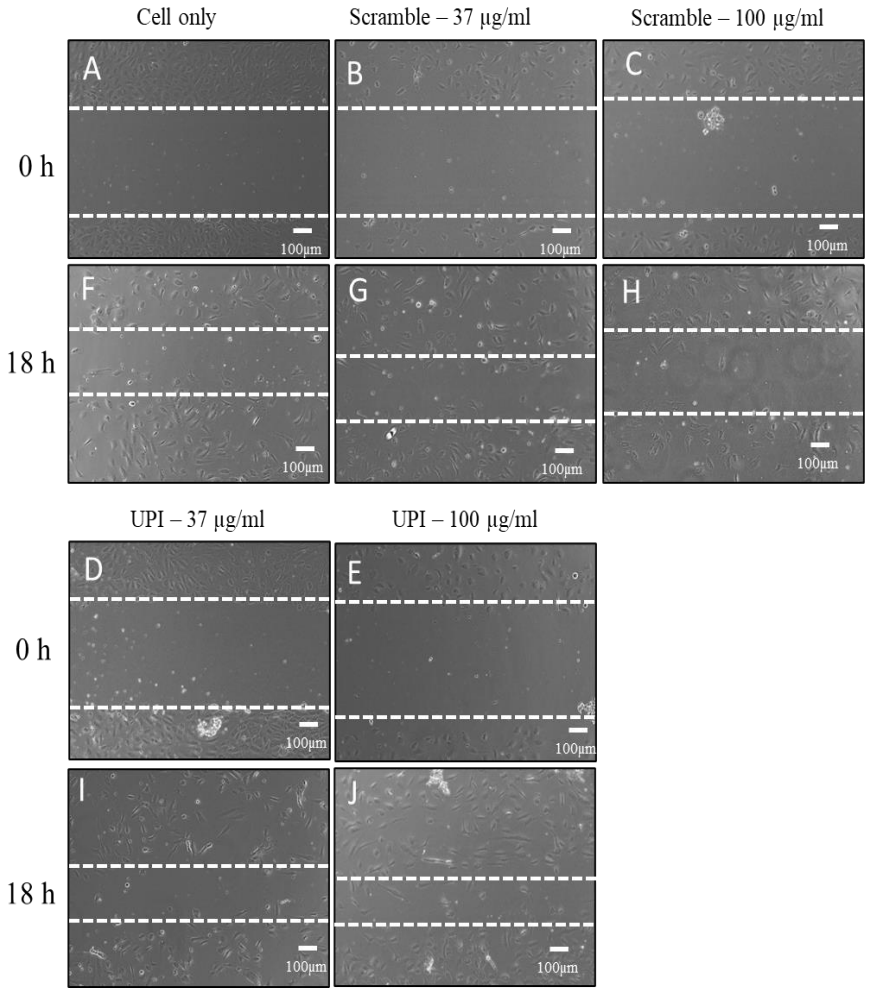
Cell only
Scramble – 37 µg/ml
Scramble – 100 µg/ml
0 h
18 h
A
B
C
F
G
H
100µm
UPI – 37 µg/ml
UPI – 100 µg/ml
D
E
I
J
K
Normalized Migration distance
1.2
1
0.8
0.6
0.4
0.2
0
3
8
18
Time (h)
*
*
*
#
Cells only
Scramble-low
Scramble-high
UPI-low
UPI-high

Figure 4.4. Images for the cell migration test. Representative phase contrast images of HUVECs with and without UPI and scramble peptides over time. n=3 samples / condition. * Indicates the statistical difference from the UPI peptide at 100 µg/ml concentration condition at 18 hours time point. # Indicates the statistical difference from the UPI peptide at 37 µg/ml concentration condition at 18 hours time point. n=3 samples / condition.

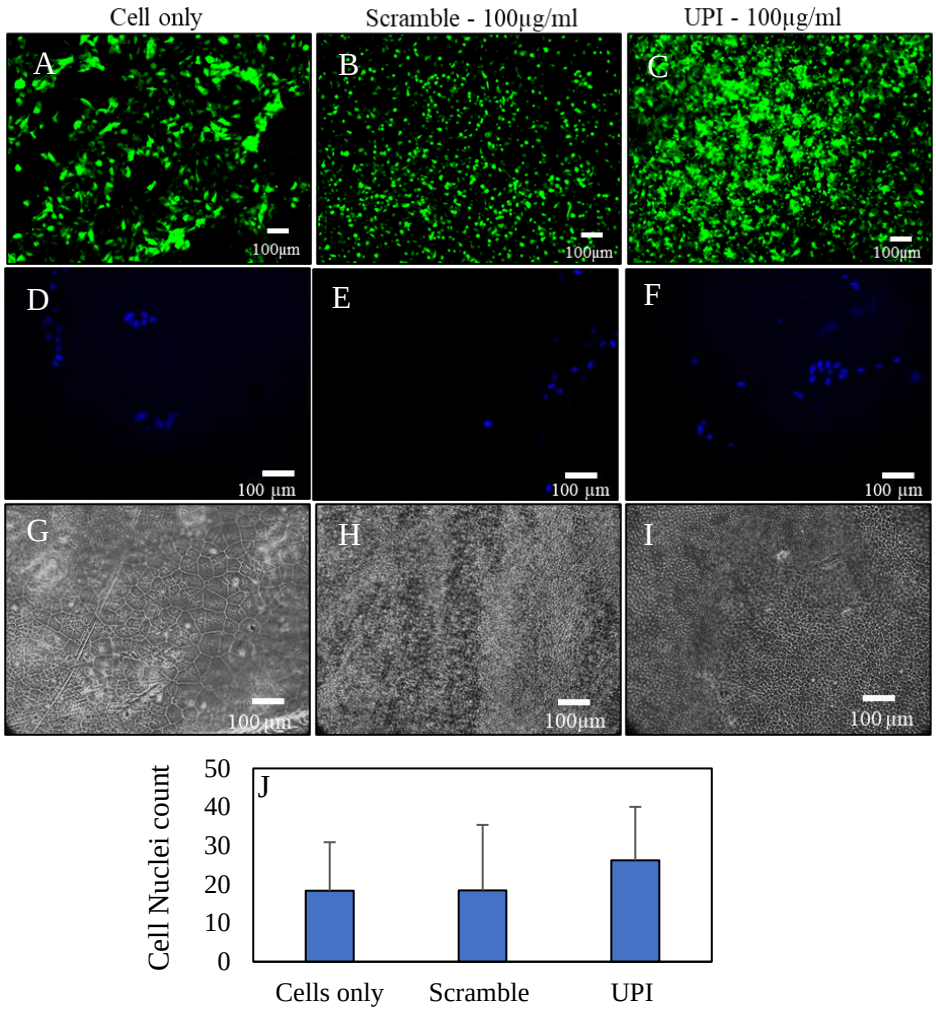

Figure 4.5. Representative immunoflourecense images of GFP+ HUVECS and HUVECs with and without UPI and scramble peptides over time. GFP+ cells only (A), with scramble peptide (B), and with UPI peptide (C). Immunofluorescence and corresponding phase contrast images of HUVECs only (D, G), with scramble peptide (E, H), and with UPI peptide (F, I). Semi-quantitative analysis of HUVECs on PCL spin coated meshes (J). n=3 samples / condition.

4.4 Conclusion

Overall, PLGA microparticles were created using double emulsion techniques (W1/O/W2) and were loaded with UPI peptide. The UPI peptide appeared to show sustained release from the PLGA microparticles for up to 28 days without reaching a plateau yet. PCL constructs, with lumens coated with 5% gelatin, showed mostly a consistent coating layer on the meshes. Furthermore, PLGA microparticles were distributed within the gelatin-coated PCL lumen.

The impact of the UPI peptide on HUVECs was demonstrated through cell migration and attachment assays. HUVECs exhibited increased migration when the UPI peptide was incorporated compared to the control conditions. Additionally, the migration assay revealed a dose-dependent effect of the UPI peptide, as higher dosages enhanced ECs cell migration. Cell attachment assays on PCL spin-coated meshes indicated that cells displayed a more elongated morphology in the presence of the UPI peptide compared to the incorporation of a scrambled peptide, where they appeared more rounded.

The specificity of the UPI peptide must be confirmed by incorporating it within other cell types in vitro. Additionally, the release study needs a larger sample size to be validated for extended release. Furthermore, validation of this study *in vivo* is necessary to uncover the extended impact of the UPI peptide on rapid endothelialization. In summary, these findings demonstrate that incorporating UPI peptides within microparticles improves sustained release, and the exogenous addition of the UPI peptide positively affects HUVECs' migration and attachment.

Chapter 5: Conclusion and future work

5.1 Summary of dissertation

The primary objective of this study was to enhance endothelization within two specific applications. This dissertation aimed to 1) Improve endothelization at the BBB, thereby mitigating cognitive impairment diseases. 2) Enhance patency of small-diameter grafts by augmenting endothelization and decreasing the risk of intimal hyperplasia. 3) Enhance the long-term release of active compounds through the incorporation of more stable carriers, consequently improving endothelization at graft sites.

One important objective was to enhance endothelization by delivering an appropriate dosage of CO at the BBB. To achieve this, two perfluorocarbons (PFCs) with distinct boiling points were utilized as microbubbles for CO incorporation. The stability of these microbubbles was assessed over time in an incubator. Microbubbles with a low boiling point were employed for CO delivery. The biocompatibility of these microbubbles was evaluated in vitro using endothelial cells, demonstrating that the proper dosage of CO improved endothelization. Furthermore, the application of ultrasound on microbubbles was examined to determine optimal ultrasound settings. These settings were applied to CO-loaded microbubbles on GFP+ HUVECs seeded on gelatin constructs, revealing enhanced endothelization in the presence of CO-loaded microbubbles following ultrasound application. Additionally, the endocytosis of these microbubbles by HUVECs was assessed through time-lapse imaging, indicating MB internalization by HUVECs.

The second objective of this dissertation aimed to enhance the endothelization of small-diameter vascular grafts through the delivery of UPI peptides using electrospun constructs. To achieve this, we electrospuned 13% PCL and characterized the thickness and diameter of the constructs. The release of UPI peptide was assessed from constructs using physical adsorption and fibrin coating methods. Furthermore, the UPI peptide's effects were evaluated in vitro and in vivo using rodents for one week. The results indicated a random orientation of PCL meshes and consistent distribution of fibrin coating. The release study demonstrated that incorporating UPI peptide within the fibrin coating improved drug loading efficiency. Moreover, the incorporation of UPI peptide with fibrin coating exhibited enhanced endothelization *in vitro*. *In vivo*, findings revealed that UPI peptide improved cell infiltration and graft remodeling at low concentrations. Additionally, consistent monolayer formation of endothelial cells at the lumen was observed, along with VE-Cadherin signals indicating functional endothelial cells.

The third objective of this study was to enhance the release of the UPI peptide and evaluate the specificity of the peptide *in vitro*. PLGA-based microparticles were fabricated using a double emulsion technique and loaded with peptides to accomplish this. A 3D-printed construct was utilized to coat the lumen of the PCL constructs with gelatin and microbubbles. The release of UPI peptide was evaluated using UPI peptide-loaded microparticles. The specificity of UPI peptide was assessed through cell migration and attachment studies. The results suggested extended release of UPI peptide up to 28 days without reaching a plateau yet. Additionally, the incorporation

of UPI peptide allowed the cells to migrate further and have more elongated morphology compared to the control conditions.

In this dissertation, some significant results were achieved: 1) delivery of a proper dose of CO via MBs showed better endothelization, 2) delivery of a proper UPI peptide dosage via fibrin-coated constructs provided better endothelization in vivo and in vitro, which can lead to better small diameter graft patency, and 3) incorporation of UPI peptide within the MP provided a more extended-release. Additionally, the proper dose of UPI peptide improves cell migration and attachment.

5.2 Future work

The potential of CO and UPI peptides for enhancing endothelialization is promising, yet further investigations are needed to assess the full potential of these active compounds. 1) investigating the impact of extended release of UPI peptide within microparticles and the gelatin coating *in vivo*, and 2) investigating the covalent binding of UPI peptide with the PCL scaffold surface.

5.2.1 Investigating the impact of extended release of UPI peptide within microparticles and the gelatin coating *in vivo*

In this work, we will assess the release of UPI peptide loaded within the microparticles and gelatin-coating *in vivo*. In previous work, we demonstrated a burst release of UPI peptide from our fibrin coating, which showed an early-stage endothelization. However, for the clinical transition of these grafts, more extended release of UPI peptide is needed. Moreover, the incorporation of microparticles

within the gelatin coating needs further investigation, as microparticles with larger diameters may lead to blood clots and graft failure concerns after graft implantation. First, we propose to modify the fabrication process to achieve microparticles with smaller diameter and assess the UPI peptide release from microparticles *in vitro*. Further, we intend to introduce specific concentrations of UPI peptide within the gelatin coating as well to induce an initial burst release. We also incorporate a proper dosage within microparticles to facilitate a sustained and long-term release profile in rodent models. Further, more long-term grafting is also needed to assess the effects of more extended release on endothelization and tissue generation. By systematically analyzing the release and subsequent biological responses, we aim to delineate an optimized strategy for achieving enhanced graft performance suitable for clinical translation.

5.2.2 Investigating the covalent binding of UPI peptide with the PCL scaffold surface *in vitro* and *in vivo*

Long-term graft patency is crucial for the clinical transition of TEVGs. Prevention of intimal hyperplasia and thrombosis, as well as generation of a monolayer of ECs to prevent platelet adhesion on the surface of TEVGs, is essential. Pre-seeding the scaffolds with ECs has shown promise in reducing the risk of early-stage thrombosis. However, *in vivo* exposure to bloodstream shear stress often leads to EC detachment, leaving portions of the scaffold surface. To address this, it is imperative to modify scaffold surfaces to promote EC adhesion from endothelial progenitor cells (EPCs) and facilitate neighboring EC migration. Scaffold surfaces

have been modified with immobilizing cell adhesion sequences, including extracellular matrix proteins such as RGD and the peptides that originate from them. Furthermore, active compounds binding to polymer surfaces have demonstrated sustained release over time. For example, covalently immobilizing sulfated silk fibroin on poly (lactic-co-glycolic acid) has shown sustained release up to 30 days. For this purpose, we propose the covalent binding of UPI peptide within the PCL scaffold surface.

We suggest that covalently binding the UPI peptide to the surface will enhance endothelialization of the scaffold by facilitating peptide interaction with VEGR2 from neighboring ECs and stimulating EC migration. Additionally, the iRGD sequence within the UPI peptide is expected to improve the attachment of circulating EPCs. Furthermore, we hypothesize that the covalent binding of this peptide will also result in a sustained release over time which reduces the risk of hyperplasia over time.

5.3 Conclusion

This research project aimed to enhance endothelialization by delivering active compounds through carriers and recruiting ECs from patients. The study enabled the evaluation of various dosages of CO and UPI peptides and their effects on ECs in vitro. Furthermore, delivery of the UPI peptide resulted in cell infiltration and tissue remodeling within our scaffold in vivo. A fabrication technique was also developed to encapsulate the UPI peptide within microparticles, improving its release profile. Future work involves incorporating UPI peptides into microparticles and gelatin

coating on our scaffold to assess longer-term release effects. Moreover, assessing the covalent binding of the UPI peptide within the scaffold in vitro and in vivo on the recruitment of autologous cells is planned. Achieving these tasks successfully marks a significant step forward in advancing the development of our proposed TEVG to clinical transitions.

Reference

[1] C. Michiels, « Endothelial cell functions », *J Cell Physiol*, vol. 196, n° 3, p. 430-443, 2003.

[2] V. V Sevostyanova *et al.*, « Endothelialization of polycaprolactone vascular graft under the action of locally applied vascular endothelial growth factor », *Bull Exp Biol Med*, vol. 165, n° 2, p. 264-268, 2018.

[3] C. Sturtzel, « Endothelial cells », *The Immunology of Cardiovascular Homeostasis and Pathology*, p. 71-91, 2017.

[4] E. A. Jaffe, « Cell biology of endothelial cells », *Hum Pathol*, vol. 18, n° 3, p. 234-239, 1987.

[5] S. E. J. Chambers *et al.*, « Current concepts on endothelial stem cells definition, location, and markers », *Stem Cells Transl Med*, vol. 10, n° S2, p. S54-S61, 2021.

[6] T. Gori *et al.*, « Both flow-mediated dilation and constriction are associated with changes in blood flow and shear stress: two complementary perspectives on endothelial function », *Clin Hemorheol Microcirc*, vol. 64, n° 3, p. 255-266, 2016.

[7] A. Krüger-Genge, A. Blocki, R.-P. Franke, et F. Jung, « Vascular endothelial cell biology: an update », *Int J Mol Sci*, vol. 20, n° 18, p. 4411, 2019.

[8] H. Ali, « SCUBE2, vascular endothelium, and vascular complications: A systematic review », *Biomedicine & Pharmacotherapy*, vol. 127, p. 110129, 2020.

[9] H. J. Carpenter, A. Gholipour, M. H. Ghayesh, A. C. Zander, et P. J. Psaltis, « A review on the biomechanics of coronary arteries », *Int J Eng Sci*, vol. 147, p. 103201, 2020.

[10] M. K. Pugsley et R. Tabrizchi, « The vascular system: An overview of structure and function », *J Pharmacol Toxicol Methods*, vol. 44, n° 2, p. 333-340, 2000.

[11] M. A. Young et S. F. Vatner, « Regulation of large coronary arteries. », *Circ Res*, vol. 59, n° 6, p. 579-596, 1986.

[12] L. G. Griffith et G. Naughton, « Tissue engineering--current challenges and expanding opportunities », *Science (1979)*, vol. 295, n° 5557, p. 1009-1014, 2002.

[13] R. Lanza, R. Langer, J. P. Vacanti, et A. Atala, *Principles of tissue engineering*. Academic press, 2020.

[14] D. W. Hutmacher, J. C. H. Goh, et S. H. Teoh, « An introduction to biodegradable materials for tissue engineering applications », *Annals-academy of medicine singapore*, vol. 30, n° 2, p. 183-191, 2001.

[15] K. Berger, L. R. Sauvage, A. M. Rao, et S. J. Wood, « Healing of arterial prostheses in man: its incompleteness. », *Ann Surg*, vol. 175, nº 1, p. 118, 1972.

[16] T. Asahara *et al.*, « Isolation of putative progenitor endothelial cells for angiogenesis », *Science (1979)*, vol. 275, nº 5302, p. 964-966, 1997.

[17] R. A. Perez, A. El-Fiqi, J.-H. Park, T.-H. Kim, J.-H. Kim, et H.-W. Kim, « Therapeutic bioactive microcarriers: co-delivery of growth factors and stem cells for bone tissue engineering », *Acta Biomater*, vol. 10, nº 1, p. 520-530, 2014.

[18] J. E. Babensee, L. V McIntire, et A. G. Mikos, « Growth factor delivery for tissue engineering », *Pharm Res*, vol. 17, nº 5, p. 497-504, 2000.

[19] D. Wang *et al.*, « Programmed release of multimodal, cross-linked vascular endothelial growth factor and heparin layers on electrospun polycaprolactone vascular grafts », *ACS Appl Mater Interfaces*, vol. 11, nº 35, p. 32533-32542, 2019.

[20] B. D. Ratner, « The biocompatibility of implant materials », in *Host response to biomaterials*, Elsevier, 2015, p. 37-51.

[21] K. S. Vasanthan, A. Subramanian, U. M. Krishnan, et S. Sethuraman, « Role of biomaterials, therapeutic molecules and cells for hepatic tissue engineering », *Biotechnol Adv*, vol. 30, nº 3, p. 742-752, 2012.

[22] I. Martin, D. Wendt, et M. Heberer, « The role of bioreactors in tissue engineering », *Trends Biotechnol*, vol. 22, n° 2, p. 80-86, 2004.

[23] N. Plunkett et F. J. O'Brien, « Bioreactors in tissue engineering », *Technology and Health Care*, vol. 19, n° 1, p. 55-69, 2011.

[24] H.-C. Chen et Y.-C. Hu, « Bioreactors for tissue engineering », *Biotechnol Lett*, vol. 28, n° 18, p. 1415-1423, 2006.

[25] G. Khang, S. J. Lee, M. S. Kim, et H. B. Lee, « Biomaterials: tissue engineering and scaffolds », *Encyclopedia of Medical devices and instrumentation*, vol. 2, p. 366-383, 2006.

[26] S. Ullah et X. Chen, « Fabrication, applications and challenges of natural biomaterials in tissue engineering », *Appl Mater Today*, vol. 20, p. 100656, 2020.

[27] M. J. Beckman, K. J. Shields, et R. F. Diegelmann, « Collagen. Encyclopedia of Biomaterials and biomedical engineering ». New York: Marcel Dekker, 2004.

[28] G. C. M. Steffens *et al.*, « Modulation of angiogenic potential of collagen matrices by covalent incorporation of heparin and loading with vascular endothelial growth factor », *Tissue Eng*, vol. 10, n° 9-10, p. 1502-1509, 2004.

[29] P. Gupta *et al.*, « Bioresorbable silk grafts for small diameter vascular tissue engineering applications: In vitro and in vivo functional analysis », *Acta Biomater*, vol. 105, p. 146-158, 2020.

[30] C. C. Canver, « Conduit options in coronary artery bypass surgery », *Chest*, vol. 108, n° 4, p. 1150-1155, 1995.

[31] P. Dunlop, R. D. Sayers, A. R. Naylor, P. R. F. Bell, et N. J. M. London, « The effect of a surveillance programme on the patency of synthetic infrainguinal bypass grafts », *European journal of vascular and endovascular surgery*, vol. 11, n° 4, p. 441-445, 1996.

[32] M. Goldberg, R. Langer, et X. Jia, « Nanostructured materials for applications in drug delivery and tissue engineering », *J Biomater Sci Polym Ed*, vol. 18, n° 3, p. 241-268, 2007.

[33] F. Opitz *et al.*, « Tissue engineering of aortic tissue: dire consequence of suboptimal elastic fiber synthesis in vivo », *Cardiovasc Res*, vol. 63, n° 4, p. 719-730, 2004.

[34] A. J. Van Rensburg, N. H. Davies, A. Oosthuysen, C. Chokoza, P. Zilla, et D. Bezuidenhout, « Improved vascularization of porous scaffolds through growth factor delivery from heparinized polyethylene glycol hydrogels », *Acta Biomater*, vol. 49, p. 89-100, 2017.

[35] S. Adepu et S. Ramakrishna, « Controlled drug delivery systems: current status and future directions », *Molecules*, vol. 26, n° 19, p. 5905, 2021.

[36] K. Wang *et al.*, « Enhanced vascularization in hybrid PCL/gelatin fibrous scaffolds with sustained release of VEGF », *Biomed Res Int*, vol. 2015, 2015.

[37] J. R. Weiser et W. M. Saltzman, « Controlled release for local delivery of drugs: barriers and models », *Journal of Controlled Release*, vol. 190, p. 664-673, 2014.

[38] T. R. Hoare et D. S. Kohane, « Hydrogels in drug delivery: Progress and challenges », *Polymer (Guildf)*, vol. 49, n° 8, p. 1993-2007, 2008.

[39] K. J. Rambhia et P. X. Ma, « Controlled drug release for tissue engineering », *Journal of Controlled Release*, vol. 219, p. 119-128, 2015.

[40] S. Li, D. Xia, et M. R. Prausnitz, « Efficient Drug Delivery into Skin Using a Biphasic Dissolvable Microneedle Patch with Water-Insoluble Backing », *Adv Funct Mater*, vol. 31, n° 44, p. 2103359, 2021.

[41] I. R. Calori, G. Braga, P. da C. C. de Jesus, H. Bi, et A. C. Tedesco, « Polymer scaffolds as drug delivery systems », *Eur Polym J*, vol. 129, p. 109621, 2020.

[42] K. Wang *et al.*, « Functional modification of electrospun poly (ε-caprolactone) vascular grafts with the fusion protein VEGF–HGFI enhanced vascular regeneration », *ACS Appl Mater Interfaces*, vol. 9, n° 13, p. 11415-11427, 2017.

[43] M. J. Mitchell, M. M. Billingsley, R. M. Haley, M. E. Wechsler, N. A. Peppas, et R. Langer, « Engineering precision nanoparticles for drug delivery », *Nat Rev Drug Discov*, vol. 20, n° 2, p. 101-124, 2021.

[44] B. Almería, W. Deng, T. M. Fahmy, et A. Gomez, « Controlling the morphology of electrospray-generated PLGA microparticles for drug delivery », *J Colloid Interface Sci*, vol. 343, n° 1, p. 125-133, 2010.

[45] M. Iqbal, N. Zafar, H. Fessi, et A. Elaissari, « Double emulsion solvent evaporation techniques used for drug encapsulation », *Int J Pharm*, vol. 496, n° 2, p. 173-190, 2015.

[46] A. Kumar, R. Kaur, V. Kumar, S. Kumar, R. Gehlot, et P. Aggarwal, « New insights into water-in-oil-in-water (W/O/W) double emulsions: Properties, fabrication, instability mechanism, and food applications », *Trends Food Sci Technol*, 2022.

[47] T. K. Giri, C. Choudhary, A. Alexander, H. Badwaik, et D. K. Tripathi, « Prospects of pharmaceuticals and biopharmaceuticals loaded microparticles prepared by double emulsion technique for controlled delivery », *Saudi Pharmaceutical Journal*, vol. 21, n° 2, p. 125-141, 2013.

[48] Y. Chen et L. Liu, « Modern methods for delivery of drugs across the blood–brain barrier », *Adv Drug Deliv Rev*, vol. 64, n° 7, p. 640-665, 2012.

[49] R. Daneman et A. Prat, « The blood–brain barrier », *Cold Spring Harb Perspect Biol*, vol. 7, n° 1, p. a020412, 2015.

[50] P. B. L. Pun, J. I. A. Lu, et S. Moochhala, « Involvement of ROS in BBB dysfunction », *Free Radic Res*, vol. 43, n° 4, p. 348-364, 2009.

[51] S. Brilha, C. W. M. Ong, B. Weksler, N. Romero, P.-O. Couraud, et J. S. Friedland, « Matrix metalloproteinase-9 activity and a downregulated Hedgehog pathway impair blood-brain barrier function in an in vitro model of CNS tuberculosis », *Sci Rep*, vol. 7, n° 1, p. 16031, 2017.

[52] Z. G. Zhang *et al.*, « Correlation of VEGF and angiopoietin expression with disruption of blood–brain barrier and angiogenesis after focal cerebral ischemia », *Journal of Cerebral Blood Flow & Metabolism*, vol. 22, n° 4, p. 379-392, 2002.

[53] A. C. Yang *et al.*, « Physiological blood–brain transport is impaired with age by a shift in transcytosis », *Nature*, vol. 583, n° 7816, p. 425-430, 2020.

[54] L. A. Boven, J. Middel, J. Verhoef, C. J. A. De Groot, et H. Nottet, « Monocyte infiltration is highly associated with loss of the tight junction protein zonula occludens in HIV-1-associated dementia », *Neuropathol Appl Neurobiol*, vol. 26, n° 4, p. 356-360, 2000.

[55] M. D. Sweeney, Z. Zhao, A. Montagne, A. R. Nelson, et B. V Zlokovic, « Blood-brain barrier: from physiology to disease and back », *Physiol Rev*, vol. 99, n° 1, p. 21-78, 2019.

[56] M. M. Patel et B. M. Patel, « Crossing the blood–brain barrier: recent advances in drug delivery to the brain », *CNS Drugs*, vol. 31, n° 2, p. 109-133, 2017.

[57] Y. Sun, K. Shi, et F. Wan, « Methotrexate-loaded microspheres for nose to brain delivery: In vitro/in vivo evaluation », *J Drug Deliv Sci Technol*, vol. 22, n° 2, p. 167-174, 2012.

[58] S. R. Sirsi et M. A. Borden, « Microbubble compositions, properties and biomedical applications », *Bubble Sci Eng Technol*, vol. 1, n° 1-2, p. 3-17, 2009.

[59] S. R. Sirsi et M. A. Borden, « State-of-the-art materials for ultrasound-triggered drug delivery », *Adv Drug Deliv Rev*, vol. 72, p. 3-14, 2014.

[60] E. Buchner Santos, J. K. Morris, E. Glynos, V. Sboros, et V. Koutsos, « Nanomechanical properties of phospholipid microbubbles », *Langmuir*, vol. 28, nº 13, p. 5753-5760, 2012.

[61] N. Rapoport *et al.*, « Ultrasound-mediated tumor imaging and nanotherapy using drug loaded, block copolymer stabilized perfluorocarbon nanoemulsions », *Journal of Controlled Release*, vol. 153, nº 1, p. 4-15, 2011.

[62] J. F. Jordão *et al.*, « Antibodies targeted to the brain with image-guided focused ultrasound reduces amyloid-β plaque load in the TgCRND8 mouse model of Alzheimer's disease », *PLoS One*, vol. 5, nº 5, p. e10549, 2010.

[63] C.-Y. Ting *et al.*, « Concurrent blood–brain barrier opening and local drug delivery using drug-carrying microbubbles and focused ultrasound for brain glioma treatment », *Biomaterials*, vol. 33, nº 2, p. 704-712, 2012.

[64] C.-H. Fan *et al.*, « Folate-conjugated gene-carrying microbubbles with focused ultrasound for concurrent blood-brain barrier opening and local gene delivery », *Biomaterials*, vol. 106, p. 46-57, 2016.

[65] R. Wang, « Gasotransmitters: growing pains and joys », *Trends Biochem Sci*, vol. 39, nº 5, p. 227-232, 2014.

[66] G. P. Kealey, « Carbon monoxide toxicity », *Journal of burn care & research*, vol. 30, n° 1, p. 146-147, 2009.

[67] C. Szabo, « Gaseotransmitters: new frontiers for translational science », *Sci Transl Med*, vol. 2, n° 59, p. 59ps54-59ps54, 2010.

[68] R. Motterlini et L. E. Otterbein, « The therapeutic potential of carbon monoxide », *Nat Rev Drug Discov*, vol. 9, n° 9, p. 728-743, 2010.

[69] K. Sato *et al.*, « Carbon monoxide generated by heme oxygenase-1 suppresses the rejection of mouse-to-rat cardiac transplants », *The Journal of Immunology*, vol. 166, n° 6, p. 4185-4194, 2001.

[70] L. Rodella *et al.*, « Carbon monoxide and biliverdin prevent endothelial cell sloughing in rats with type I diabetes », *Free Radic Biol Med*, vol. 40, n° 12, p. 2198-2205, 2006.

[71] E. Bathoorn *et al.*, « Anti-inflammatory effects of inhaled carbon monoxide in patients with COPD: a pilot study », *European Respiratory Journal*, vol. 30, n° 6, p. 1131-1137, 2007.

[72] K. Okrainec, D. K. Banerjee, et M. J. Eisenberg, « Coronary artery disease in the developing world », *Am Heart J*, vol. 148, n° 1, p. 7-15, 2004.

[73] J. L. Mehta, T. G. P. Saldeen, et K. Rand, « Interactive role of infection, inflammation and traditional risk factors in atherosclerosis and coronary artery disease », *J Am Coll Cardiol*, vol. 31, n° 6, p. 1217-1225, 1998.

[74] N. Alie, M. Eldib, Z. A. Fayad, et V. Mani, « Inflammation, atherosclerosis, and coronary artery disease: PET/CT for the evaluation of atherosclerosis and inflammation », *Clin Med Insights Cardiol*, vol. 8, p. CMC-S17063, 2014.

[75] E. L. Barrett-Connor, « Obesity, atherosclerosis, and coronary artery disease », *Ann Intern Med*, vol. 103, n° 6_Part_2, p. 1010-1019, 1985.

[76] G. K. Hansson, « Inflammation, atherosclerosis, and coronary artery disease », *New England Journal of Medicine*, vol. 352, n° 16, p. 1685-1695, 2005.

[77] M. G. Davies et P. O. Hagen, « Pathobiology of intimal hyperplasia », *Journal of British Surgery*, vol. 81, n° 9, p. 1254-1269, 1994.

[78] B. Mills, T. Robb, et D. F. Larson, « Intimal hyperplasia: slow but deadly », *Perfusion*, vol. 27, n° 6, p. 520-528, 2012.

[79] P. Gupta et B. B. Mandal, « Tissue-engineered vascular grafts: emerging trends and technologies », *Adv Funct Mater*, vol. 31, n° 33, p. 2100027, 2021.

[80] B. Sigel *et al.*, « Intimal hyperplasia producing thrombus organization in an experimental venous thrombosis model », *J Vasc Surg*, vol. 19, n° 2, p. 350-360, 1994.

[81] J. C. Jennette et J. R. Stone, « Diseases of medium-sized and small vessels », in *Cellular and Molecular Pathobiology of Cardiovascular Disease*, Elsevier, 2014, p. 197-219.

[82] M. Alghrairi, N. Sulaiman, et S. Mutashar, « Health Care Monitoring and Treatment for Coronary Artery Diseases: Challenges and Issues », *Sensors*, vol. 20, n° 15, p. 4303, 2020.

[83] S. Pashneh-Tala, S. MacNeil, et F. Claeyssens, « The tissue-engineered vascular graft—past, present, and future », *Tissue Eng Part B Rev*, vol. 22, n° 1, p. 68-100, 2016.

[84] M. Desai, A. M. Seifalian, et G. Hamilton, « Role of prosthetic conduits in coronary artery bypass grafting », *European Journal of Cardio-Thoracic Surgery*, vol. 40, n° 2, p. 394-398, 2011.

[85] R. Y. Kannan, H. J. Salacinski, P. E. Butler, G. Hamilton, et A. M. Seifalian, « Current status of prosthetic bypass grafts: a review », *Journal of Biomedical Materials Research Part B: Applied Biomaterials: An Official Journal of The Society for Biomaterials, The Japanese Society for Biomaterials, and The Australian Society for Biomaterials and the Korean Society for Biomaterials*, vol. 74, n° 1, p. 570-581, 2005.

[86] M. R. Jackson *et al.*, « The consequences of a failed femoropopliteal bypass grafting: comparison of saphenous vein and PTFE grafts », *J Vasc Surg*, vol. 32, n° 3, p. 498-505, 2000.

[87] M. Carrabba et P. Madeddu, « Current strategies for the manufacture of small size tissue engineering vascular grafts », *Front Bioeng Biotechnol*, vol. 6, p. 41, 2018.

[88] U. G. Sampath, Y. C. Ching, C. H. Chuah, J. J. Sabariah, et P.-C. Lin, « Fabrication of porous materials from natural/synthetic biopolymers and their composites », *Materials*, vol. 9, n° 12, p. 991, 2016.

[89] A. McDougal, B. Miller, M. Singh, et M. Kolle, « Biological growth and synthetic fabrication of structurally colored materials », *Journal of Optics*, vol. 21, n° 7, p. 73001, 2019.

[90] Y. Zhang, H. Ouyang, C. T. Lim, S. Ramakrishna, et Z. Huang, « Electrospinning of gelatin fibers and gelatin/PCL composite fibrous scaffolds », *Journal of Biomedical Materials Research Part B: Applied Biomaterials: An Official Journal of The Society for Biomaterials, The Japanese Society for Biomaterials, and The Australian Society for Biomaterials and the Korean Society for Biomaterials*, vol. 72, n° 1, p. 156-165, 2005.

[91] T. Subbiah, G. S. Bhat, R. W. Tock, S. Parameswaran, et S. S. Ramkumar, « Electrospinning of nanofibers », *J Appl Polym Sci*, vol. 96, n° 2, p. 557-569, 2005.

[92] N. Bhardwaj et S. C. Kundu, « Electrospinning: a fascinating fiber fabrication technique », *Biotechnol Adv*, vol. 28, n° 3, p. 325-347, 2010.

[93] A. Haider, S. Haider, et I.-K. Kang, « A comprehensive review summarizing the effect of electrospinning parameters and potential applications of nanofibers in biomedical and biotechnology », *Arabian Journal of Chemistry*, vol. 11, n° 8, p. 1165-1188, 2018.

[94] C. S. Ong, X. Zhou, C. Y. Huang, T. Fukunishi, H. Zhang, et N. Hibino, « Tissue engineered vascular grafts: current state of the field », *Expert Rev Med Devices*, vol. 14, n° 5, p. 383-392, 2017.

[95] K. S. Washington et C. A. Bashur, « Delivery of antioxidant and anti-inflammatory agents for tissue engineered vascular grafts », *Front Pharmacol*, vol. 8, p. 659, 2017.

[96] J. P. Cuenca *et al.*, « Physico-mechanical and biological evaluation of heparin/VEGF-loaded electrospun polycaprolactone/decellularized rat aorta extracellular matrix for small-diameter vascular grafts », *J Biomater Sci Polym Ed*, vol. 33, n° 13, p. 1664-1684, 2022.

[97] X. Geng *et al.*, « Hydrogel complex electrospun scaffolds and their multiple functions in in situ vascular tissue engineering », *ACS Appl Bio Mater*, vol. 4, n° 3, p. 2373-2384, 2021.

[98] S. Aslani, M. Kabiri, S. HosseinZadeh, H. Hanaee-Ahvaz, E. S. Taherzadeh, et M. Soleimani, « The applications of heparin in vascular tissue engineering », *Microvasc Res*, vol. 131, p. 104027, 2020.

[99] S. Ma *et al.*, « E-selectin-targeting delivery of microRNAs by microparticles ameliorates endothelial inflammation and atherosclerosis », *Sci Rep*, vol. 6, n° 1, p. 22910, 2016.

[100] F. R. Formiga *et al.*, « Sustained release of VEGF through PLGA microparticles improves vasculogenesis and tissue remodeling in an acute myocardial ischemia–reperfusion model », *Journal of Controlled Release*, vol. 147, n° 1, p. 30-37, 2010.

[101] J. M. Morais, F. Papadimitrakopoulos, et D. J. Burgess, « Biomaterials/tissue interactions: possible solutions to overcome foreign body response », *AAPS J*, vol. 12, n° 2, p. 188-196, 2010.

[102] E. Mariani, G. Lisignoli, R. M. Borzì, et L. Pulsatelli, « Biomaterials: foreign bodies or tuners for the immune response? », *Int J Mol Sci*, vol. 20, n° 3, p. 636, 2019.

[103] Z. Xia et J. T. Triffitt, « A review on macrophage responses to biomaterials », *Biomedical materials*, vol. 1, n° 1, p. R1, 2006.

[104] J. Zhou *et al.*, « Endothelial cell-mediated gene delivery for in situ accelerated endothelialization of a vascular graft », *ACS Appl Mater Interfaces*, vol. 13, n° 14, p. 16097-16105, 2021.

[105] S. Changizi, M. Sameti, G. L. Bazemore, H. Chen, et C. A. Bashur, « Epsin mimetic UPI peptide delivery strategies to improve endothelization of vascular grafts », *Macromol Biosci*, vol. 23, n° 9, p. 2300073, 2023.

[106] A. Thomas, S. Deshayes, M. Decaffmeyer, M. H. Van Eyck, B. Charloteaux, et R. Brasseur, « Prediction of peptide structure: how far are we? », *Proteins: Structure, Function, and Bioinformatics*, vol. 65, n° 4, p. 889-897, 2006.

[107] Y. Lei, M. Rémy, C. Labrugère, et M.-C. Durrieu, « Peptide immobilization on polyethylene terephthalate surfaces to study specific endothelial cell adhesion, spreading and migration », *J Mater Sci Mater Med*, vol. 23, p. 2761-2772, 2012.

[108] T. Ichiki et J. C. Burnett Jr, « Atrial Natriuretic Peptide—Old But New Therapeutic in Cardiovascular Diseases— », *Circulation Journal*, vol. 81, n° 7, p. 913-919, 2017.

[109] D. Tesauro *et al.*, « Peptide-based drug-delivery systems in biotechnological applications: recent advances and perspectives », *Molecules*, vol. 24, n° 2, p. 351, 2019.

[110] A. Kumar, J. D. Potts, et D. J. DiPette, « Protective role of α-calcitonin gene-related peptide in cardiovascular diseases », *Front Physiol*, vol. 10, p. 821, 2019.

[111] Y. Xue, M. L. O'Mara, P. P. T. Surawski, M. Trau, et A. E. Mark, « Effect of poly (ethylene glycol)(PEG) spacers on the conformational properties of small peptides: a molecular dynamics study », *Langmuir*, vol. 27, n° 1, p. 296-303, 2011.

[112] Y.-Y. Wang, L.-X. Lü, J.-C. Shi, H.-F. Wang, Z.-D. Xiao, et N.-P. Huang, « Introducing RGD peptides on PHBV films through PEG-containing cross-linkers to improve the biocompatibility », *Biomacromolecules*, vol. 12, n° 3, p. 551-559, 2011.

[113] W. Zheng *et al.*, « Endothelialization and patency of RGD-functionalized vascular grafts in a rabbit carotid artery model », *Biomaterials*, vol. 33, n° 10, p. 2880-2891, 2012.

[114] R. Sivkova *et al.*, « Surface design of antifouling vascular constructs bearing biofunctional peptides for tissue regeneration applications », *Int J Mol Sci*, vol. 21, n° 18, p. 6800, 2020.

[115] S. Patan, « Vasculogenesis and angiogenesis », *Angiogenesis in brain tumors*, p. 3-32, 2004.

[116] J. Dong *et al.*, « Therapeutic efficacy of a synthetic epsin mimetic peptide in glioma tumor model: uncovering multiple mechanisms beyond the VEGF-associated tumor angiogenesis », *J Neurooncol*, vol. 138, n° 1, p. 17-27, 2018.

[117] Y. Dong *et al.*, « Mimetic peptide of ubiquitin-interacting motif of epsin as a cancer therapeutic-perspective in brain tumor therapy through regulating VEGFR2 signaling », *Vessel Plus*, 2018.

[118] F. Li et H. Zhang, « Targeting Macrophage Epsins to Reverse Atherosclerosis », *Circulation research*, vol. 132, n° 1. Am Heart Assoc, p. 7-9, 2023.

[119] H. Chen *et al.*, « Embryonic arrest at midgestation and disruption of Notch signaling produced by the absence of both epsin 1 and epsin 2 in mice », *Proceedings of the National Academy of Sciences*, vol. 106, nº 33, p. 13838-13843, 2009.

[120] H. N. A. Rahman *et al.*, « Selective targeting of a novel epsin–VEGFR2 interaction promotes VEGF-mediated angiogenesis », *Circ Res*, vol. 118, nº 6, p. 957-969, 2016.

[121] X. Liu *et al.*, « Temporal and spatial regulation of epsin abundance and VEGFR3 signaling are required for lymphatic valve formation and function », *Sci Signal*, vol. 7, nº 347, p. ra97-ra97, 2014.

[122] K. Song *et al.*, « Endothelial epsins as regulators and potential therapeutic targets of tumor angiogenesis », *Cellular and molecular life sciences*, vol. 74, nº 3, p. 393-398, 2017.

[123] Y. Dong *et al.*, « Motif mimetic of epsin perturbs tumor growth and metastasis », *J Clin Invest*, vol. 125, nº 12, p. 4349-4364, 2015.

[124] D. B. Cines *et al.*, « Endothelial cells in physiology and in the pathophysiology of vascular disorders », *Blood, The Journal of the American Society of Hematology*, vol. 91, nº 10, p. 3527-3561, 1998.

[125] M. A. Gimbrone Jr et G. García-Cardeña, « Endothelial cell dysfunction and the pathobiology of atherosclerosis », *Circ Res*, vol. 118, nº 4, p. 620-636, 2016.

[126] L. L. Rubin, « Staddon. The cell biology of the blood-brain barrier », *Ann Rev Neurosci*, vol. 22, p. 11-28, 1999.

[127] R. Daneman, « The blood–brain barrier in health and disease », *Ann Neurol*, vol. 72, n° 5, p. 648-672, 2012.

[128] B. Hussain, C. Fang, et J. Chang, « Blood–brain barrier breakdown: an emerging biomarker of cognitive impairment in normal aging and dementia », *Front Neurosci*, vol. 15, p. 688090, 2021.

[129] M.-K. Sun, « Potential therapeutics for vascular cognitive impairment and dementia », *Curr Neuropharmacol*, vol. 16, n° 7, p. 1036-1044, 2018.

[130] M. D. Maines, « The heme oxygenase system: a regulator of second messenger gases », *Annu Rev Pharmacol Toxicol*, vol. 37, n° 1, p. 517-554, 1997.

[131] R. Foresti, M. G. Bani-Hani, et R. Motterlini, « Use of carbon monoxide as a therapeutic agent: promises and challenges », *Intensive Care Med*, vol. 34, p. 649-658, 2008.

[132] P.-M. Yang, Y.-T. Huang, Y.-Q. Zhang, C.-W. Hsieh, et B.-S. Wung, « Carbon monoxide releasing molecule induces endothelial nitric oxide synthase activation through a calcium and phosphatidylinositol 3-kinase/Akt mechanism », *Vascul Pharmacol*, vol. 87, p. 209-218, 2016.

[133] H. P. Kim, S. W. Ryter, et A. M. K. Choi, « CO as a cellular signaling molecule », *Annu. Rev. Pharmacol. Toxicol.*, vol. 46, p. 411-449, 2006.

[134] S. Brouard *et al.*, « Carbon monoxide generated by heme oxygenase 1 suppresses endothelial cell apoptosis », *J Exp Med*, vol. 192, n° 7, p. 1015-1026, 2000.

[135] M. P. Soares *et al.*, « Expression of heme oxygenase-1 can determine cardiac xenograft survival », *Nat Med*, vol. 4, n° 9, p. 1073-1077, 1998.

[136] K. S. Washington et C. A. Bashur, « Gasotransmitters: Antimicrobial Properties and Impact on Cell Growth for Tissue Engineering », *Racing for the Surface: Antimicrobial and Interface Tissue Engineering*, p. 183-205, 2020.

[137] E. Michael, N. Abeyrathna, A. V Patel, Y. Liao, et C. A. Bashur, « Incorporation of photo-carbon monoxide releasing materials into electrospun scaffolds for vascular tissue engineering », *Biomedical Materials*, vol. 11, n° 2, p. 25009, 2016.

[138] J. E. Clark *et al.*, « Cardioprotective actions by a water-soluble carbon monoxide–releasing molecule », *Circ Res*, vol. 93, n° 2, p. e2-e8, 2003.

[139] A. Elgattar *et al.*, « Poly (butyl cyanoacrylate) nanoparticle containing an organic photoCORM », *Photochemical & Photobiological Sciences*, vol. 18, p. 2666-2672, 2019.

[140] M. Zhang *et al.*, « Photo-degradable micelles capable of releasing of carbon monoxide under visible light irradiation », *Macromol Rapid Commun*, vol. 41, n° 18, p. 2000323, 2020.

[141] M. C. Cochran *et al.*, « Disposition of ultrasound sensitive polymeric drug carrier in a rat hepatocellular carcinoma model », *Acad Radiol*, vol. 18, n° 11, p. 1341-1348, 2011.

[142] K. Gandhi, A. Barzegar-Fallah, A. Banstola, S. B. Rizwan, et J. N. J. Reynolds, « Ultrasound-mediated blood–brain barrier disruption for drug delivery: A systematic review of protocols, efficacy, and safety outcomes from preclinical and clinical studies », *Pharmaceutics*, vol. 14, n° 4, p. 833, 2022.

[143] R. ’Jourdain, V. K. ’Chivukula, et C. A. ’ ’Bashur, « Modeling gasotransmitter availability to brain capillary endothelial cells with ultrasound-sensitive microbubbles », *pharmaceutical research* , p. 1-30, sept. 2023.

[144] D. S. Li, S. Schneewind, M. Bruce, Z. Khaing, M. O’Donnell, et L. Pozzo, « Spontaneous nucleation of stable perfluorocarbon emulsions for ultrasound contrast agents », *Nano Lett*, vol. 19, n° 1, p. 173-181, 2018.

[145] W. Feng, D. Liu, S. Feng, et G. Feng, « Readily available fluorescent probe for carbon monoxide imaging in living cells », *Anal Chem*, vol. 88, n° 21, p. 10648-10653, 2016.

[146] Y. Kim, H. Rhim, M. J. Choi, H. K. Lim, et D. Choi, « High-intensity focused ultrasound therapy: an overview for radiologists », *Korean J Radiol*, vol. 9, n° 4, p. 291-302, 2008.

[147] W. Guo *et al.*, « Ultrasound-mediated antitumor therapy via targeted acoustic release carrier of carbon monoxide (TARC-CO) », *ACS Appl Mater Interfaces*, vol. 14, n° 45, p. 50664-50676, 2022.

[148] L. Yue, Y. Tang, H. Huang, W. Song, et W. Lin, « A fluorogenic probe for detecting CO with the potential integration of diagnosis and therapy (IDT) for cancer », *Sens Actuators B Chem*, vol. 344, p. 130245, 2021.

[149] A. Dauba *et al.*, « Recent advances on ultrasound contrast agents for blood-brain barrier opening with focused ultrasound », *Pharmaceutics*, vol. 12, n° 11, p. 1125, 2020.

[150] R. H. Abou-Saleh *et al.*, « Freeze-dried therapeutic microbubbles: Stability and gas exchange », *ACS Appl Bio Mater*, vol. 3, n° 11, p. 7840-7848, 2020.

[151] H. Lea-Banks, M. A. O'reilly, et K. Hynynen, « Ultrasound-responsive droplets for therapy: A review », *Journal of Controlled Release*, vol. 293, p. 144-154, 2019.

[152] E. G. Schutt, D. H. Klein, R. M. Mattrey, et J. G. Riess, « Injectable microbubbles as contrast agents for diagnostic ultrasound imaging: the key role of perfluorochemicals », *Angewandte Chemie International Edition*, vol. 42, n° 28, p. 3218-3235, 2003.

[153] J. Hauser, M. Hauser, G. Muhr, et S. Esenwein, « Ultrasound-induced modifications of cytoskeletal components in osteoblast-like SAOS-2 cells », *Journal of Orthopaedic Research*, vol. 27, n° 3, p. 286-294, 2009.

[154] Y. Sun, D. E. Kruse, P. A. Dayton, et K. W. Ferrara, « High-frequency dynamics of ultrasound contrast agents », *IEEE Trans Ultrason Ferroelectr Freq Control*, vol. 52, n° 11, p. 1981-1991, 2005.

[155] A. Carovac, F. Smajlovic, et D. Junuzovic, « Application of ultrasound in medicine », *Acta Informatica Medica*, vol. 19, n° 3, p. 168, 2011.

[156] O. Supponen *et al.*, « The effect of size range on ultrasound-induced translations in microbubble populations », *J Acoust Soc Am*, vol. 147, n° 5, p. 3236-3247, 2020.

[157] M. Olsman *et al.*, « Focused ultrasound and microbubble treatment increases delivery of transferrin receptor-targeting liposomes to the brain », *Ultrasound Med Biol*, vol. 47, n° 5, p. 1343-1355, 2021.

[158] S. R. Thom, D. Fisher, Y. A. Xu, K. Notarfrancesco, et H. Ischiropoulos, « Adaptive responses and apoptosis in endothelial cells exposed to carbon monoxide », *Proceedings of the National Academy of Sciences*, vol. 97, n° 3, p. 1305-1310, 2000.

[159] J. Jägers, A. Wrobeln, et K. B. Ferenz, « Perfluorocarbon-based oxygen carriers: from physics to physiology », *Pflügers Archiv-European Journal of Physiology*, vol. 473, p. 139-150, 2021.

[160] M. P. Desai, V. Labhasetwar, E. Walter, R. J. Levy, et G. L. Amidon, « The mechanism of uptake of biodegradable microparticles in Caco-2 cells is size dependent », *Pharm Res*, vol. 14, p. 1568-1573, 1997.

[161] Y. He et K. Park, « Effects of the microparticle shape on cellular uptake », *Mol Pharm*, vol. 13, n° 7, p. 2164-2171, 2016.

[162] L. Kou, J. Sun, Y. Zhai, et Z. He, « The endocytosis and intracellular fate of nanomedicines: Implication for rational design », *Asian J Pharm Sci*, vol. 8, n° 1, p. 1-10, 2013.

[163] P. Foroozandeh et A. A. Aziz, « Insight into cellular uptake and intracellular trafficking of nanoparticles », *Nanoscale Res Lett*, vol. 13, p. 1-12, 2018.

[164] A. S. Go *et al.*, « Heart disease and stroke statistics—2013 update: a report from the American Heart Association », *Circulation*, vol. 127, n° 1, p. e6-e245, 2013.

[165] D. Radke *et al.*, « Tissue engineering at the blood-contacting surface: A review of challenges and strategies in vascular graft development », *Adv Healthc Mater*, vol. 7, n° 15, p. 1701461, 2018.

[166] M. Shojaee et C. A. Bashur, « Compositions including synthetic and natural blends for integration and structural integrity: engineered for different vascular graft applications », *Adv Healthc Mater*, vol. 6, n° 12, p. 1700001, 2017.

[167] E. D. Giol *et al.*, « Endothelialization and Anticoagulation Potential of Surface-Modified PET Intended for Vascular Applications », *Macromol Biosci*, vol. 18, n° 7, p. 1800125, 2018.

[168] J. Shi *et al.*, « Rapid endothelialization and controlled smooth muscle regeneration by electrospun heparin-loaded polycaprolactone/gelatin hybrid vascular grafts », *J Biomed Mater Res B Appl Biomater*, vol. 107, n° 6, p. 2040-2049, 2019.

[169] J. Shi *et al.*, « Rapid endothelialization and controlled smooth muscle regeneration by electrospun heparin-loaded polycaprolactone/gelatin hybrid vascular grafts », *J Biomed Mater Res B Appl Biomater*, vol. 107, n° 6, p. 2040-2049, 2019.

[170] K. T. Kurpinski, J. T. Stephenson, R. R. R. Janairo, H. Lee, et S. Li, « The effect of fiber alignment and heparin coating on cell infiltration into nanofibrous PLLA scaffolds », *Biomaterials*, vol. 31, n° 13, p. 3536-3542, 2010.

[171] Y. Heo, Y. M. Shin, Y. Bin Lee, Y. M. Lim, et H. Shin, « Effect of immobilized collagen type IV on biological properties of endothelial cells for the enhanced endothelialization of synthetic vascular graft materials », *Colloids Surf B Biointerfaces*, vol. 134, p. 196-203, 2015.

[172] L. Zhao *et al.*, « Evaluation of remodeling and regeneration of electrospun PCL/fibrin vascular grafts in vivo », *Materials Science and Engineering: C*, vol. 118, p. 111441, 2021.

[173] D. J. Brown, E. M. Rzucidlo, B. L. Merenick, R. J. Wagner, K. A. Martin, et R. J. Powell, « Endothelial cell activation of the smooth muscle cell phosphoinositide 3-kinase/Akt pathway promotes differentiation », *J Vasc Surg*, vol. 41, n° 3, p. 509-516, 2005.

[174] J. A. van Aalst, D.-M. Zhang, K. Miyazaki, S. M. Colles, P. L. Fox, et L. M. Graham, « Role of reactive oxygen species in inhibition of endothelial cell migration by oxidized low-density lipoprotein », *J Vasc Surg*, vol. 40, n° 6, p. 1208-1215, 2004.

[175] E. C. Filipe *et al.*, « Rapid endothelialization of off-the-shelf small diameter silk vascular grafts », *JACC Basic Transl Sci*, vol. 3, n° 1, p. 38-53, 2018.

[176] R. J. Smith *et al.*, « Endothelialization of arterial vascular grafts by circulating monocytes », *Nat Commun*, vol. 11, n° 1, p. 1-16, 2020.

[177] F. Zhang et M. W. King, « Immunomodulation Strategies for the Successful Regeneration of a Tissue-Engineered Vascular Graft », *Adv Healthc Mater*, p. 2200045, 2022.

[178] E. Pektok *et al.*, « Degradation and healing characteristics of small-diameter poly (ε-caprolactone) vascular grafts in the rat systemic arterial circulation », *Circulation*, vol. 118, n° 24, p. 2563-2570, 2008.

[179] A. W. Clowes, T. R. Kirkman, et M. A. Reidy, « Mechanisms of arterial graft healing. Rapid transmural capillary ingrowth provides a source of intimal endothelium and smooth muscle in porous PTFE prostheses. », *Am J Pathol*, vol. 123, n° 2, p. 220, 1986.

[180] J. P. Hytönen *et al.*, « Improved endothelialization of small-diameter ePTFE vascular grafts through growth factor therapy », *Vascular Biology*, vol. 1, n° 1, p. 1-9, 2019.

[181] F. Kuwabara *et al.*, « Novel small-caliber vascular grafts with trimeric peptide for acceleration of endothelialization », *Ann Thorac Surg*, vol. 93, n° 1, p. 156-163, 2012.

[182] K. L. Tessneer *et al.*, « Epsin family of endocytic adaptor proteins as oncogenic regulators of cancer progression », *J Can Res Updates*, vol. 2, n° 3, p. 144, 2013.

[183] C. Chen et X. Zhuang, « Epsin 1 is a cargo-specific adaptor for the clathrin-mediated endocytosis of the influenza virus », *Proceedings of the National Academy of Sciences*, vol. 105, n° 33, p. 11790-11795, 2008.

[184] K. L. Tessneer *et al.*, « Genetic reduction of vascular endothelial growth factor receptor 2 rescues aberrant angiogenesis caused by epsin deficiency », *Arterioscler Thromb Vasc Biol*, vol. 34, n° 2, p. 331-337, 2014.

[185] M. L. Brophy *et al.*, « Myeloid-specific deletion of epsins 1 and 2 reduces atherosclerosis by preventing LRP-1 downregulation », *Circ Res*, vol. 124, n° 4, p. e6-e19, 2019.

[186] J. Dong *et al.*, « Therapeutic efficacy of a synthetic epsin mimetic peptide in glioma tumor model: uncovering multiple mechanisms beyond the VEGF-associated tumor angiogenesis », *J Neurooncol*, vol. 138, n° 1, p. 17-27, 2018.

[187] C. C. Larsen, F. Kligman, C. Tang, K. Kottke-Marchant, et R. E. Marchant, « A biomimetic peptide fluorosurfactant polymer for endothelialization of ePTFE with limited platelet adhesion », *Biomaterials*, vol. 28, n° 24, p. 3537-3548, 2007.

[188] E. Luong-Van, L. Grøndahl, K. N. Chua, K. W. Leong, V. Nurcombe, et S. M. Cool, « Controlled release of heparin from poly (ε-caprolactone) electrospun fibers », *Biomaterials*, vol. 27, n° 9, p. 2042-2050, 2006.

[189] J. Táborská, Z. Riedelová, E. Brynda, P. Májek, et T. Riedel, « Endothelialization of an ePTFE vessel prosthesis modified with an antithrombogenic fibrin/heparin coating enriched with bound growth factors », *RSC Adv*, vol. 11, n° 11, p. 5903-5913, 2021.

[190] Q. Tan *et al.*, « Controlled release of chitosan/heparin nanoparticle-delivered VEGF enhances regeneration of decellularized tissue-engineered scaffolds », *Int J Nanomedicine*, vol. 6, p. 929, 2011.

[191] J. W. Heng, M. D. Yazid, M. R. Abdul Rahman, et N. Sulaiman, « Coatings in Decellularized Vascular Scaffolds for the Establishment of a Functional Endothelium: A Scoping Review of Vascular Graft Refinement », *Front Cardiovasc Med*, p. 836, 2021.

[192] M. Likhitpanichkul *et al.*, « Fibrin-genipin annulus fibrosus sealant as a delivery system for anti-TNFα drug », *The Spine Journal*, vol. 15, n° 9, p. 2045-2054, 2015.

[193] L. Zhao *et al.*, « Evaluation of remodeling and regeneration of electrospun PCL/fibrin vascular grafts in vivo », *Materials Science and Engineering: C*, vol. 118, p. 111441, 2021.

[194] O. Kaplan *et al.*, « Low-thrombogenic fibrin-heparin coating promotes in vitro endothelialization », *J Biomed Mater Res A*, vol. 105, n° 11, p. 2995-3005, 2017.

[195] X. Ren *et al.*, « Surface modification and endothelialization of biomaterials as potential scaffolds for vascular tissue engineering applications », *Chem Soc Rev*, vol. 44, n° 15, p. 5680-5742, 2015.

[196] B. H. Walpoth *et al.*, « Enhanced intimal thickening of expanded polytetrafluoroethylene grafts coated with fibrin or fibrin-releasing vascular endothelial growth factor in the pig carotid artery interposition model », *J Thorac Cardiovasc Surg*, vol. 133, n° 5, p. 1163-1170, 2007.

[197] M. Sameti *et al.*, « Reduced Platelet Adhesion for Blended Electrospun Meshes with Low Amounts of Collagen Type I », *Macromol Biosci*, vol. 22, n° 1, p. 2100267, 2022.

[198] M. Ma *et al.*, « Local delivery of antimicrobial peptides using self-organized TiO2 nanotube arrays for peri-implant infections », *J Biomed Mater Res A*, vol. 100, n° 2, p. 278-285, 2012.

[199] A. P. J. Middelberg, C. J. Radke, et H. W. Blanch, « Peptide interfacial adsorption is kinetically limited by the thermodynamic stability of self association », *Proceedings of the National Academy of Sciences*, vol. 97, n° 10, p. 5054-5059, 2000.

[200] C. Grobler *et al.*, « Covid-19: The rollercoaster of fibrin (ogen), d-dimer, von willebrand factor, p-selectin and their interactions with endothelial cells, platelets and erythrocytes », *Int J Mol Sci*, vol. 21, n° 14, p. 5168, 2020.

[201] Z. Li et B. H. Tan, « Towards the development of polycaprolactone based amphiphilic block copolymers: molecular design, self-assembly and biomedical applications », *Materials Science and Engineering: C*, vol. 45, p. 620-634, 2014.

[202] N. Prasain et T. Stevens, « The actin cytoskeleton in endothelial cell phenotypes », *Microvasc Res*, vol. 77, n° 1, p. 53-63, 2009.

[203] M. Pensalfini, S. Meneghello, V. Lintas, K. Bircher, A. E. Ehret, et E. Mazza, « The suture retention test, revisited and revised », *J Mech Behav Biomed Mater*, vol. 77, p. 711-717, 2018.

[204] S. Baker *et al.*, « The mechanical properties of dry, electrospun fibrinogen fibers », *Materials Science and Engineering: C*, vol. 32, n° 2, p. 215-221, 2012.

[205] D. D. Swartz, J. A. Russell, et S. T. Andreadis, « Engineering of fibrin-based functional and implantable small-diameter blood vessels », *American Journal of Physiology-Heart and Circulatory Physiology*, vol. 288, n° 3, p. H1451-H1460, 2005.

[206] Z. H. Syedain, J. S. Weinberg, et R. T. Tranquillo, « Cyclic distension of fibrin-based tissue constructs: evidence of adaptation during growth of engineered connective tissue », *Proceedings of the National Academy of Sciences*, vol. 105, n° 18, p. 6537-6542, 2008.

[207] P. H. Mangin *et al.*, « Immobilized fibrinogen activates human platelets through glycoprotein VI », *Haematologica*, vol. 103, n° 5, p. 898, 2018.

[208] R. Safiullin *et al.*, « Fibrinogen matrix deposited on the surface of biomaterials acts as a natural anti-adhesive coating », *Biomaterials*, vol. 67, p. 151-159, 2015.

[209] T. Hasegawa, K. Okada, Y. Takano, Y. Hiraishi, et Y. Okita, « Thrombin-free Fibrin Coating on Small Caliber Vascular Prostheses Has High Antithrombogenicity in Rabbit Model », *Artif Organs*, vol. 29, n° 11, p. 880-886, 2005.

[210] S. de Valence *et al.*, « Long term performance of polycaprolactone vascular grafts in a rat abdominal aorta replacement model », *Biomaterials*, vol. 33, n° 1, p. 38-47, 2012.

[211] M. Shojaee, K. B. Wood, L. K. Moore, et C. A. Bashur, « Peritoneal pre-conditioning reduces macrophage marker expression in collagen-containing engineered vascular grafts », *Acta Biomater*, vol. 64, p. 80-93, 2017.

[212] M. Sameti, M. Shojaee, B. M. Saleh, L. K. Moore, et C. A. Bashur, « Peritoneal pre-conditioning impacts long-term vascular graft patency and remodeling », *Biomaterials Advances*, p. 213386, 2023.

[213] Z. H. Syedain, L. A. Meier, J. W. Bjork, A. Lee, et R. T. Tranquillo, « Implantable arterial grafts from human fibroblasts and fibrin using a multi-graft pulsed flow-stretch bioreactor with noninvasive strength monitoring », *Biomaterials*, vol. 32, n° 3, p. 714-722, 2011.

[214] U. Repnik, M. H. Česen, et B. Turk, « The endolysosomal system in cell death and survival », *Cold Spring Harb Perspect Biol*, vol. 5, n° 1, p. a008755, 2013.

[215] C. R. Reis, P.-H. Chen, N. Bendris, et S. L. Schmid, « TRAIL-death receptor endocytosis and apoptosis are selectively regulated by dynamin-1 activation », *Proceedings of the National Academy of Sciences*, vol. 114, n° 3, p. 504-509, 2017.

[216] Z. Zhang, J. Ni, L. Chen, L. Yu, J. Xu, et J. Ding, « Encapsulation of cell-adhesive RGD peptides into a polymeric physical hydrogel to prevent postoperative tissue adhesion », *J Biomed Mater Res B Appl Biomater*, vol. 100, n° 6, p. 1599-1609, 2012.

[217] P. R. Somanath, N. L. Malinin, et T. V Byzova, « Cooperation between integrin α ν β 3 and VEGFR2 in angiogenesis », *Angiogenesis*, vol. 12, p. 177-185, 2009.

[218] L. Zhen *et al.*, « Precision-porous polyurethane elastomers engineered for application in pro-healing vascular grafts: Synthesis, fabrication and detailed biocompatibility assessment », *Biomaterials*, vol. 279, p. 121174, 2021.

[219] J. H. Campbell, J. L. Efendy, et G. R. Campbell, « Novel vascular graft grown within recipient's own peritoneal cavity », *Circ Res*, vol. 85, n° 12, p. 1173-1178, 1999.

[220] J.-E. Won *et al.*, « Hierarchical microchanneled scaffolds modulate multiple tissue-regenerative processes of immune-responses, angiogenesis, and stem cell homing », *Biomaterials*, vol. 227, p. 119548, 2020.

[221] M. Gaudino *et al.*, « Mechanisms, consequences, and prevention of coronary graft failure », *Circulation*, vol. 136, n° 18, p. 1749-1764, 2017.

[222] C. S. Ong, X. Zhou, C. Y. Huang, T. Fukunishi, H. Zhang, et N. Hibino, « Tissue engineered vascular grafts: current state of the field », *Expert Rev Med Devices*, vol. 14, n° 5, p. 383-392, 2017.

[223] N. Hibino *et al.*, « Tissue-engineered vascular grafts form neovessels that arise from regeneration of the adjacent blood vessel », *The FASEB Journal*, vol. 25, n° 8, p. 2731, 2011.

[224] J. Horakova *et al.*, « An Assessment of Blood Vessel Remodeling of Nanofibrous Poly (ε-Caprolactone) Vascular Grafts in a Rat Animal Model », *J Funct Biomater*, vol. 14, n° 2, p. 88, 2023.

[225] J. A. Hubbell, S. P. Massia, N. P. Desai, et P. D. Drumheller, « Endothelial cell-selective materials for tissue engineering in the vascular graft via a new receptor », *Bio/technology*, vol. 9, n° 6, p. 568-572, 1991.

[226] B. D. Plouffe *et al.*, « Peptide-mediated selective adhesion of smooth muscle and endothelial cells in microfluidic shear flow », *Langmuir*, vol. 23, n° 9, p. 5050-5055, 2007.

[227] P. Kingshott et H. J. Griesser, « Surfaces that resist bioadhesion », *Curr Opin Solid State Mater Sci*, vol. 4, n° 4, p. 403-412, 1999.

[228] H. Chen *et al.*, « Epsin is an EH-domain-binding protein implicated in clathrin-mediated endocytosis », *Nature*, vol. 394, n° 6695, p. 793-797, 1998.

[229] W. Chaisri, W. E. Hennink, et S. Okonogi, « Preparation and characterization of cephalexin loaded PLGA microspheres », *Curr Drug Deliv*, vol. 6, n° 1, p. 69-75, 2009.

[230] J. Zhou *et al.*, « Influence of encapsulation variables on formation of leuprolide-loaded PLGA microspheres », *J Colloid Interface Sci*, vol. 636, p. 401-412, 2023.

Appendix A: In vitro and in-silico validation, tracking and delivery of ultrasound-sensitive Microbubbles

Rubens Jourdain[1], Shirin Changizi[1], Aiguo Han[2], Venkat Keshav Chivukula[1], and Chris A. Bashur[1]

[1]Department of Biomedical Engineering a, Florida Institute of Technology,

Melbourne, FL 32901, USA

[2] Virginia Tech, Blacksburg, VA, 24061

Shirin Changizi was responsible for the experimental assays in this project.

Abstract

Disruption of the blood-brain barrier (BBB) is associated with vascular cognitive impairment and dementia (VCID). Current treatments for VCID involve using high-frequency ultrasound to open the BBB for drug delivery, targeting already established diseases. Our proposed method aims to address the root cause of VCID by delivering carbon monoxide (CO)-loaded microbubbles (MBs) to the BBB to restore endothelial cell (EC) integrity. Through experimental and computational studies, we investigated the effects of low-intensity ultrasound on MBs, demonstrating partial MB rupture and subsequent CO release impacting ECs. Our experiments revealed ultrasound-induced MB movement against blood flow with varied speeds. Computational fluid dynamics modeling showed approximately

17.2% of released MBs reaching the BBB region within 10 seconds. Additionally, 1.4% of the released MBs reached the BBB wall at 10s. Preliminary experiments confirmed that employing ultrasound at full intensity results in the bursting of 82% of the released MBs, whereas only 67% of MBs are burst when using 50% intensity. Additionally, MB accumulation within ECs indicated successful static CO delivery *in vitro*. Our findings underscore the impact of ultrasound parameters on MB delivery rates and highlight the importance of integrating traditional ultrasound analysis with MB movement. Additional simulations to assess the MBs movements due to the ultrasound waves and blood flow is ongoing. Overall, our approach holds promise for BBB restoration in VCID, but further research is warranted.